FINAL REPORT

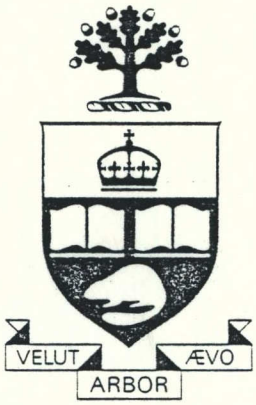

EHF CONTROLLED-BEAM ANTENNAS

FOR SATCOM PHASE B STUDY

By: J.L. Yen, Department of Electrical Engineering
University of Toronto, Toronto M5S 1A4

For: Department of Communications, Ottawa, Ont.

Under: Department of Supplies and Services
Contract Serial No. OSV82-00027

For period ending March 31, 1983.

EHF CONTROLLED-BEAM ANTENNAS FOR SATCOM: ~~PHASE B STUDY~~ FINAL REPORT

Principal Investigator: J.L. Yen
Department of Electrical Engineering
University of Toronto
TORONTO, Ontario.

Submitted to: Department of Communications
OTTAWA, Ontario.

Under DSS Contract OSV82-00027

For period ending March 31, 1983.

SUMMARY

Detailed scanning properties of multi-beam and phased array reflector antennas and the feeds required are analyzed. Sample designs for uplink and downlink applications are given. Design of zoned dielectric lens for broadband applications and the feeds are examined. Environmental effects on lenses and their remedies are considered. The results suggest that a one meter diameter multi-beam lens antenna is possible for the downlink but rather difficult for the uplink. The unique SATCOM requirements on beam control are analyzed. A system based on precise determination of jammer locations with respect to beacon transmissions is described. A combination of slow acting broadband nulling and fast acting narrow band nulling is proposed. Feed forward and feed back implementation of an intellegent adaptive array capable of nearby nulling is considered. The operation of an experimental two-element analog adaptive array using the LMS algorithm is described. Dynamic pattern adaptation in the presence of varying jamming situation is presented and compared with analysis. Recommendations for further studies in Phase C for future SATCOM are presented.

TABLE OF CONTENTS

Chapter 1

INTRODUCTION AND OVERVIEW

The task of Phase B study of EHF Controlled-Beam Antennas for SATCOM is to propose promising implementation alternatives for a specific baseline SATCOM application as described in the Statement of Work supported by numerical performance analysis and simulations. The alternatives are selected to satisfy the diverse communication objectives within the physical limitations of each configuration. Programs for numerical analysis of antenna performance and beam control are assembled and experimental facilities acquired and planned in preparation for the detailed evaluation and verification of the proposed concepts in subsequent Phase C study. The overall objective of the study is to provide technological basis for the planning of future generation SATCOM systems capable of high capacity interference resistant multi-user integrated service by maximizing the use of spacecraft resource while minimizing the requirements on user terminals.

In this Chapter an overview of the system concepts whose implementation are investigated in detail in the period reported and their rational are given. These concepts are derived from considerations of overall communications objectives, antenna capabilities and signal structures required to achieve them, and balance between spacecraft complexity and performance. The concepts adhere to the specific baseline application given in the Statement of Work, although they are more complete in nature. The remainder of this Report describes in detail the use of reflector antennas, lens antennas, their feeds and beam control for interference rejection to implement the basic system. Specific system components that should be investigated in the detailed Phase C study are proposed.

1.

Traffic Scenario, Resource Allocation and Signal Structure.

The specific baseline application in future EHF SATCOM requires a system to serve multiple user communities having different requirements. The antennas must have high gain and narrow beam so that small mobile earth terminals can be employed. When many users densely packed in a theater-of-operations require frequent service, an uplink beam can be steered to the area and remain there to provide continuing service while the spacecraft resource is shared by

frequency division multiplex (FDM). If the area covers more than a single beam width, capability for two or more beams must be provided by the spacecraft antenna. Some users however may be widely separated and requiring only occassional service. Such demands are best served in time division multiplex (TDM) employing an additional hopping narrow uplink beam. To accomodate data rates ranging from teletype rate of ten's of bits per second to voice rate of say 2400 bits per second, an M-ary frequency shift keying (FSK) modulated signal is adopted to permit inter-operability among all users and minimize the need to develop diverse terminal types [1,2]. To protect the spacecraft against uplink jamming frequency hopping over a wide bandwidth is used. To maximize downlink effective isotopic radiated power (eirp), time division multiplex using a hopping beam is most effective. The uplink signal is first dehopped, then converted from FDM to TDM using say a surface acoustic wave device, frequency hopped and then switched to an appropriate downlink beam as shown in Figure 1. To protect against downlink jamming frequency hopping can also be used. To allocate the transponder resource a portion of uplink and downlink time must be reserved for network control and handling of traffic requests and assignments.

A possible uplink signal structure assumes a maximum of 50 users. Assuming each user sends one of eight tones for 50 μs and then hops to a different frequency, i.e. at a rate faster then the data rate, then the user instanteaneous bandwidth is about 8 x 40 kHZ. To accomodate 50 users in FDM, a total instantaneous bandwidth of 16 MHz is required. If the frequencies are hopped over a 2 GHz band then processing gain contributed by total to instantaneous bandwidth ratio is 21 dB.

2.

Antenna Gain, Foot Print, Field of View and Number of Beams or Antennas.

As stated before the spacecraft antennas must have large areas and high gain narrow beams so that very small earth terminals can be served. In addition, the spacecraft must be able to serve users distributed over as large an area as possible using electronic beam control alone. These two requirements can be met only at the expense of a large number of beams if implementd in a multi-beam antenna, or, a large number of elements if a phased array is used. As discussed in Chapter 2 of this Report and in Chapter 3 of Phase A Report [3] the number of beams N of a multi-beam antenna with gain G and beam solid angle $4\pi/G$ required to cove a field of view of solid angle Ω_f is

$$N = k\ \Omega_f\ G/4\pi$$

where k is a filling factor slightly greater than one to account for beam packing. The relation also holds for the number of elements required in a phased array in which case the factor k is due to element beam spilling over the field of view. However, the main beam solid angle of a thinned phased array can be much smaller than $4\pi/G$ due to the presence of grating lobes or grating plateaus. For full earth field of view of 17 °beam angle, the required beam or element number becomes

$$10 \log_{10} N = G_{dB} - 22.6 + 10 \log_{10} K$$

The specific baseline application requires one meter diameter antennas for both uplink and downlink. This basic specification is derived from minimum user terminal considerations. Assuming an aperture efficiency of 60 percent, the uplink gain at 44 GHz is 51 dB. To have full earth coverage the beam or element number N must be greater than 1000, a number judged to mean excessive spacecraft complexity, weight and power. The specified field of view is therefore 4 x 4 degrees so that N comes in at the reasonable value of slightly greater than 75. The diameter of the uplink field of view is about 2500 km at the subsatellite point with a beam foot print diameter of approximately 325 km. Both areas are of course enlarged when the satellite zenith angle is increased from zero. To cover the entire earth, mechnical beam steering must be used. The same size antenna at the downlink frequency of 22 GHz would have a gain of 45 dB, requiring an N of about 250 to cover the earth with a sub-satellite point foot print of about 650 km. Using 60 beams or elements would result in a downlink field of view of 5000 km diameter. To cover the entire earth mechanical scanning is again necessary. These parameters are important in the design of a system to serve widely separated users.

3.

Uplink Anti-Jam Nulling.

The fact that the sytsem is required to serve small terminals means it is very easy for an adversary to use a much higher power jammer with an eirp of 90-100 dBw, to interfere. Compared with a small terminal of 50 dBw eirp there is a jammer power advantage of 40 to 50 dB. To provide sufficient protection against interference spatial discrimination must be introduced in addition to signal discrimination. The specific baseline reference system requires nulling of 3 to 4 jammers with 1 or 2 in the main beam with null depth greater than 15 dB. Although adaptive antennas have been very well studied [4] including considerations of frequency hopping [5], [6] and many have been implemented, the complexity of the SATCOM situation requires considerable rethinking of the many issues so that perhaps an intelligent adaptive antenna can be devised to counter 'smart' jammers.

4.

References

1. **McElroy, D.R.,** "EHF System Concepts for Serving Mobile Users." *9th AIAA Communications Satellite Systems Conference*, Paper No. 82-0489, March 1982.

2. **Euves, R.E. and D.P. Kolba,** "Multiple Beam EHF Antenna/Receiver Configuration for Unified Satellite Communications Uplink Coverage." *9th AIAA Communications Satellite Systems Conference*, Paper No. 82-0485, March 1982.

3. **Yen, J.L., et al.** "Study of EHF Controlled-Beam Antennas for SATCOM." Final Report, Phase A Study, DSS Contract Serial No. OSO-81-00336, May 1982.

4. **Mayhan, J.T.,** "Adaptive Nulling with Satellite Antennas." *ICC 80*, Paper No. 59.1, June 1980.

5. **Spellman, M.,** "A Comparison Between Frequency Hopping and Direct Spread PN as Antijam Techniques." *IEEE Eastcom*, Paper No. 14.4, June 1982.

6. **Castro, A.A.,** "Uplink Antenna Nulling for High Data Rate EHF Satellite Communications." *IEEE Eastcom*, Paper No. 25.4, June 1982.

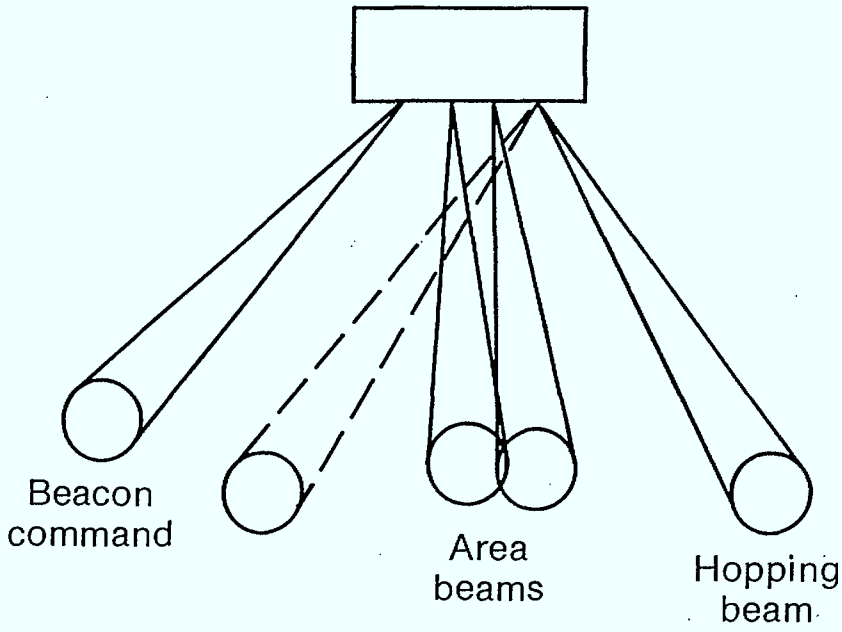

a. Uplink beams

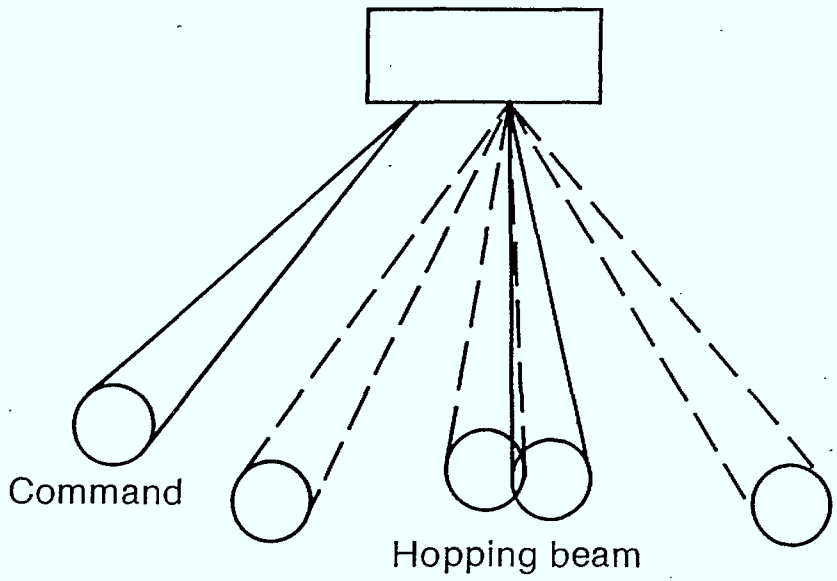

b. Downlink beams

Fig. 1.

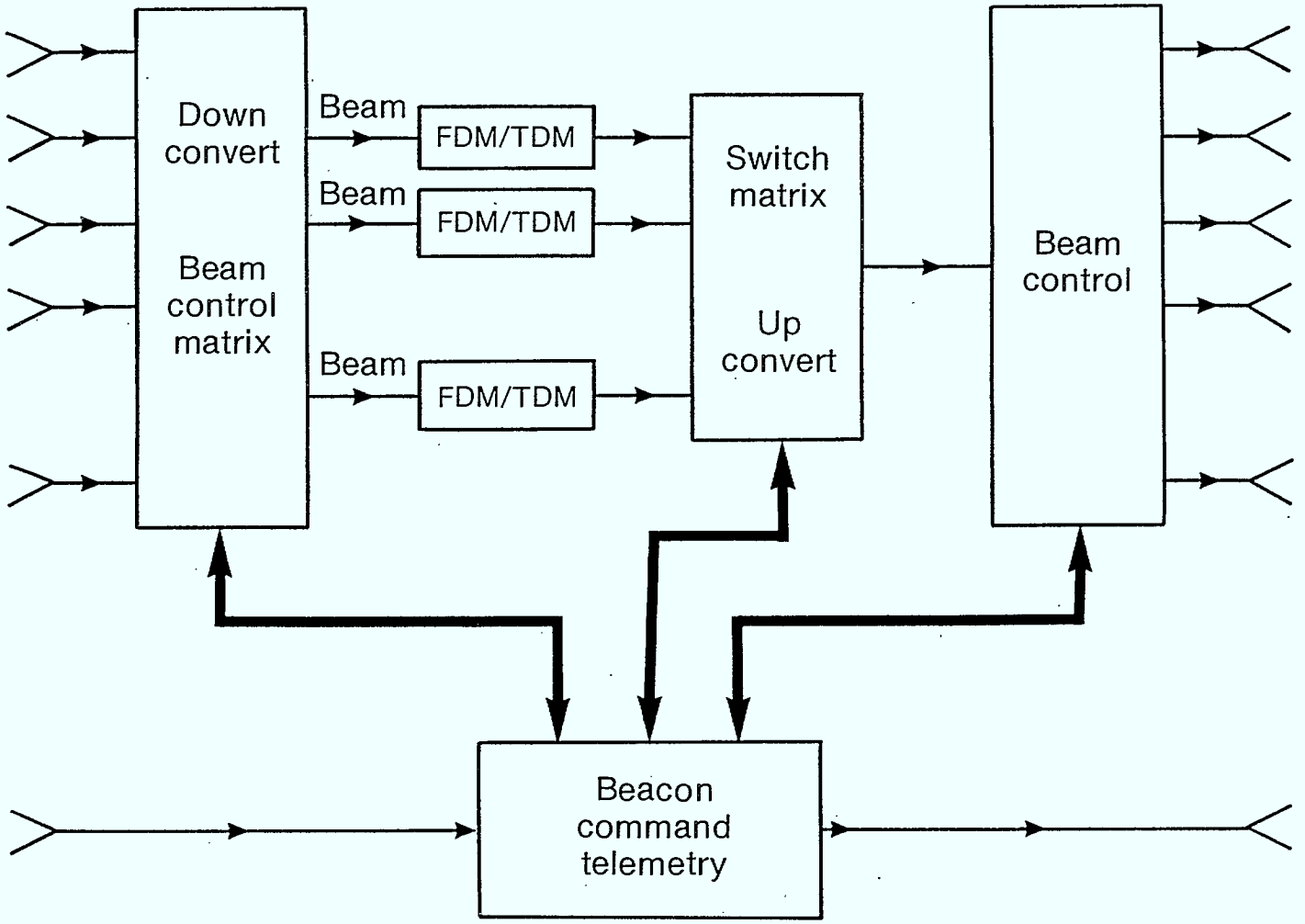

Fig. 1c. Space segment

Chapter 2

REFLECTOR ANTENNAS

S. Dmitrevsky

1.

Introduction

This chapter will review the performance of reflector antennas employed in communications systems requiring scan and beam shaping capabilities. It will be shown that these capabilities impose severe demands on the dimensions and complexity of the antennas themselves and the associated feed elements.

The basic conclusions with regard to the scan performance of a reflector antenna sytem of a given gain are:

(i) The volume of the combined antenna and feed system increases approximately linearly with the scan angle and,

(ii) the number of independently controlled elements in the feed is proportional to the square of the angle.

2.

Reflectors and Their Limitations

The common element of a reflector antenna system is a circular section of a paraboloid of revolution or a surface derived from it. In the simplest arrangement it is illuminated by a feed or feed array located near the focus.

It is usually necessary to locate the feed outside the antenna beam in order to reduce the sidelobe level. The circular section of the paraboloid surface forming the reflector is then not the central portion, but an offset one with respect to the axis. The undesirable features accruing from this arrangement are:

(i) Increase in the distortion of the feed polarization by the reflector,

(ii) enhanced effect of geometric-optical aberrations for off-axis feed elements and illumination and,

(iii) increase in the dimensions of the antenna system.

An example of an offset paraboloid reflector is shown in Figure 1.

Quantitative discussion of these effects is different for the two main types of controlled beam reflector antenna configurations:

(i) The multi-beam and,

(ii) the phase array system.

In the multi-beam antenna configuration a footprint of the beam is imaged on a particular element of the feed array. In the phased array configuration the beam is formed and steered by the generation of a suitable amplitude and phase distribution of the field in the aperture of the main reflector. The necessary field distribution is generated by corresponding excitation of all elements of the feed array which is imaged by means of a system of auxiliary reflectors (or other quasi-optical elements) on the main aperture. Samples of the two configurations are shown in Figures 2 and 3.

In the two types of systems mentioned above the complexity of the feed system is governed by the scan angle and diffraction effects while the dimensions are determined by the combined effects of the diffraction and geometric-optical aberrations.

Basic quantitative relations pertaining to these effects will be discussed in the following section.

3.

Theoretical Background

This section contains basic formulae needed for the quantitative description of antenna performances and their limitations. The expressions to be introduced have been derived under assumptions rendering the results simple but, of necessity approximate. Numerical values have been obtained for the case of the main reflector diameter of 1 m and for the operating frequencies of 44.5 GHz ($\lambda = 6.7$ mm) and 21.7 GHz ($\lambda = 13.7$ mm) corresponding to the downlink and uplink centre frequencies respecitvely of the satellite communications system considered.

3.1.

Antenna beamwidth

It is assumed that the beamwidth θ of a uniformely illuminated circular aperture of diameter D at wavelength λ is given by the equation

$$\theta = \lambda/D \tag{1}$$

3.2.

Effect of geometric-optical aberrations

The deterioration of a reflector performance at beam directions deviating by angle α from the axis of the paraboloid are caused primarily by coma and and spherical aberration. Their effect will be described by considering the field distribution in the focal plane of a reflector due to a plane wave impinging on the aperture at an angle α with respect to the axis as shown in Figure 4. The spread of the focal pattern in this case, as compared with that for axial illumination ($\alpha = 0$) is due primarily to the change of phase in the argument of the Kirchhoff-Huyghens integral, present for the case of α different from zero [3], [4]. The maximum value of the phase distortion $\Delta\Phi$ is

$$\Delta\Phi = 0.25kf(\alpha \sin^3\phi - \alpha^2 \sin^2\phi) \tag{2}$$

where $k = 2\pi/\lambda$ and f is the focal length of the paraboloid and ϕ is the direction of the ray of maximum deviation (see Figure 4).

Computer evaluation of the integral has indicated that the focal pattern does not deteriorate appreciably if $\Delta\Phi$ is less than 0.7π. The criterion accepted in future for the limit of admissible performance in this connection is

$$\Delta\Phi = 0.25kf(\alpha \sin^3\phi - \alpha^2 \sin^2\phi) = \pi/2 \tag{2a}$$

3.3.

Polarization distortion

A focal plane feed array illuminating an offset reflector is shown in Figure 5. The polarization pattern of the feed array may be controlled to a certain degree by the choice of feed elements. The polarization distortion due to the reflection by the antenna can be substantially reduced by the use of a secondary, hyperboloidal reflector inserted between the feed array and

the main reflector [1], [2]. This reflector can also be simultaneously utilized to change the size and the position of the feed array to reduce the system dimenions.

4.

Multi-Beam Beam Reflectors

4.1.

Number of feed elements

In a multi-beam reflector, or systems of such, a feed array is imaged on the area serviced by the antenna with an individual element of the feed illuminating (or receiving signal from) a particular footprint which, in the case of circular aperture subtends a solid angle of circular cross-section. If the area is to be covered completely the footprints must overlap. The number of beams required to service a given scan range specified by solid angle Ω can be approximately calculated by inscribing a hexagon into the circular beam and covering Ω by these hexagons. The number of hexagons required is equal to the number of elements in the array. If the antenna beamwidth is θ, the solid angle subtended by the inscribed hexagon is $0.65\ \theta^2$ and the number of elements N required for the feed array is

$$N = 1.5\ \Omega/\theta^2 \tag{3}$$

For the system considered the scan range is 4 °×4 °. For aperture diameter D of 1 m the realizable beamwidth θ is

$$\theta = \begin{cases} 1\ ^\circ \text{at } 21.7 \text{ GHz (downlink)} \\ 0.5\ ^\circ \text{at } 44.5 \text{ GHz (uplink)} \end{cases}$$

The number of feed elements required in the multi-beam configuration is 24 for the 21.7 GHz downlink and 96 for the 44.5 GHz uplink.

4.2.

Spillover

The need to cover completely the area serviced by the overlapping beams results in inefficient reflector illumination by feed elements which cannot overlap. Their dimensions being smaller than those required to illuminate the reflector aperture some of the power spills past the reflector and is lost to the system. To obtain an estimate of the magnitude of the effect

consider a multi-beam system shown in Figure 5. Assuming uniform illumination of both the feed and reflector apertures one obtains the following relations:

- o Main beamwith, $\theta = \lambda/D$.
- o Separation of beam centres required for gapless coverage, $\delta = \theta\sqrt{3/4}$.
- o Feed element diameter, $d = \delta f = f\,\theta\sqrt{3/4}$.
- o Feed beamwidth, $\lambda/d = (\lambda/f\ \theta)\ \sqrt{4/3} = \frac{D}{f}\sqrt{4/3}$
- o Feed beam solid angle, $\Omega_a = (\pi/3)\ (D/f)^2$
- o Reflector solid angle, $\Omega = (\pi/4)\ (D/f')^2$

where (f'/f) is a number greater than unity.

For system under discussion the typical value of the number is 1.2. The ratio of power P_h radiated from the feed to the power intercepted by the reflector P_r is thus

$$P_h/P_r = 4(1.2)^2/3 = 3\ dB$$

The scan capability thus results in a 3 dB reduction of effective power due to spillover.

4.3.

Dimensions

It will be shown below that the scan capability of ± 2 ° requires that the ratio of focal length f to diameter D be about 2.5 as shown in Figure 5. The longitudinal dimension of the antenna system required would then be about 3 m to accomodate the feed sources. This value can be reduced by bending the beam back by an auxiliary reflector as shown in Figure 6. A clearance h of about one half of the main reflector diameter is required to assure free path for the main beam. The undesirable consequence of the arrangement is the increase in the angle of deviation of the marginal ray (FA in Figure 6) resulting in increased aberration and phase deviation $\Delta\Phi$ (Eqn. 2 in Section 3 above). The tolerable value of $\Delta\Phi$ was set at $\pi/2$ (Eqn. 2a). For moderate values of D/f (see Figure 4), sin ϕ in this equation can be approximated by $(D+h)/f$ reducing the equation to the form:

$$(D/\lambda)\left[\alpha\left(\frac{D+h}{f}\right)^2 - \alpha^2\left(\frac{D+h}{f}\right)\right] = 1 \qquad (5)$$

This equation allows one to determine the value of $(D+h)/f$ required to retain acceptable antenna performance at scan angle α.

The relationship between the parameter f/D and α for offsets h equal to $D/2$ and $D/3$ is given in Figure 7 for $D = 1$ m and $\lambda = 13.7$ mm (21.7 GHz). It is evident from these curves that an increase of the scan angle α requires an increase in the focal length f.

There exists thus a trade-off between the scan angle and the overall dimensions of the system.

A scan range of 4 °× 4 °would require an f/D value of 2.5 with offset h equal to 0.4 D. Thus for 1 m antenna diameter the axial dimension of the system would be in excess of 2.5 m. The relatively large value of the focal length required has an adverse effect in the size of the feed elements. As shown in Eqn. 4 the feed element diameter d is 0.865 $f\theta$ which, for $\theta = \lambda/D$ is

$$d = 0.865\,\lambda\,f/D \tag{6}$$

For $f/D = 2.5$ the feed element diameter d is 2.15 λ.

It is desirable to reduce both the axial dimensions of the system and the polarization distortion caused by the lack of symmetry in the offset geometry. Both can be accomplished by a hyperboloidal reflector located between the main reflector and its focus.

By a geometrical construction described in reference [2] a confocal hyperboloid reflector shape can be developed which will allow the polarization of the feed to return to its original state after reflections from the hyperboloid and the main paraboloid reflector. An example of a system of this type is shown in Figure 8. Its parameters are:

- o Main reflector diameter, $D = 1$ m
- o Focal length, $f = 2.5$ m
- o Reflector offset, $h = 0.5$ m
- o Inclination of hyperboloid axis, $i = 15$ °
- o Separation of prime and secondary foci, $2e = 1.76$ m
- o Hyperboloid main axis, $a = 22$ cm

The advantages of the new configuration are summarized below for numerical parameters corresponding to 21.7 GHz downlink frequency.

In the original, single reflector configuration the overall length of the system is equal to the focal length plus the length required to accomodate the feed array. With feed element aperture d of 2.15 λ the horn length required would be about $3 \times 2.15\,\lambda$ which, for $\lambda = 13.7$ mm would be 9 cm. With appropriate transmission line connections one can assume that the feed might require a length of some 15 cm. The axial length of the system would thus be about 2.65 cm. The use of the auxiliary reflector (see Figure 6) removes a portion of the focal length from

the longitudinal dimension and, because of the bending of the main beam eliminate the need for length to accomodate the feed. The overall longitudinal dimension is reduced to 1.8 m. The longitudinal size reduction, however, is obtained at the expense of an increase of transverse dimensions and of the feed element aperture which is magnified by a factor M [1],

$$M = \frac{e + a}{e - a} \frac{\cos^2 \phi_1/2}{\cos^2 \phi_2/2} \tag{7}$$

For the numerical parameters considered the value of M is 1.63 and the feed aperture d increases from $2.15\,\lambda$ to $3.5\,\lambda = 4.8$ cm. The required longitudinal feed dimension of about 20 cm can be accomodated within the 1.8 m length obtained from Figure 6.

It is useful to consider the transverse dimensions of the system with and without the auxiliary reflector. With 24 feed elements required to accomodate the 4 ° scan the diameter of the feed array is six feed apertures. For a single reflector configuration this adds $3 \times 2.15\,\lambda = 9$ cm to the transverse dimension which becomes $D + D/2 + 9\,\text{cm} = 185\,\text{cm}$. The overall system volume then is approximately

$$1\,\text{m} \times 1.85\,\text{m} \times 2.65\,\text{m} = 5\,\text{m}^3$$

In the two-reflector configuration the longitudinal dimension is 1.25 m. Transverse dimension, however, increases to about 220 cm rendering the volume

$$1\,\text{m} \times 2.2\,\text{m} \times 1.8\,\text{m} = 4\,\text{m}^3$$

It can thus be seen that the overall volume remains approximately constant and is fixed primarily by the gain which determines the main reflector diameter D and the scan angle α, both affecting jointly the focal length f.

The discussion of multi-beam antennas in this section was relevant to the application in the 21.7 GHz downlink for the following reason: the beam steering in this configuration is effected by switching the signal to individual feed elements, which is readily accomplished in transmitter application at RF frequency. Because steering in the phased array systems is realized by adjusting the phase and amplitude of signals in all elements of the feed, it is more easily realizable in receiver applications where the necessary processing can take place at IF frequencies.

5.

Phased Arrays

In phased array systems beam steering and shaping is accomplished by the generation of aperture amplitude and phase distribution required to produce the desired beam shape and direction. If the feed array were to be used directly as the aperture the size of individual elements would be inconveniently large for high gain systems. It is therefore useful to generate a small image of the desired aperture distribution and magnify it by means of appropriate quasi-optical elements such as mirrors on lenses. It may be pointed out that whereas the discussion of the properties of multi-beam antennas was based on microwave analogue of optical telescope theory, the properties of phased arrays resemble those of microscopes.

A typical phased array system consists of a larger paraboloidal reflector, a feed array and a small paraboloidal reflector imaging the aray on the aperture of the large reflector. A layout of a configuration of this type is shown in Figure 8. The important parameters of the system are the main reflector diameter D, the offset h and the ratio of the focal lengths F/f of the two reflectors.

5.1

Number of feed elements

As mentioned above, the pattern of this antenna type is produced by the interference of fields radiating from individual images of array elements on the main dish aperture. The scan angle is therefore determined by the beamwidth of individual image. If Ω is the solid angle corresponding to the scan angle and θ the desired beamwidth of the antenna the number N of elements in the feed is $1.5\,\Omega\,/\,\theta^2$ as shown in the Introduction. The expresssion is the same for both the multi-beam and phased array configurations, but due to different mechanisms of aperture excitation in the two cases the patterns overlap leading to the reduction of power in the main beam produces different side effects which will be discussed later.

For the 44.5 GHz downlink for which the phased array system may be a suitable antenna type the number of feed elements N for $4\,^\circ \times 4\,^\circ$ scan and $0.5\,^\circ$ beamwidth is $1.5 \times 4 \times 4/0.5^2 = 96$..

5.2

Grating lobes

The feed array consisting of a series of discrete elements cannot produce a uniform amplitude and phase distribution over an aperture. As a consequence the pattern generated will exhibit strong 'grating' sidelobes reducing the power in the main beam by approximately 3 *dB*. The effect is analoges to the spillover in the case of multi-beam antennas with an additional adverse feature that, whereas in the case of spillover the lost power was radiated in the direction opposite to that of the main beam, the grating lobes point in the direction close to that of the main lobe. A method of eliminating the effect will be discussed later in Subsection 5.4 - Feed arrays.

5.3

Dimensions of reflectors

The three basic elements of a phased array antenna are, as discussed earlier, the main reflector, the imaging reflector and the phased array. To reduce the longitudinal dimensions of the systems it may be desirable to fold the main beam back by means of a reflector located between the main and the imaging dishes necessitating offset geometry analogous to the case of multi-beam systems, as shown in Figure 11.

The dimensions of various elements are determined by system requirements, diffraction and aberration effects.

The diameter D of the main dish is given by the gain. The optical performance of the main dish does not affect the performance of the system because individual patches of its surface are independently illuminated by suitably phased feed elements. It is limited primarily by the small imaging dish which, to use optical anology, plays the role of the objective lens in a microscope. Its purpose is to produce a magnified image of the feed array in the aperture of the main dish. The magnification is approximately equal to the ratio of the focal lengths of the two reflectors F/f and from the size requirements alone a large ratio is desirable to reduce the dimension of the feed array. Excessive reduction of the focal length f, however, leads to degradation of the performance in that it reduces the resolving power of the imaging process as will be shown below.

If a is the dimension of the feed element aperture and d the diameter of the imaging reflector, a will be properly imaged on the main aperture if its beam is intercepted by this imaging reflector, i.e., if, approximately,

$$f\lambda/a \leqslant d \tag{8}$$

For scan angle α the value of a is given by

$$(\lambda/a)\,(f/F) = \alpha \quad \text{or,} \tag{9}$$

$$a = (\lambda f)\,/\,(\alpha F) \tag{9a}$$

Substituting the expression for a into Eqn. 8 and observing that d is equal to $D f/F$ one obtains the following approximate relationship for the ratio F/f:

$$F/f \leqslant (1/\alpha)\,(D/f) \tag{10}$$

Thus there exists an upper limit for the ratio F/f. The discussion presented above is a microwave analogue of a simple theory of the resolving power of a microscope. It is evident from the last equation that the performance of the system for a given scan angle α depends both on the ratio F/f and F/D. To evaluate the effect of F/D it is necessary to consider the influence of the imaging components on geometric-optical aberrations.

For sufficiently small values of F/f the imaging parabola lies in the Fresnel region of the feed array the field of which may be considered to be a plane wave illuminating the parabola the steering angle α. This condition is obtained if

$$(f/F)^2\, D^2/\lambda > f \tag{11}$$

This requirement is easily satisfied for values of $F/f = 5$, $\lambda = 6.7\,\text{mm}$ (44.5 GHz) and $D = 1\,\text{m}$. For this range of parameters the value of the phase error $\Delta\Phi$ (Eqn. 2a) determines the imaging properties of the system. Adopting again the criterion that the maximum tolerable value of $\Delta\Phi$ is $\pi/2$ the relationship between the scan angle α, and the ratios F/f and F/D are plotted in Figure 9 for $D = 1\text{m}$, $\lambda = 6.7\text{mm}$ and offset h equal to $D/3$.

A different phenomenon dominates the imaging process for large values of f when the Fraunhofer pattern of individual array element covers the whole of the imaging reflector. The antenna performance is then limited by the diffraction of the partially intercepted feed element beam by the aperture of the imaging parabola. The requirement under these conditions is for the main beam of the diffraction pattern to illuminate only the geometrical optical image of the feed element on the main reflector aperture. With reference to Figure 8, the approximate value of ϕ in Eqn. 2 for $\Delta\Phi$ is given by

$$\phi = (\lambda/a)\,(F/f) = 2\,\alpha\,F/f \tag{12}$$

where $\pm\alpha$ are the maximum scan angles, aF/f is the dimension of individually illuminated patch on the main aperture and a is the dimension of the feed element aperture. The limits of performance in this regime are the obtained again by requiring that the maximum value $\Delta\Phi$ be

$\pi/2$. The corresponding equation (which appropriate approximations such as $\sin\phi = D/F$) is

$$(D/\lambda)\,(F/D)\,\alpha^4\left[\,8(F/f)^2 \pm 4F/f\,\right] = 1 \qquad (13)$$

The curve of α against F/D for large values of the latter parameter is plotted in Figure 9.

It is not possible to obtain simple description of the behaviour in the intermediate range and the approximate pattern of behaviour was obtained using interpolation as shown by the dotted portions of the curves in Figure 9.

An interesting feature of these curves is the fact that for a given value of the ratio F/f there exists a maximum value of the scan angle. A parallel with the behaviour of multi-beam systems also becomes apparent in that large scan angles require small values of F/f, i.e., large imaging reflectors increase in scan range requires increase in size.

For 4 °× 4 °scan range of the 44.5 GHz uplink with main dish diameter $D = 1$m and 33 cm offset a possible set of antenna system parameters is $F/f = 5$, $F/D = 1.65$.

5.4

Feed arrays

The feed array is the geometric image of the main reflector aperture and is located in the vicinity of the focal plane of the imaging reflector. Because the main reflector is not at infinity the deviation of the feed array surface from the focal plane is not negligible and must be evaluated using geometric optical methods.

The image A' of a point A in the aperture of the main reflector is given by the coordinates (see Figure 8) given by the equation

$$z = 2f\,(1 + f/F)\,/\,(1 + \cos\phi) \qquad (14)$$

The relative deviation of the image points from the focal plane, $\Delta\, z/f$ is plotted in Figure 10. For F/f equal to 5, the offset h equal to $D/3$ and F/D equal to 1.65 the distance of the central element from the focal plane is $.3f$. The average inclination of the array surface to the focal plane is 12 °as depicted in Figure 8.

The size of feed element aperture a is related to the corresponding patch in the main reflector aperture by the magnification factor F/f. For scan angle variation α, the size of the patch is λ/α and the dimension of the feed element aperture a is, from Eqn. 9

$$a = (\lambda/\alpha)\,f/F$$

For total scan of 4 ° (1/14 radian) at 44.5 GHz and the ratio F/f of 5 the size of the feed aperture is $\lambda\ 14/5 = 2.8\,\lambda = 19$ mm.

The non-uniform illumination of the main aperture by the feed array produces, as was mentioned earlier, grating lobes which affect adversely the antenna performance in that they reduce the power in the main beam and increase the sidelobe level. The latter can be partially reduced by a spatial filter (aperture) in the common focal plane of the two reflectors [5]. The explanation of the mechanism is based on the fact that the small imaging antenna produces a Fourier transform of the feed array field in its focal plane. The main reflector aperture distribution is the Fourier transform of the focal field and the far field of the main reflector is the Fourier transform of its aperture field. Thus the far fields of the main reflector is the double Fourier transformer of its focal field. In as much as the inverse of a Fourier transform is the transform itself the far field of the main reflector is the image of its own focal field. If space filtering in the focal plane eliminates grating lobes, they are automatically eliminated from the far field of the antenna system.

5.5

System dimensions

The overall system dimensions can be reduced by the insertion of a flat reflector between the focus and the main reflector as shown in Figure 11. In the case of parameters adopted ($D = 1\,m$, $F/f = 5$, $h = D/3$) the volume of the antenna system is approximately $1\,\text{m} \times 1.3\,\text{m} \times 1.6\,\text{m} = 2.1\,\text{m}^3$. In a manner analogous to the behaviour of the multi-beam antennas the system volume depends on the maximum scan angle - increase in scan angle requires an increase of the focal length F and a reduction of F/f ratio, i.e., additional increase of the imaging system dimensions.

5.6

Performance limits

The effects of diffraction and aberrations as considered in Subsection 5.3 - Dimensions of reflectors, were used to determine the optimum system configuration for a given frequency and main reflector diameter. Eqn. 8 can, however, be interpreted in a more general way. When rewritten in the form

$$f\,\lambda/d \leqslant a \tag{15}$$

where f, d and a are the focal length and diameter of the imaging parabola and a is the dimension of the feed element aperture, the equation can be viewed as establishing the

resolving power of a microscope which, for a given wavelength prossesses upper bound. The dimension a is related to the scan α by the equation (Eqn. 9)

$$\lambda f/a\ F = \alpha$$

Substituting for a in Eqn. 15 one obtains the absolute limit of the scan angle α

$$\alpha \leqslant d/F \tag{16}$$

In communications systems, as distinct from optical imaging devices the important parameter is either the diameter of the main reflector or the beamwidth. Eqn. 16 can thus be rewritten in the following form

$$\alpha \leqslant Df/F^2 \quad \text{or,} \tag{16a}$$

$$\alpha \leqslant (\lambda/\theta)\ (f/F^2) \tag{16b}$$

It can thus be seen that the maximum scan angle attainable in a phased array antenna as indicated by the existence of maxima in the curves of Figure 9 is a consequence of the existence of an upper limit of the resolving power of a microscope type system. Should a scan angle larger than the limit imposed by the dominant system parameters be required, it will be necessary to abandon the convenience afforded by the small size of feed arrays in configurations with imaging reflectors and employ the phased array itself as the main aperture.

It should be pointed out that the severe limitation on the performance of phased array antennas developed above applies if beam shaping capability is required. For beam steering capability alone the limitations can be relaxed to a certain degree, so that Eqn. 16a and 16b would acquire the form

$$\alpha \leqslant q\ D f/F^2 \tag{17}$$

$$\alpha \leqslant q\ (\lambda/\theta)\ f/F^2$$

where q is a numerical factor greater than unity.

6.

Computer Simulation

The effect of geometric-optical aberrations on the performance of offset paraboloidal reflectors was numerically evaluated for several configurations. The main purpose of the study was to develop a criterion for establishing the maximum tolerable phase error in aperture distribution in the case of off-axis illumination. The effect was observed in terms of the behaviour

of the field pattern in the focal plane of the reflector. The calculations were carried out for a range of steering angles and the amplitude distribution was displayed in a two-dimensional shaded plot.

The actual expression evaluated was the Kirchhoff-Huyghens integral

$$J(\xi,\eta) = \exp[-j\,kf\,(\xi^2+\eta^2)/2] \int \exp[j\,kf\,\Phi(\theta,\phi,\alpha,\xi,\eta)] \sin d\theta\ \ d\phi$$

The symbols in the above expressions are (see Figure 12):

- θ, ϕ - polar coordinates of aperture point,
- α - beam steering angle,
- ξ, η - coordinates in focal plane with respect to geometric image point in units of f,
- k - $2\pi/\lambda$,
- $\Phi(\theta, \phi, \alpha, \xi, \eta)$ - aperture phase function specified below (see Eqn. 2 and Ref. [?]).

$$\Phi(\theta,\phi,\alpha,\xi,\eta) = \Delta\Phi(\theta,\phi,\alpha) + (\xi\cos\phi - \eta\sin\phi)\sin\theta \tag{18}$$

$$\Delta\Phi(\theta,\phi,\alpha) = (\alpha\sin^3\theta\cos\phi - \alpha^2\sin^2\theta)/4$$

In the above expression the term $\Delta\Phi(\theta, \phi, \alpha)$ represents the phase distortion due to geometric-optical aberrations caused by the off-axis steering angle α.

The computations were carried out with input parameters simulating the following conditions:

- Aperture diameter: 1 m,
- focal length: 2.5 m,
- frequency: 44 GHz and 22 GHz,
- steering angle range: ± 2.8 °.

A sample of results in the form of beam shapes and two dimensional intensity distributions is presented in the Appendix.

As mentioned earlier the purpose of the computer simulation was to develop a criterion for the determination of maximum tolerable value of the phase derviation $\Delta\Phi$. A convenient objective (as distinct from subjective) evaluation of amplitude and phase distributions was to plot the level of first sidelobes with reference to their level for zero sterring angle α and the excentricity defined as the ratio of 3 dB pattern widths in the meridional and transverse

directions. The graphs of these parameters are shown in Figures 13 and 14.

In view of the fact that the focal pattern is the desirable feed pattern it was decided that an acceptable level of excentricity would be 1.5 , which corresponds to a value of 0.7π of the phase distortion $kf\,\Delta\Phi$. It is interesting to note that the values of α for which the excentricity becomes 1.5 coincide with the values for which the sidelobe levels begin to increase as apparent in Figure 14.

The computer simulation carried out has shown that the performance at off-axis beam direction lies within tolerable limits if the phase distortion $kf\,\Delta\Phi$ is less than 0.7π. Based on this result the adapted criterion for determining the limits of tolerable performance degradation in theoretial discussions presented earlier was

$$kf\,\Delta\Phi\,(\theta\,,\phi\,,\alpha) \leqslant \pi/2 \tag{19}$$

7.

Conclusions

7.1

General

The central problem considered in this chapter was the relationship between the scan angle and the dimensions of the components in controlled beam reflector antennas.

The behaviour of the multi-beam and phased array systems in this context is different as summarized below

(a) In multi-beam antennas the scan angle determines the focal length, i.e., the distance from, and the size of the feed array. The performance limitations are imposed primarily by geometric-optical aberrations and their effect on system parameters is expressed through the curves of Figure 7. Some improvement of performance retaining the given dimensions can be achieved by the use of reflecting surfaces other than paraboloids or systems with annular rather than offset geometry. In the latter case enhanced sidelobe level would have to be tolerated.

(b) In phased array systems the scan performance is limited by the resolving power of the imaging reflectors, which beyond a certain value of the scan angle would have to be larger than the main reflector itself. The curves of Figures 9 and 10 provide a summary of system design criteria.

The general performance features of the two types of configurations can be easily, if approximately understood in terms of analogy with their optical counterparts. The scan

performance of multi-beam systems is a microwave analogue of the field of view capability of telescopic devices while the scan performance in phased array systems has its counterpart in the resolving power of a microscope.

7.2

SATCOM

Antenna configurations suitable for employment in SATCOM system are:

(a) Downlink, 21.2 - 22.2 GHz, electrical steering range 4 °× 4 °, main reflector diameter $D = 1m$,

- multi-beam configuration, $F/D = 2.5$,
- auxiliary hyperboloid reflector as shown in Figure 6,
- feed element aperture $3.5\lambda = 4.8$ cm,
- 24 element feed array.

(b) Uplink, 43.5 - 45.5 GHz, electrical steering range 4 °× 4 °, main reflector diameter $D = 1m$,

- Phased array configuration with imaging reflector as shown in Figure 11,
- $F/D = 1.65$, $F/f = 5$,
- feed element aperture $a = 2.8\lambda = 19\ mm$,
- 96 element feed array.

(c) Full earth disc coverage.

The full earth disc coverage requires pointing range of ±8.5 °. For the configurations considered above this can be achieved through mechanical steering only. Due to the fact that the antennas proposed operate at the limit of their performance capability the mechanical steering system cannot employ dislocation of internal antenna elements. The steering method recommended is to employ flat movable reflectors (mirrors) in front of the main reflectors.

7.3

Increase of electronic steering range

Steering range of multi-beam downlink system can be increased to full earth disc coverage by increasing the F/D ratio to approximately 4 and the array size to $14 \times 24 = 336$ elements. The large number of elements can be reduced if lower antenna gain can be tolerated. The F/D ratio can be somewhat reduced by employing main reflector surface other than paraboloid.

The steering performance of the phased array uplink system can be improved by increasing the main reflector diameter and reducing the F/f ratio. In as much as the increase of the main dish diameter would require increase of the number of feed array elements by factor of 16 times the square of the diameter ratio the realization of a system of this type would be prohibitive. A feasible configuration in this case would be a direct feed array aperture.

8.

References

1. **Dragone, C.,** "Conformal mapping and complex coordinates in Cassegraimian and Gregorian Reflector Antennas." *Bell System Technical Journal*, Vol. 60, No. 10, pp. 2397-2420 (December), 1981.

2. **Dragone, C.,** "Offset multi-reflector antennas with perfect pattern symmetry and polarization discrimination." *Bell System Technical Journal*, Vol. 57, No. 7, pp. 2663-2684 (September), 1978.

3. **Born, M. and E. Wolf,** "*Principles of Optics.*" pp. 458-463, Pergamon Press, New York, London, Paris, Los Angles, 1959.

4. **Synge, J.L.,** " *Geometrical Optics*". Cambridge University Press, 1937.

5. **Dragone, C. and M.H. Gans,** "Satellite Phased Arrays: Use of Imaging Reflectors with Spatial Filtering in the Focal Plane to Reduce Grating Lobes." *Bell System Technical Journal*, Vol. 59, No. 3, pp. 449-461 (March), 1980.

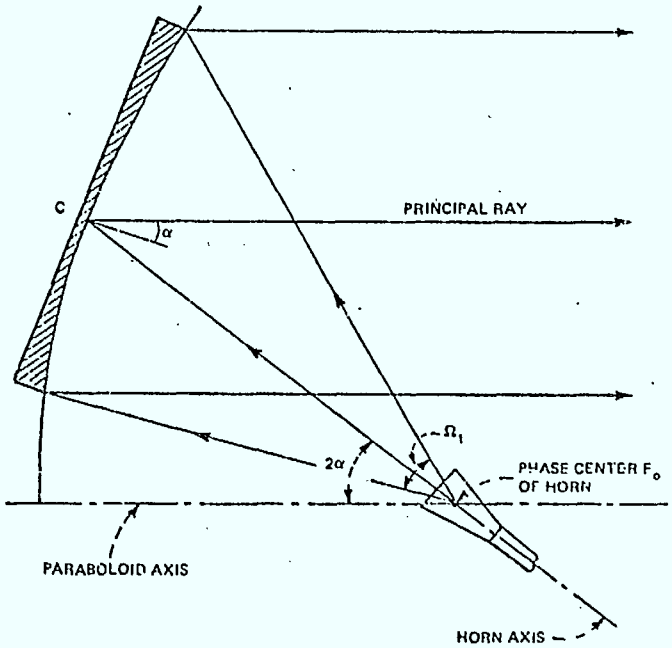

The spherical wave radiated from F_0 by a corrugated feed is transformed by an offset paraboloid into a plane wave.

Fig. 1.
Offset paraboloid reflector,
(C. Dragone, BSTJ, Vol. 57, No. 7,
p. 2664).

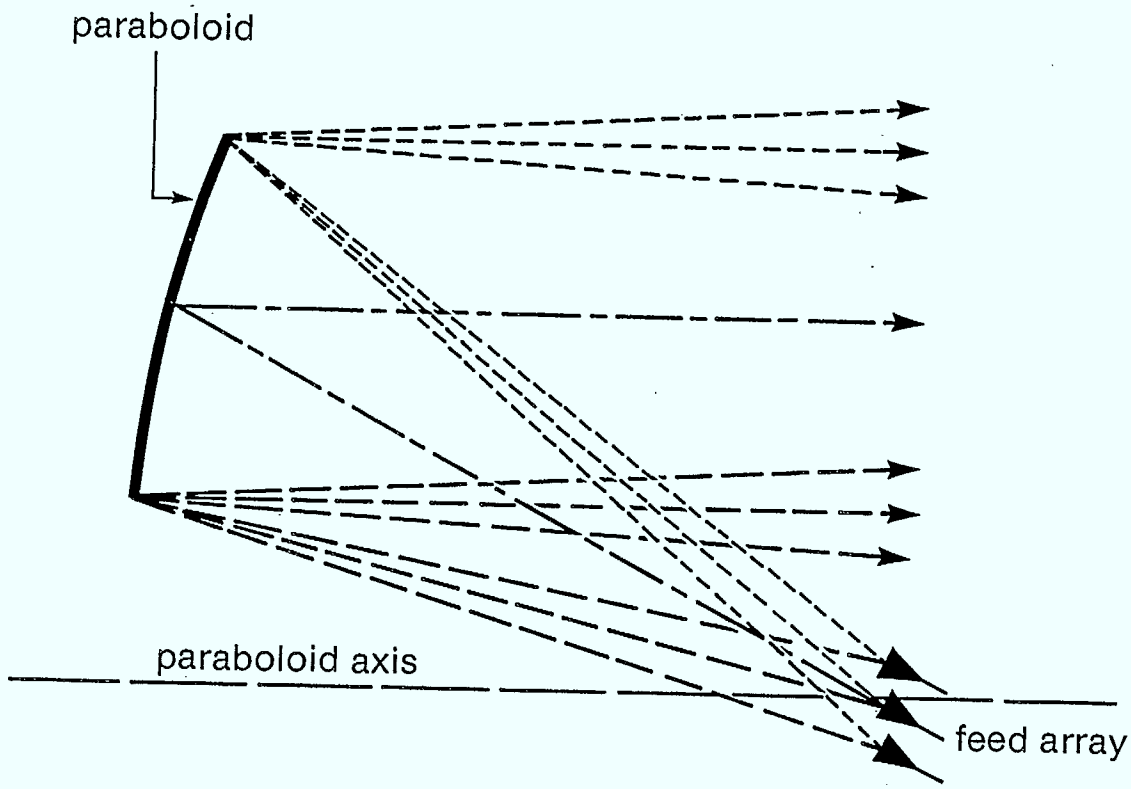

Fig. 2. Multibeam reflector antenna.

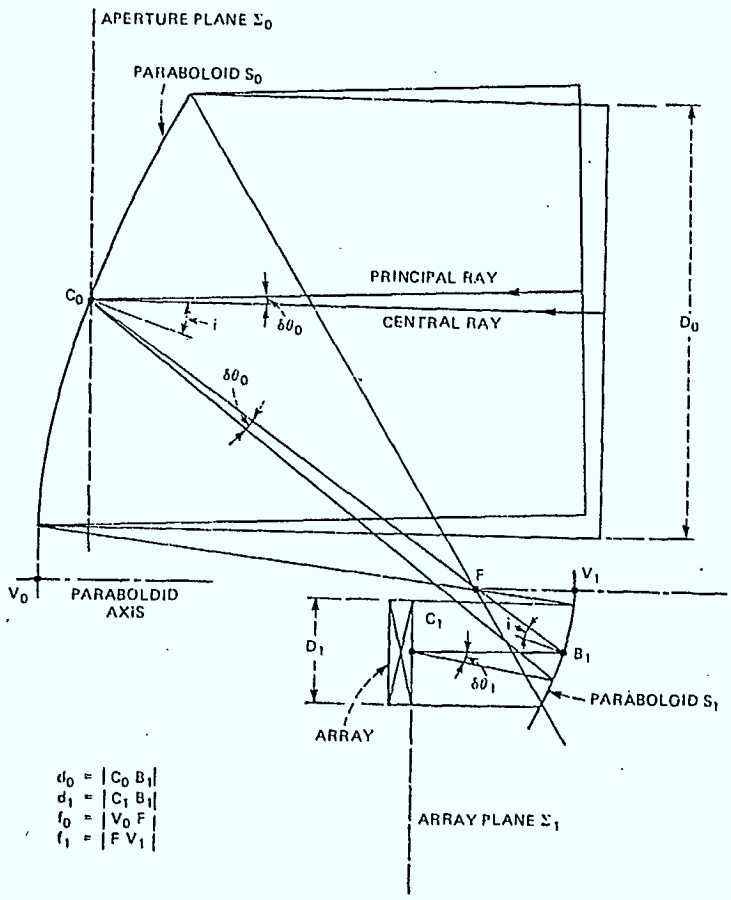

Fig. 3. Phased array reflector antenna (C. Dragone, M.J. Gans, BSTJ Vol. 58, No. 2, p. 503)

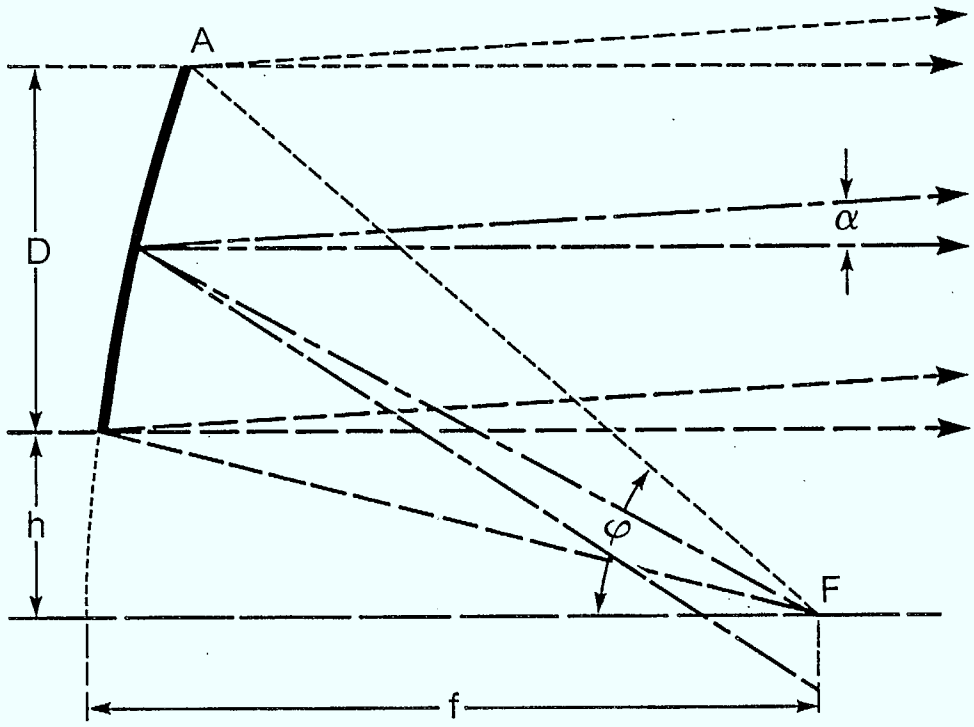

Fig. 4. Beam steering angle α
in offset paraboloid refelector.

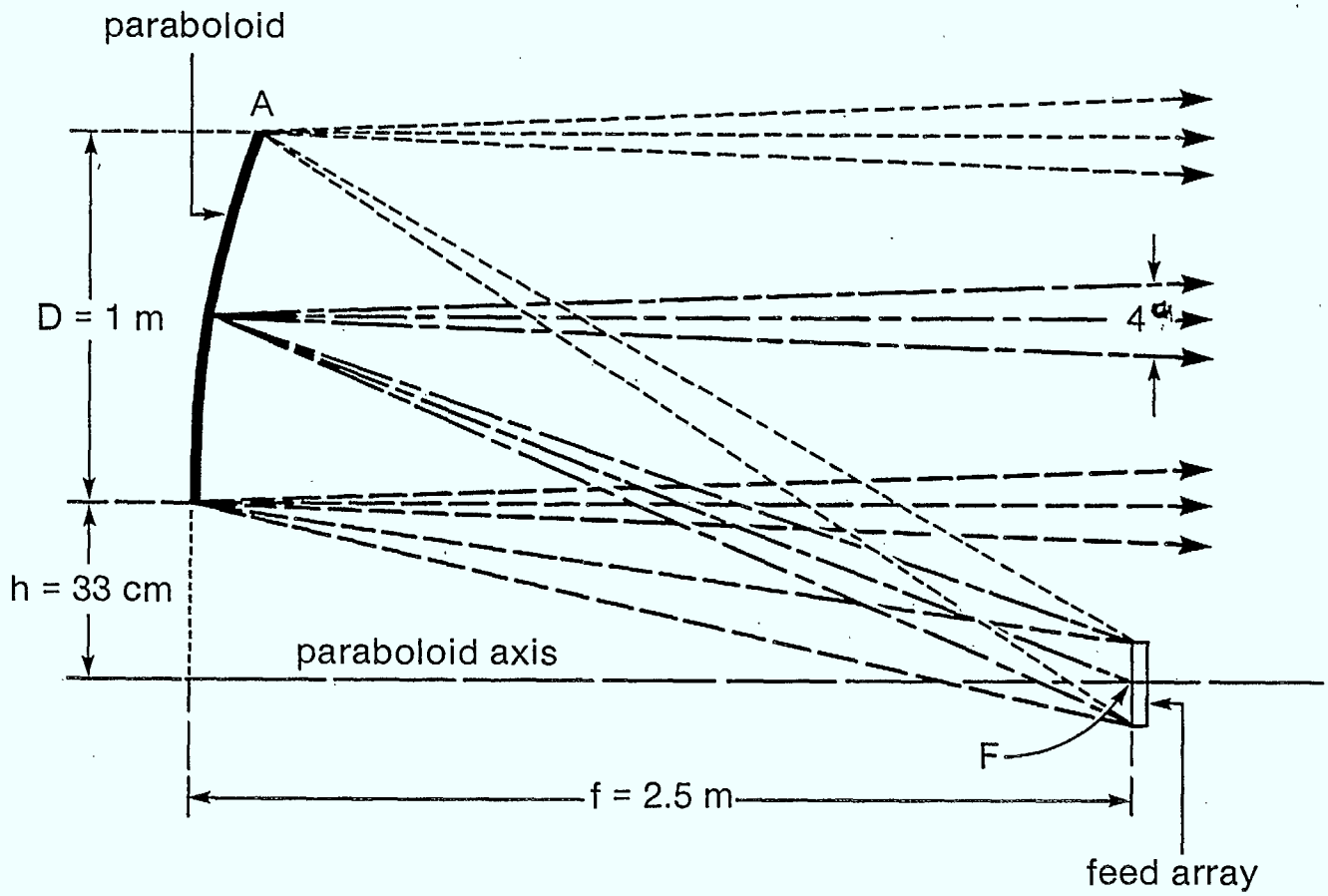

Fig. 5. Offset paraboloid reflector antenna for multibeam operation.
D/f = 2.5, h = D/3, steering angle $\alpha = \pm 2°$,
frequency = 21.7 GHz.

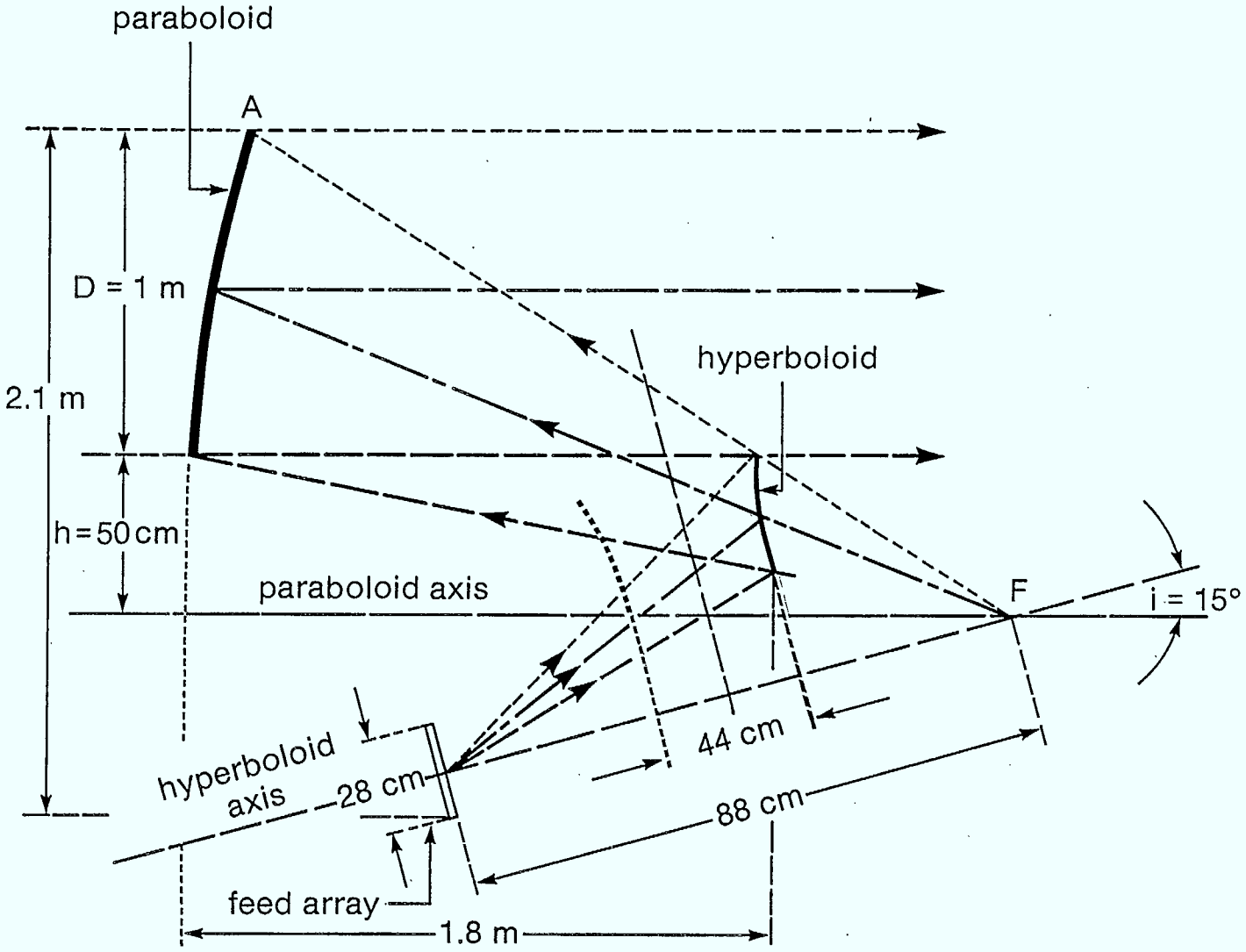

Fig. 6. Multibeam antenna with auxiliary reflector.
D/f = 2.5, D = 1 m, h = D/3,
frequency = 21.7 GHz.

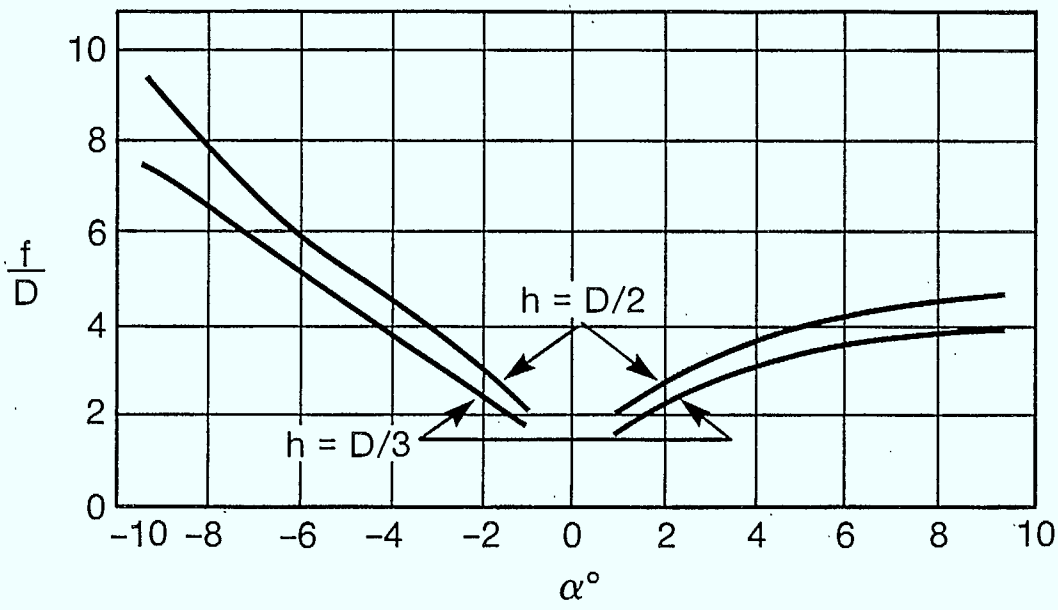

Fig. 7. Plot of maximum steering angle against f/D in multibeam offset paraboloid reflector

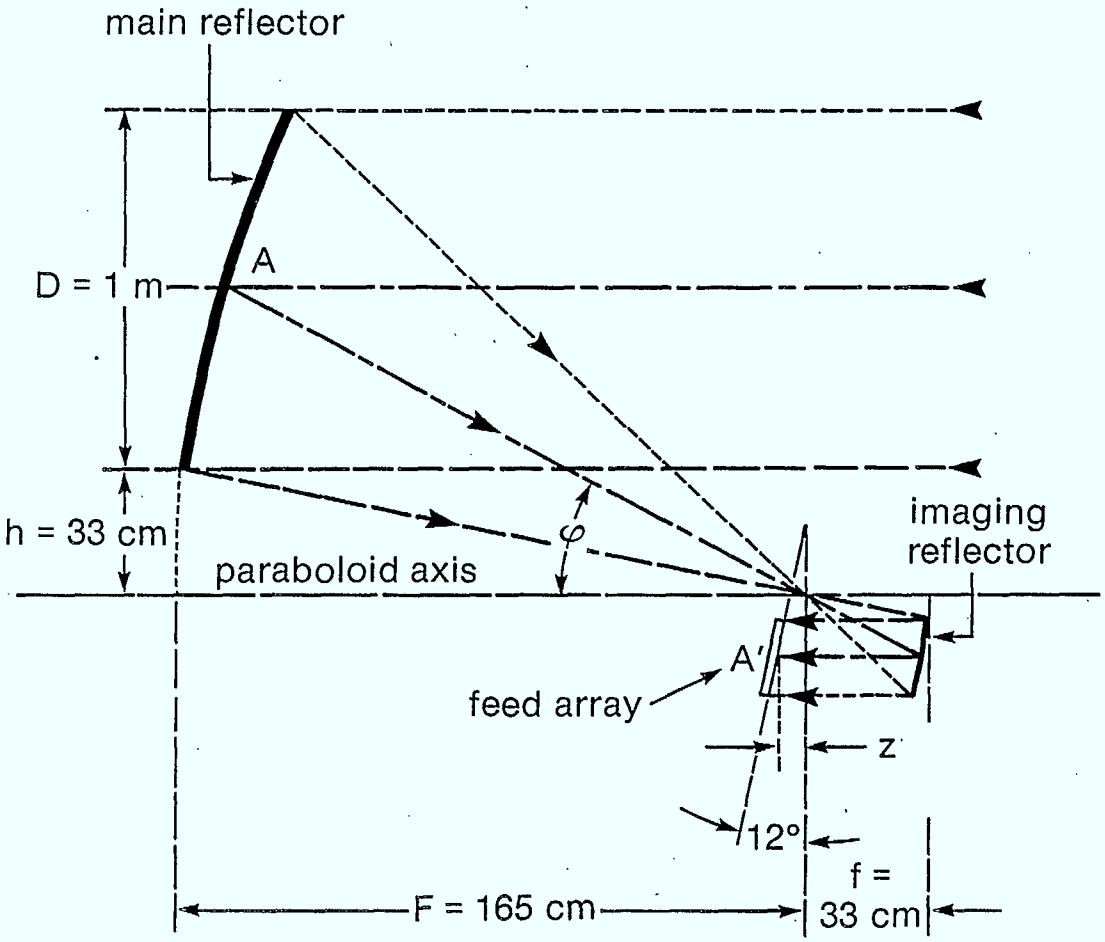

Fig. 8. Phased array antenna system.
F/D = 1.65, D = 1 m, h/D = 1/3, F/f = 5,
steering angle $\alpha = \pm 2°$, frequency = 44.5 GHz.

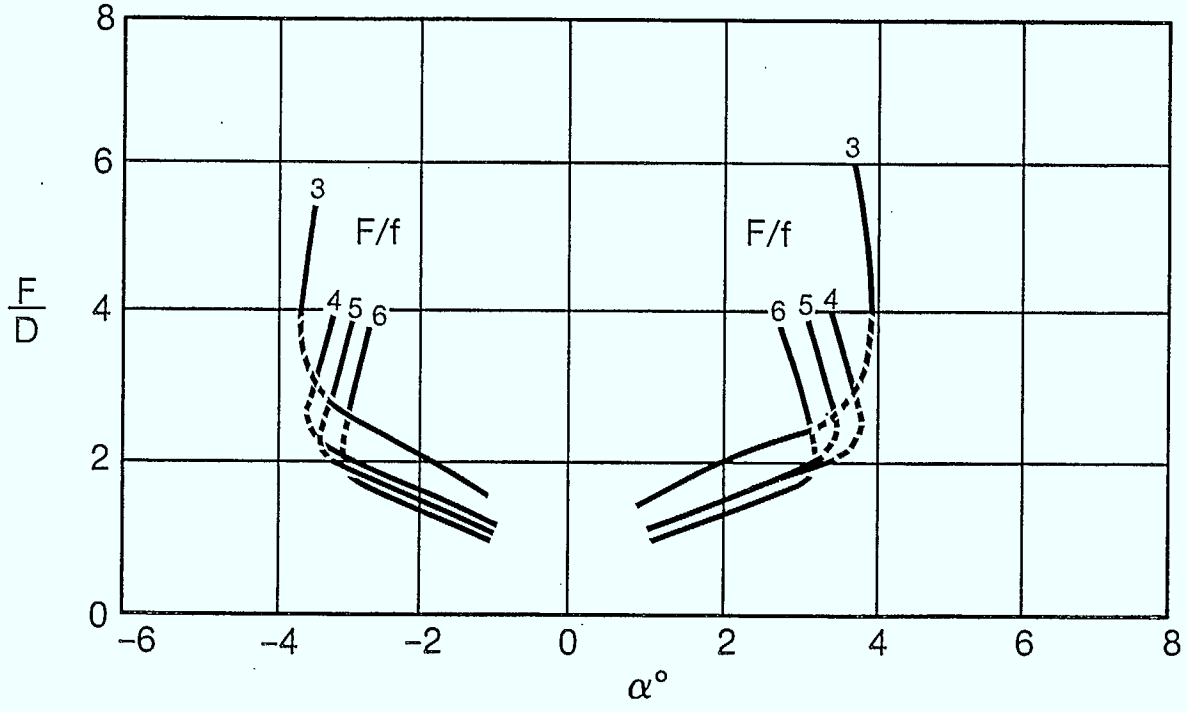

Fig. 9. Plot of F/D ratio vs. steering angle α.

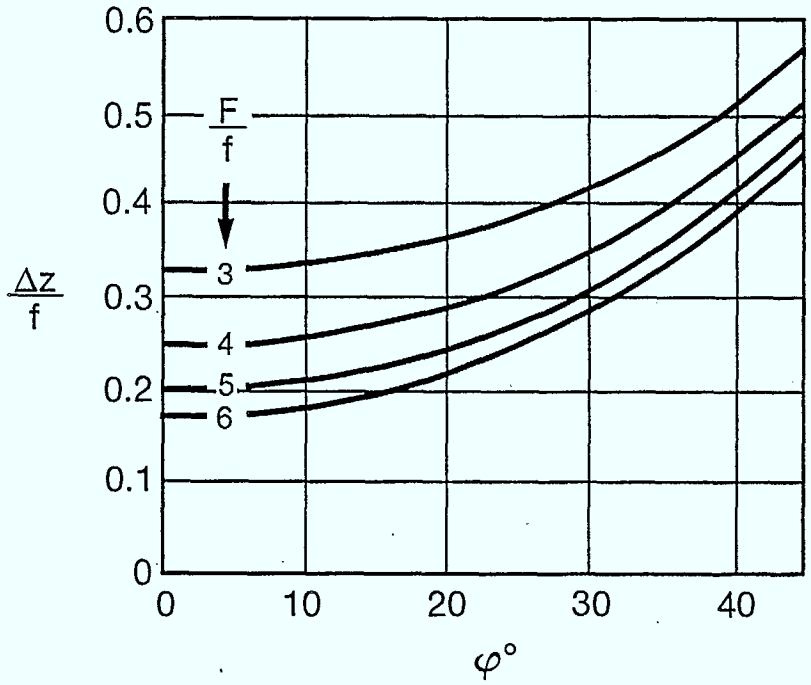

Fig. 10. Main reflector image deviation from focal plane, Δ. F = focal length of main reflector, f = focal length of imaging reflector, φ = polar angle of point imaged.

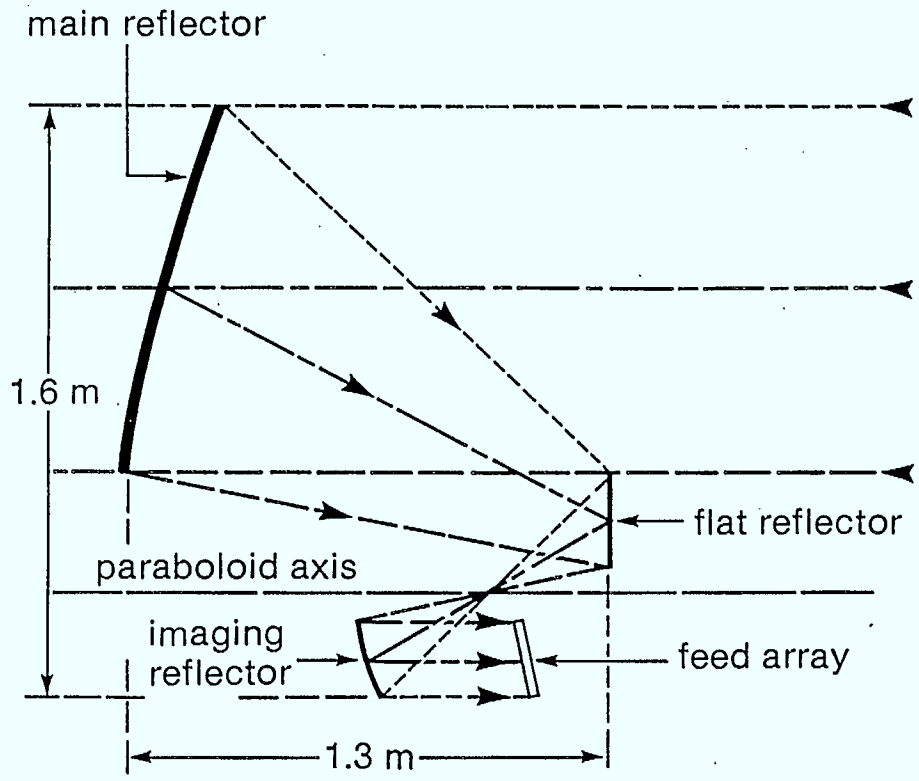

Fig. 11. Phased array reflector antenna with folded beam.

D = 1 m, F/D = 1.65, F/f = 5,
steering angle $\alpha = \pm 2°$, frequency = 44.5 GHz.

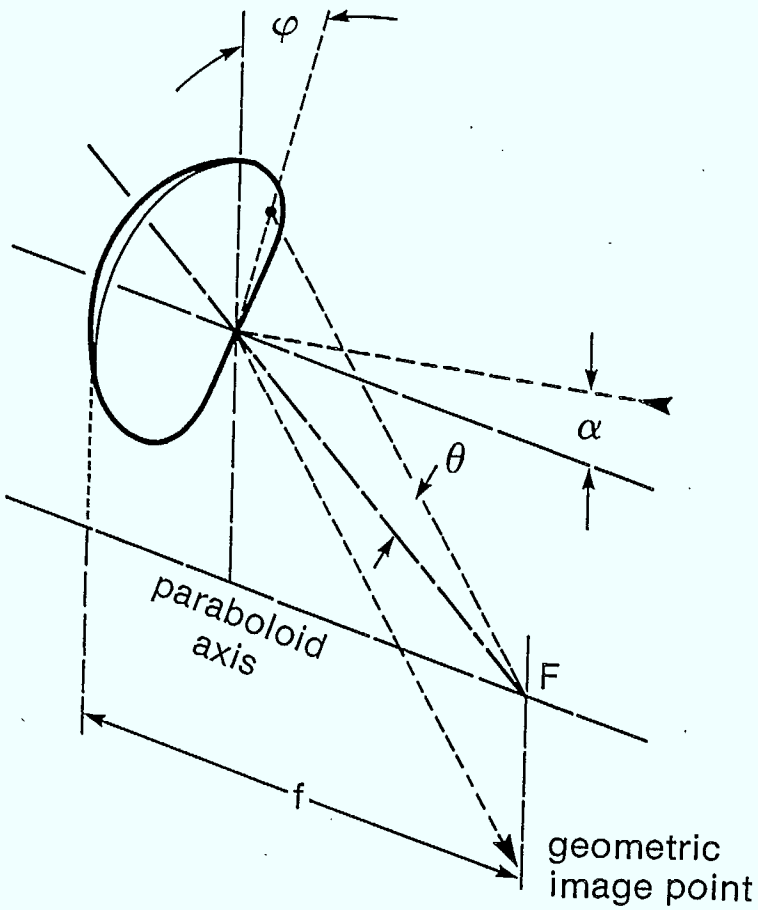

Fig. 12. Polar coordinate system for computer simulation.

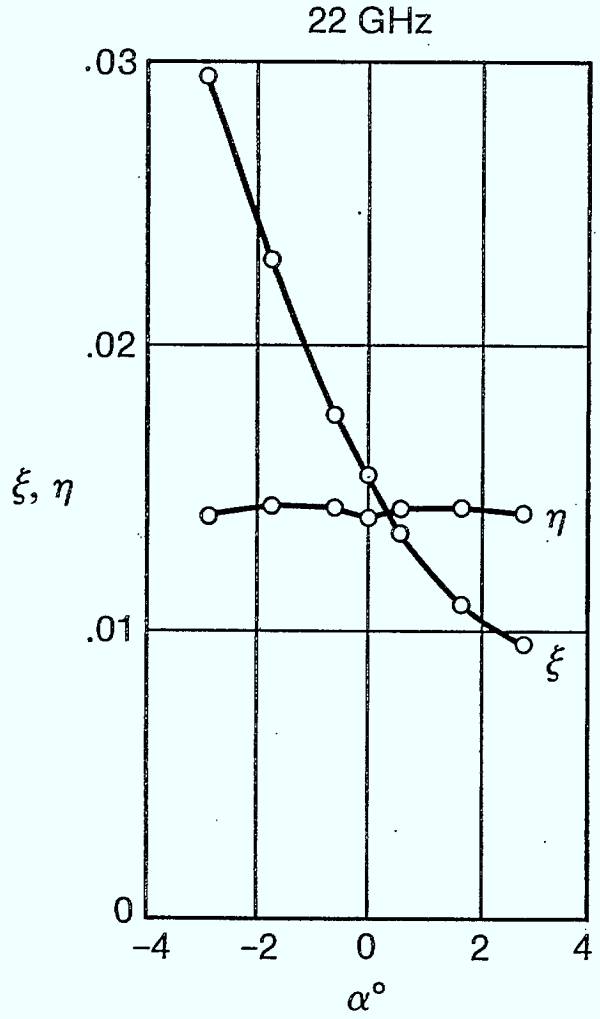

Meridional (ξ) and transverse (η) beamwidths of focal plane pattern.

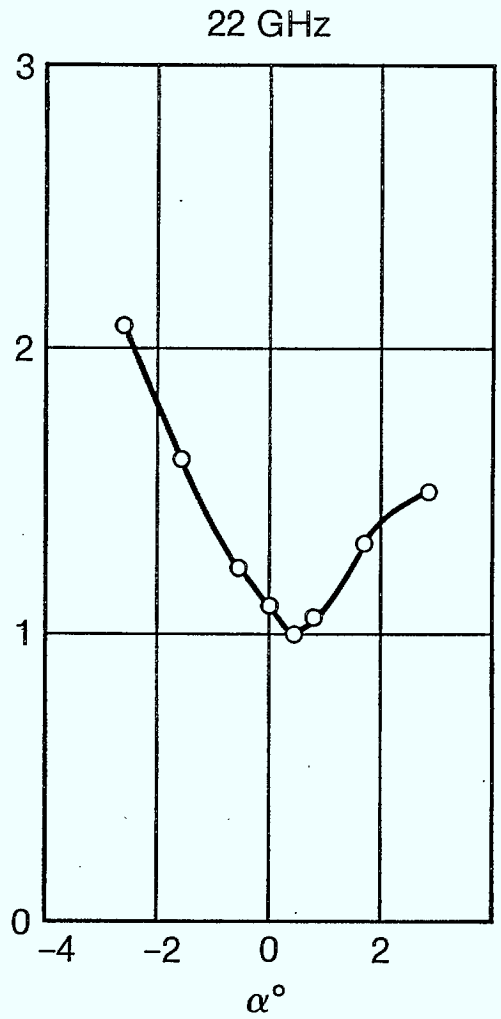

Eccentricity of focal plane pattern.

Fig. 13.

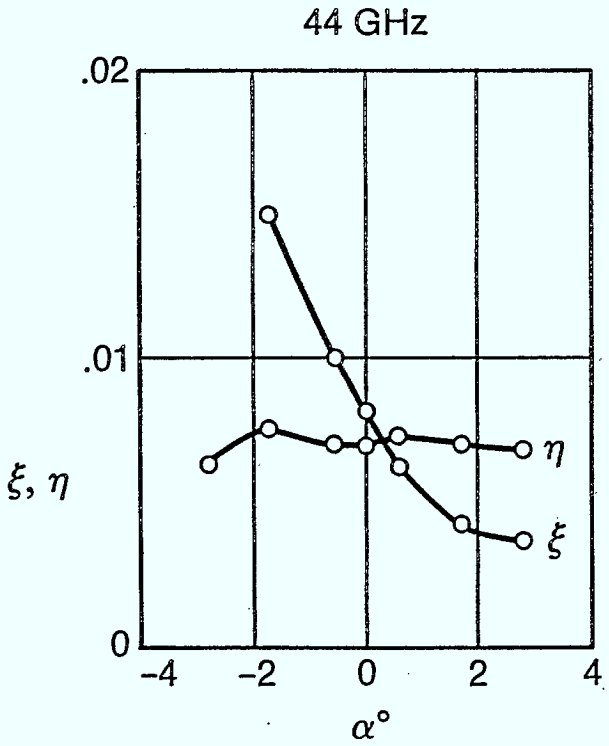

Meridional (ξ) and transverse (η) beamwidths of focal plane pattern.

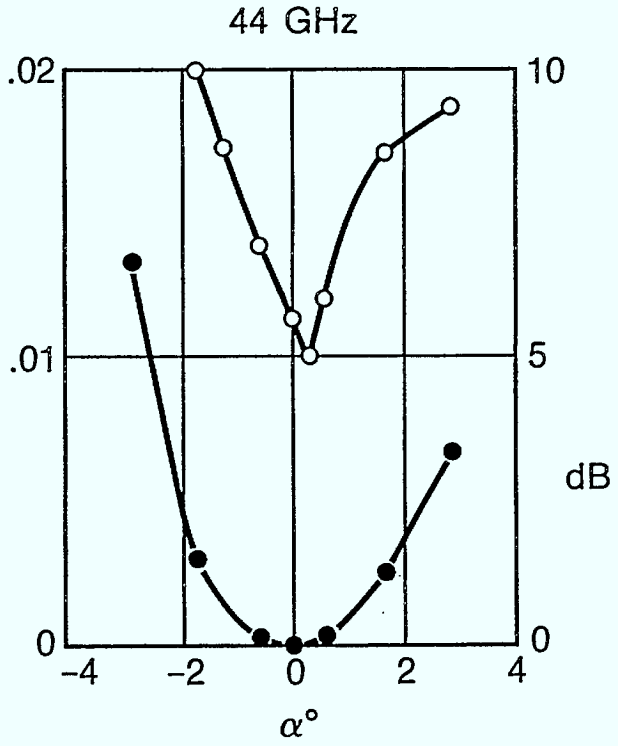

Eccentricity (o) and relative sidelobe levels (●) of focal plane pattern.

Fig. 14.

9.

Appendix

This Appendix contains diagrams of calculated focal plane patterns of reflector antenna described below (see Figure 4):

Shape: paraboloid

Diameter D: 1 m

Offset h: 0.5 m

f/D ratio: 2.5

Operating conditions and diagram designations:

DIAGRAM TYPE	STEERING ANGLE	DIAGRAM No. at 22 GHz	DIAGRAM No. at 44 GHz
Shaded pattern	−1.7 °	A1	B1
	0 °	A2	B2
	+1.7 °	A3	B3
Meridional beam cross-section	−1.7 °	A4	B4
	0 °	A5	B5
	+1.7 °	A6	B6
Transverse beam cross-section	−1.7 °	A7	B7
	0 °	A8	B8
	+1.7 °	A9	B9

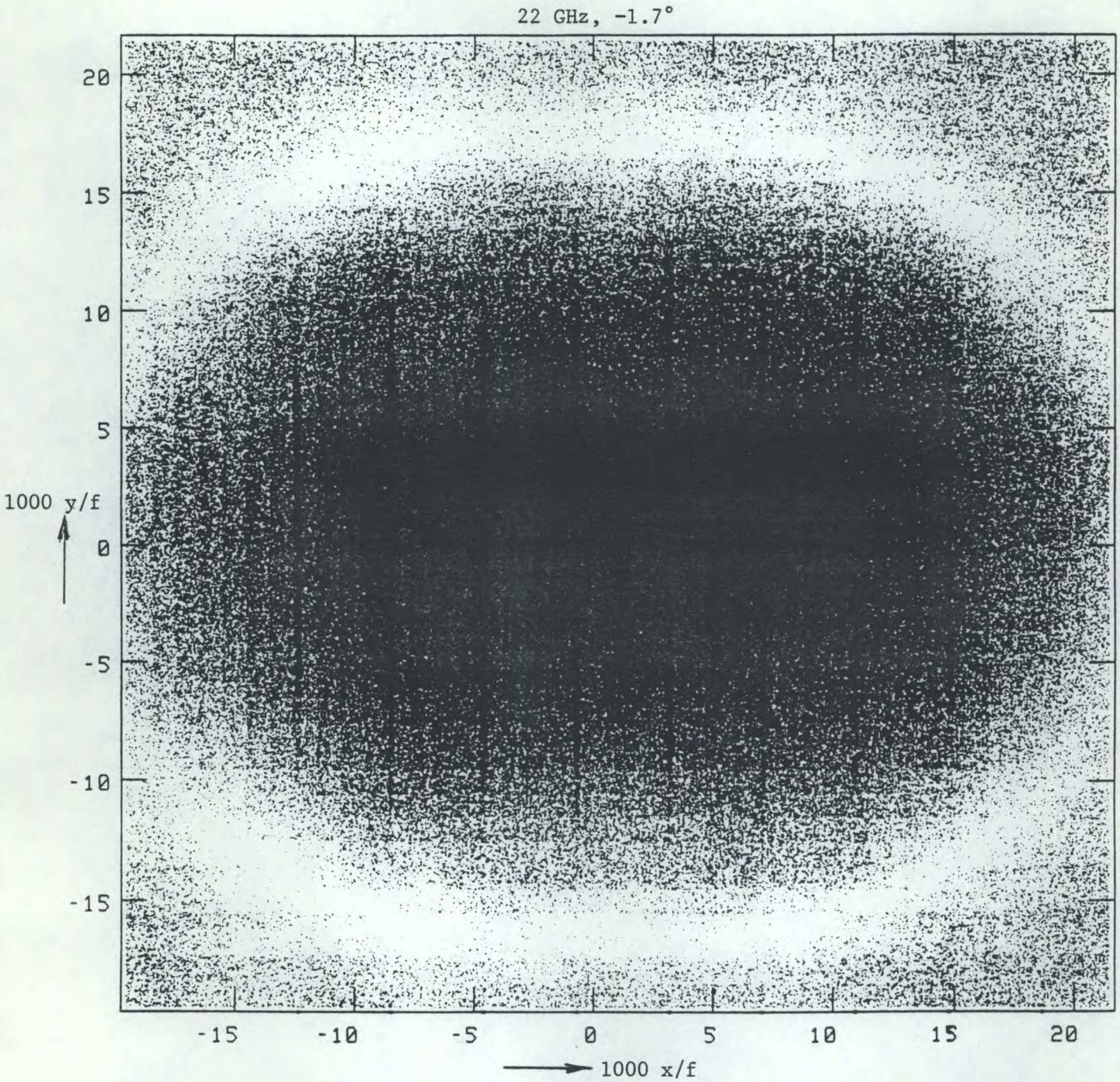

A1

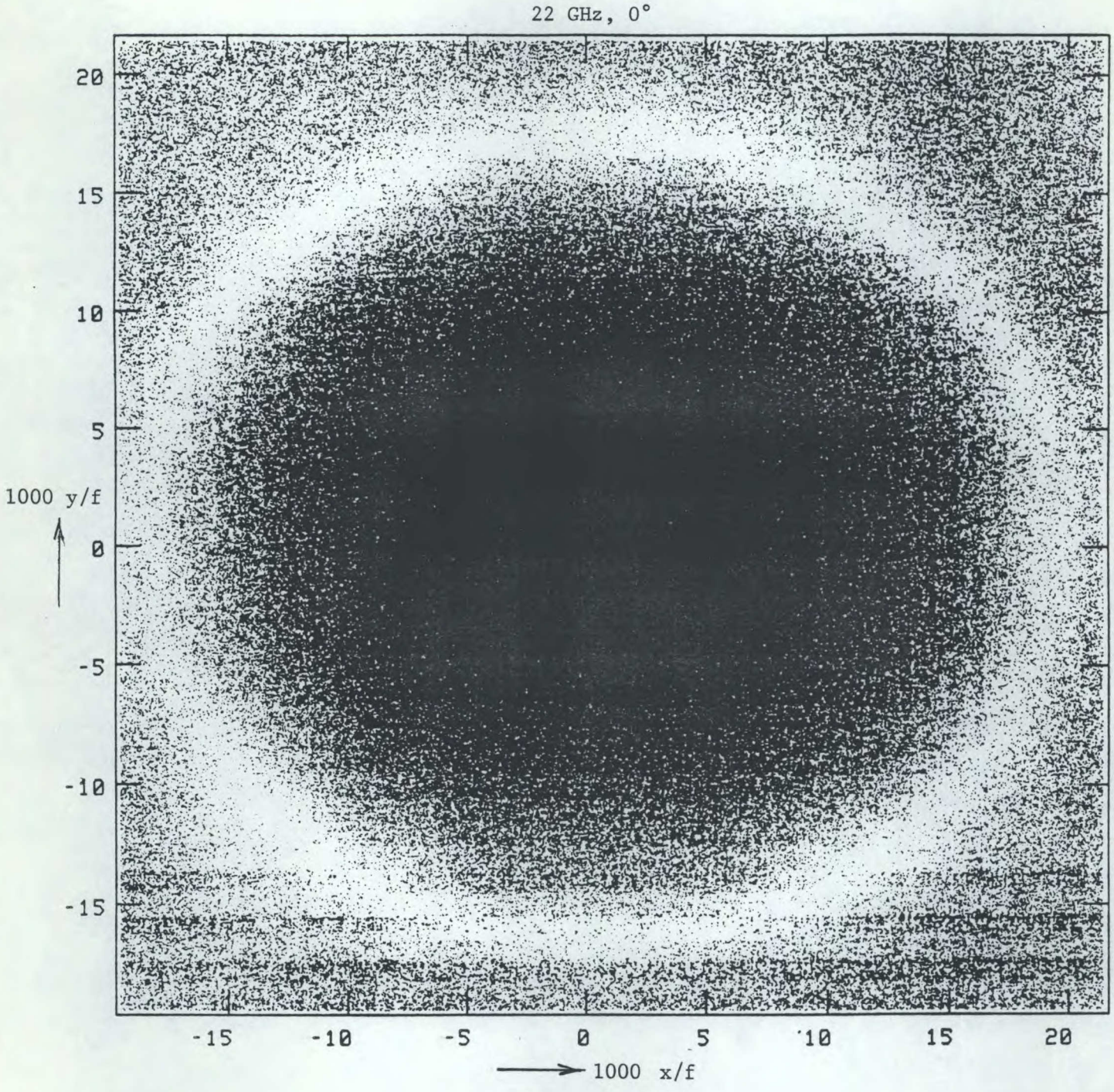

A2

22 GHz, 1.7°

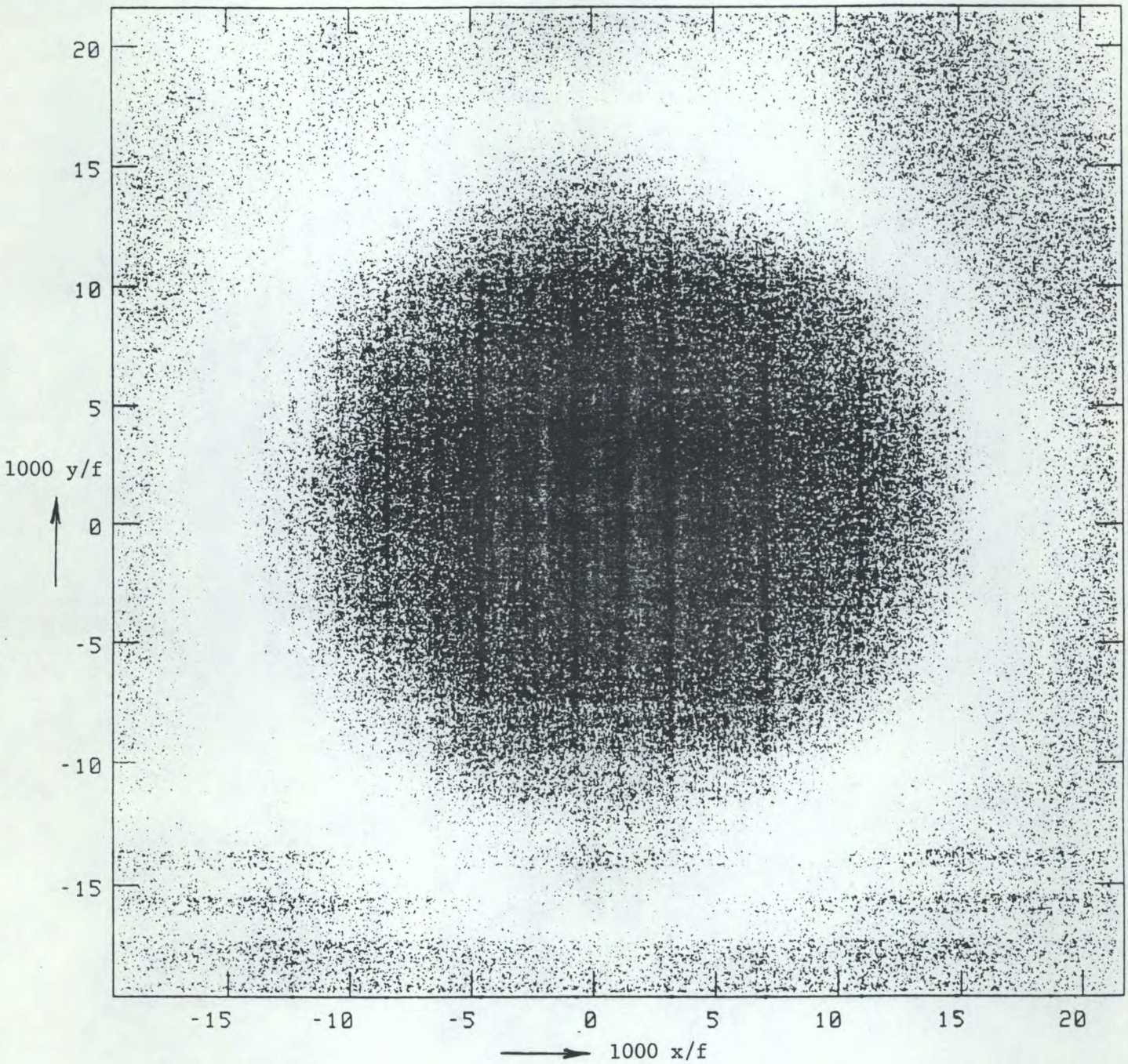

A3

22 GHz

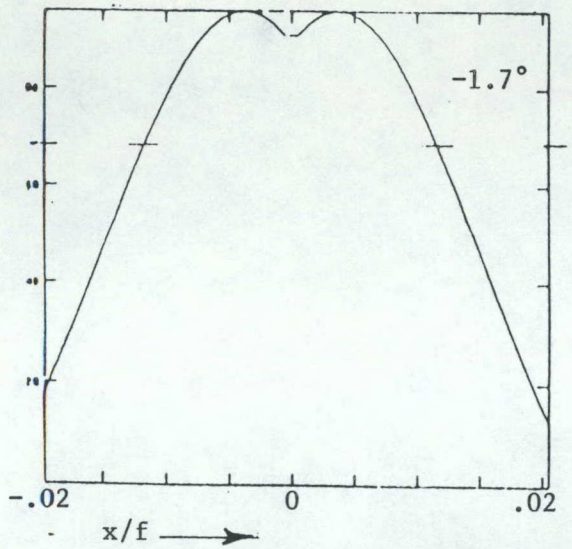

A4

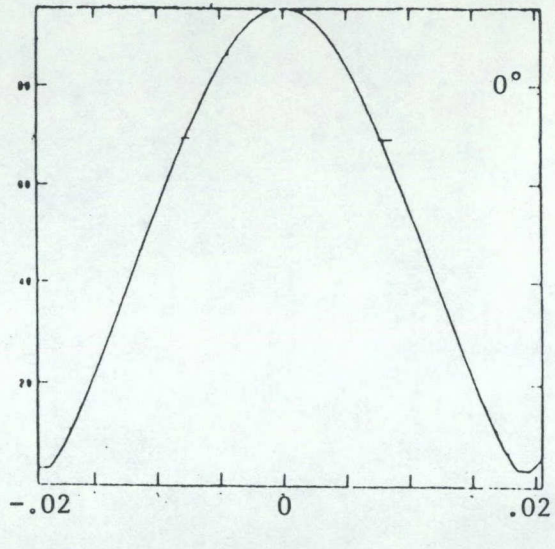

A5

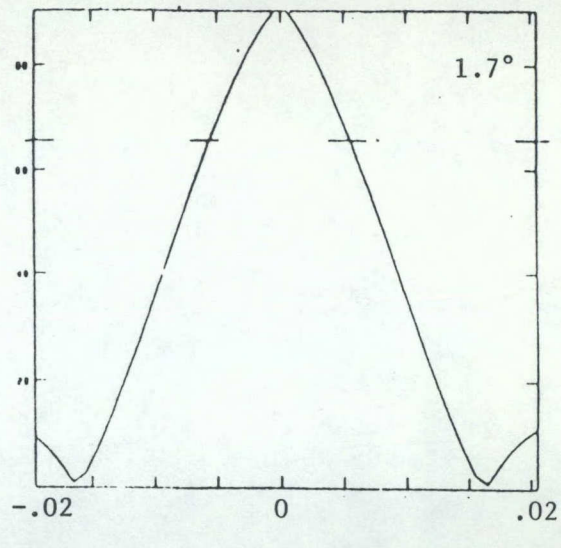

A6

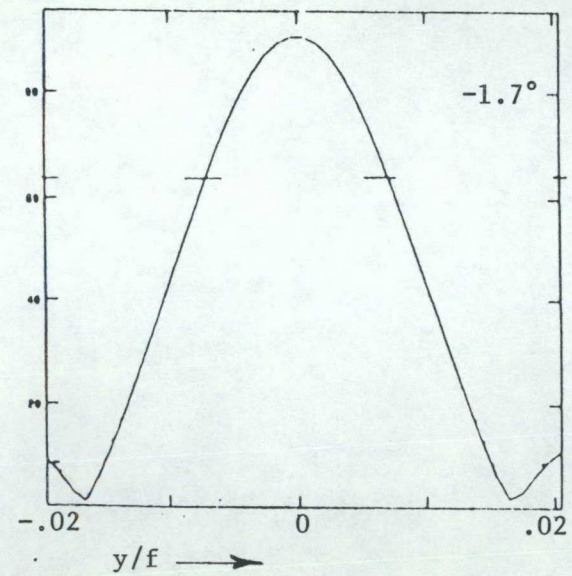

A7

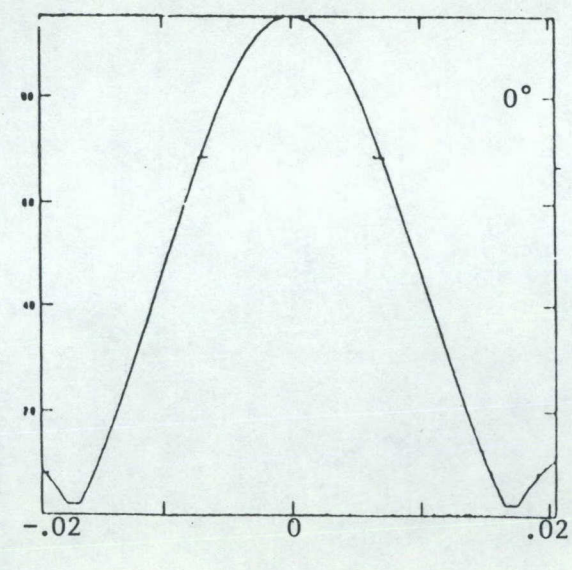

A8

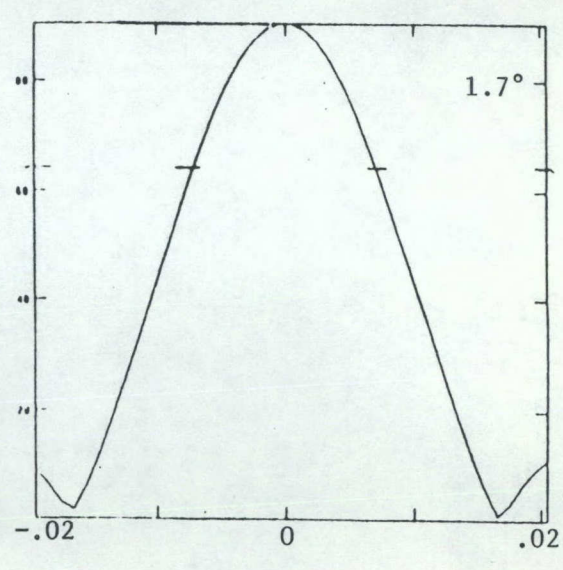

A9

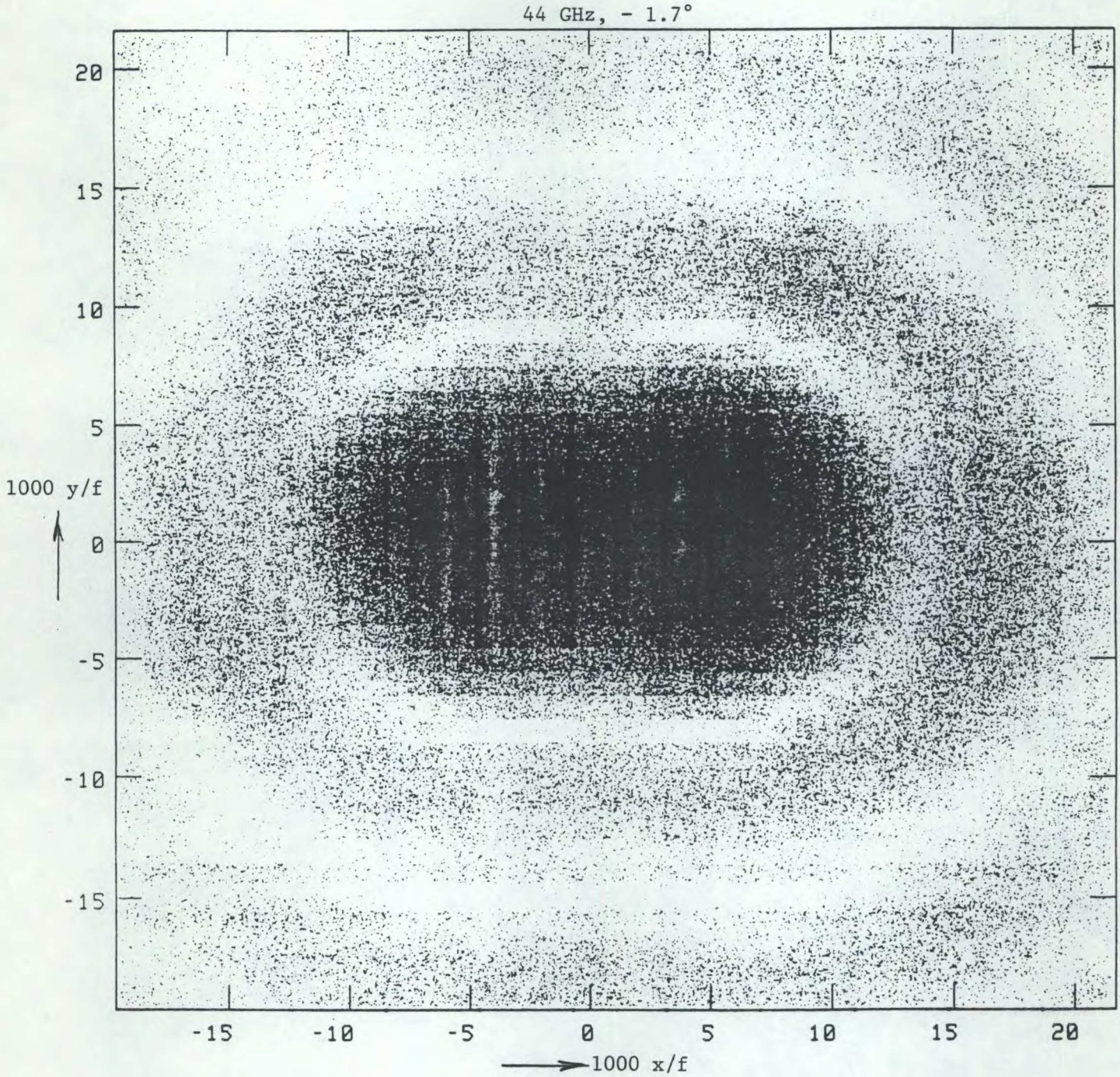

B1

44 GHz, 0°

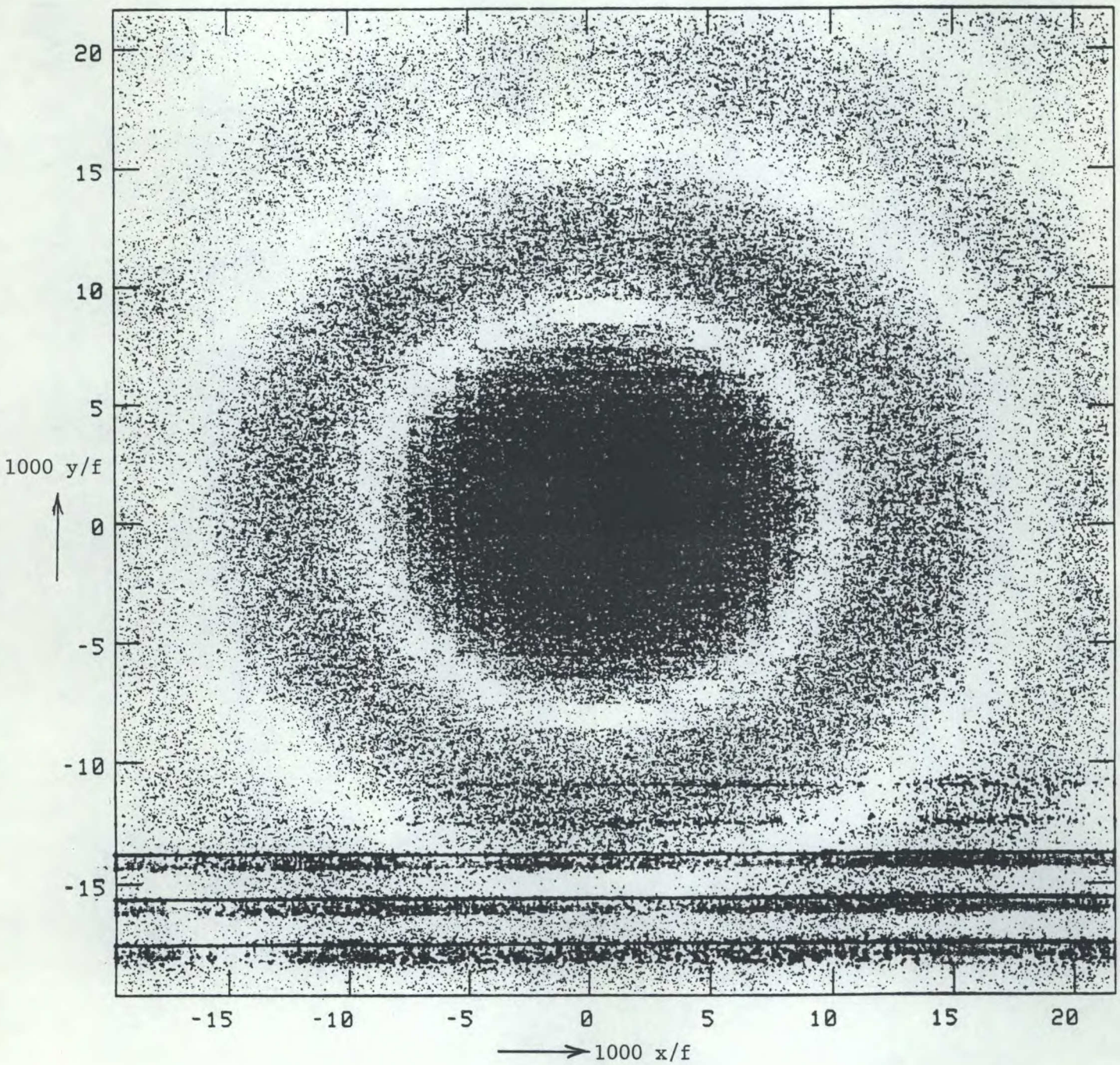

B2

44 GHz, 1.7°

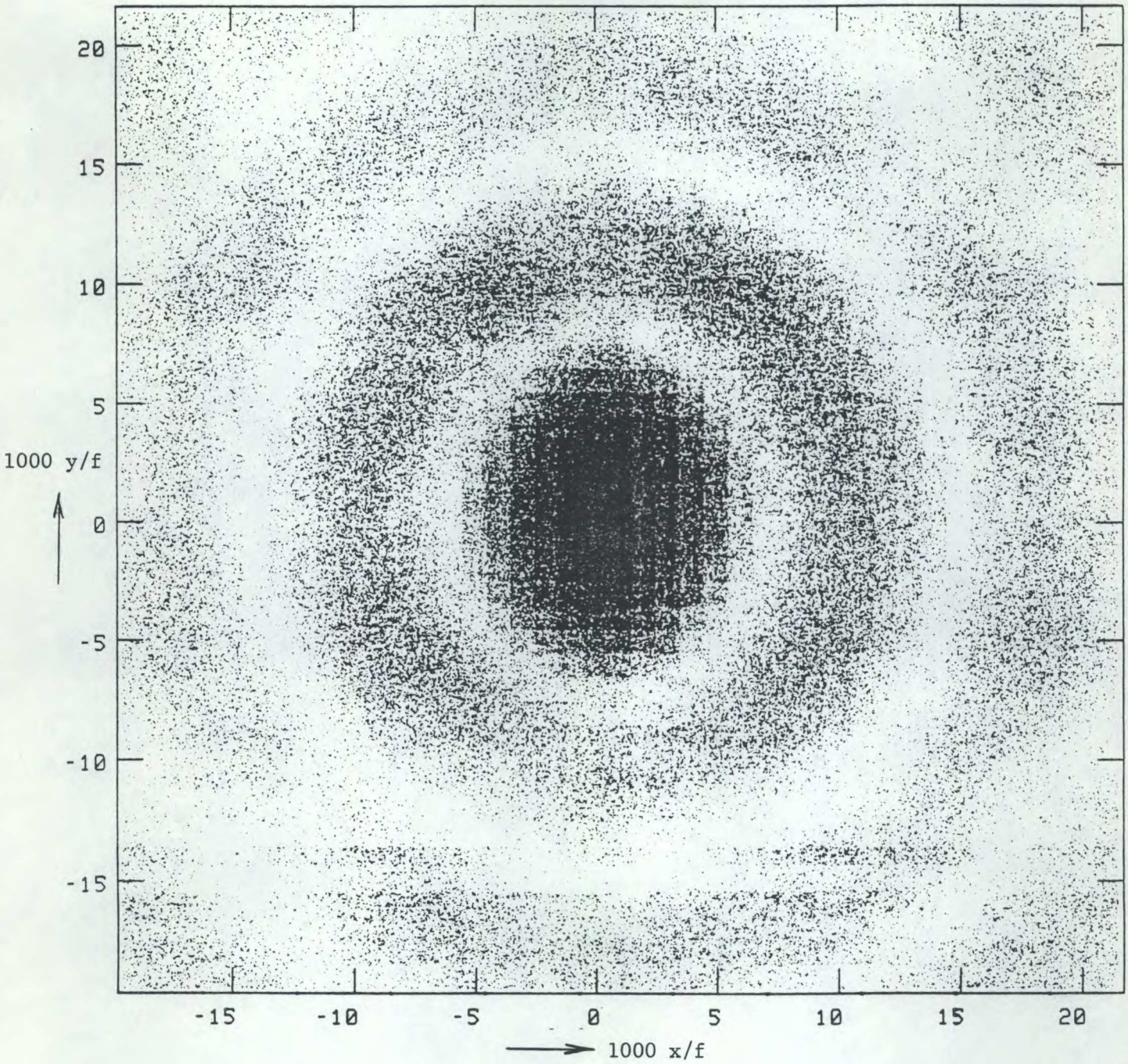

B3

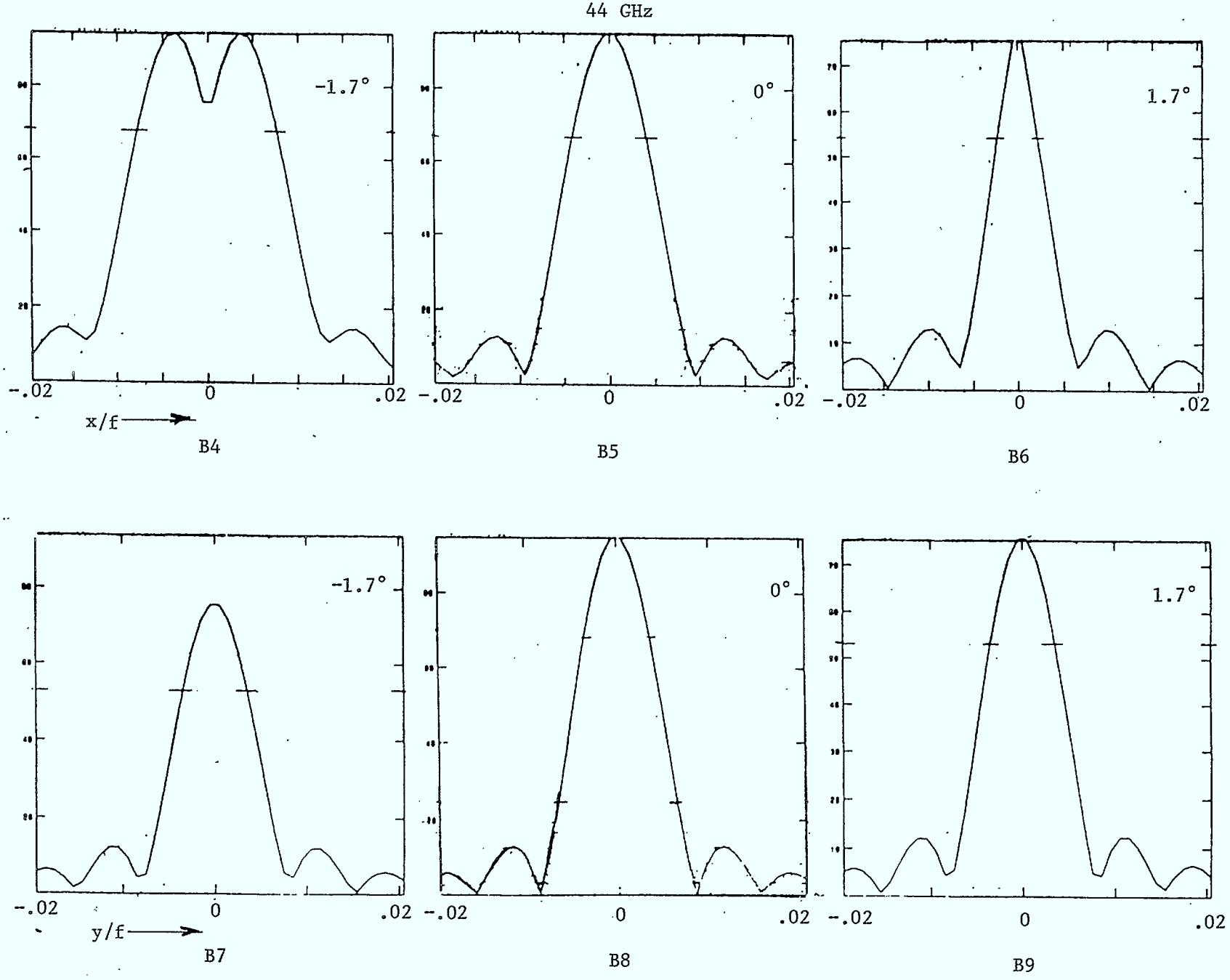
44 GHz
-1.7°
0°
1.7°
-.02
0
.02
x/f
B4
B5
B6
-1.7°
0°
1.7°
-.02
0
.02
y/f
B7
B8
B9

Chapter 3

LENS ANTENNAS

K.G. Balmain

1.

Basic Formulas for Scanning Lens Antennas.

A multiple beam, single-lens antenna is depicted in Figure 1, and Figure 2 shows how an offset feed can produce a scanned beam by generating fields of constant phase in a tilted aperture plane or equivalently, fields of linear transverse phase variation in a plane normal the axis. The basic design concept used here is that of Rotman [1] and Shinn [2], which involves a thin lens with a spherical outer surface of radius R and a stepped (zoned) inner surface. The focal length F is made equal to R to satisfy the Abbe sine condition, thereby minimizing coma aberration (cubic transverse phase variation) as the feed horn is moved away from the focus along the focal arc. Spherical aberration (quadratic phase variation) in the scan plane can be eliminated by the use of a focal arc of constant length $l = F$; spherical aberration in the orthogonal plane can be eliminated by the use of the focal arc of length $l = F \cos^2 \alpha$, where α is the scan angle. These different focal loci indicate astigmatism. Rotman [1] and Cheston and Shinn [3] recommend a compromise focal arc of length

$$l = \tfrac{1}{2} F (1 + \cos^2 \alpha) \tag{1}$$

which should be useful although it does not completely eliminate the effects of astigmatism. Of course, aberrations will be present due to scattering from the steps between lens zones, due to edge diffraction, and due to the fact that the lens is not absolutely thin.

The feed-horn aperture diameter d imposes a fundamental limitation on the set of available scan angles when scanning is achieved by switching between any pair of horns in fixed positions. The closest centre-to-centre horn spacing is d and so the smallest off-axis scan angle is given by

$$\tan \alpha = d/F$$

or, for small angles,

$$\alpha = d/F \tag{2}$$

The feed horn beamwidth θ_f for a given beam-edge criterion (or relative lens edge illumination level I, in dB) can be expressed as

$$\theta_f(I) = K_f(I)\ \lambda/d \tag{3}$$

If D is the lens diameter and if the lens edges subtend the total angle θ_f at the feed horn, then $\tan(\theta_f/2) = D/2F$, or for small angles,

$$\theta_f = D/F \tag{4}$$

Finally the width of the main beam formed by the lens aperture can be expressed as follows for a particular choice of beam-edge criterion C (dB) and lens edge illumination I (dB):

$$\theta_a(C,I) = K_a(C,I)\ \lambda/D \tag{5}$$

Elimination of θ_f from (3) and (4) gives

$$\frac{d}{F} = K_f(I)\ \frac{\lambda}{D} \tag{6}$$

Taking the scan angle α equal to the beamwidth $\theta_a\ (C,I)$ as defined by the beam-edge criterion C and elimination of θ_a from (2) and (5) gives

$$\frac{d}{F} = K_a(C,I)\ \frac{\lambda}{D} \tag{7}$$

Examination of the literature ([4], [5], [6]) suggests that a useful empirical approximation for K_a may be

$$K_a\ (C,I) = \left[1 + \frac{I}{59.0}\right] K_a(C,O) \tag{8}$$

Note that $K_a\ (C,O)$ is the value of $K_a\ (C,I)$ appropriate for a uniformly illuminated circular aperture. Taking the ratio of (6) and (8) produces the final result

$$K_a(C,O) = K_f(I)\,/\,(1 + I/59.0) \tag{9}$$

This suggests the following trial design procedure: 1) Establish the feed horn type and the lens edge illumination I, giving $K_f\ (I)$; 2) Calculate $K_a\ (C,O)$; 3) From a table of values of $K_a\ (C,O)$ estimate the beam-edge criterion C (in dB) which is also the scanned-beam cross-over level. Such a table can be deduced readily from uniform circular aperture theory and is as follows:

C	$K_a(C,O)$
3 dB	59.0 degrees
4	67.3
5	74.4
6	80.7
7	86.2
8	91.1
9	95.6
10	99.7

As for the horns to be considered as candidates in a scanning application, the main problem is finding a sufficiently complete and accurate tabulation of their radiation patterns. Consider for example the set of scalar (corrugated) circular horns which have been optimized for maximum gain [7]. These horns have very regular patterns which can be described by the following table:

I	$K_f(I)$
3 dB	100 degrees
4	120
5	137
6	153
7	168
8	183
9	196
10	208

As a trial design, select an optimum scalar horn to provide a relative lens edge illumination I of 3 dB down from the lens centre. This means $K_f(3) = 100\ ^\circ$ and $K_a\ (C,O) = 100/(1 + 3/59.0) = 95.2\ ^\circ$ From the appropriate table, the scanned beam crossover level C is about 9 dB down from the beam maximum. Such a crossover level would be unsatisfactory in most applications which means that optimum scalar horns have apertures that are too large for use in multiple beam antennas.

Very long scalar horns could be considered but the currently available data is sketchy [7]. It does indicate for a $5\ ^\circ$ half flare angle that $K_f(3) = 74.0\ ^\circ$ which means that

$K_a\ (C,O) = 74.0\ /\ (1 + 3/59.0) = 70.4$ °. From the appropriate table, $C = 4.4dB$ which is an acceptable crossover although the 3 dB edge illumination suggests excessive spillover. This data is incomplete but it does indicate that long scalar (corrugated) horns should be given careful consideration for multiple-beam antennas. Data on long non-corrugated horns [8] suggests that in the limit a 3 dB crossover could be obtained with a 3 dB lens edge illumination, and that in general the limit $C = I$ probably could be approached in general, with sufficient attention being given to horn design. This postulate can be checked by examining actual designs of multiple-beam antennas. The paper of Dion and Ricardi [9] refers to an X-band waveguide lens design with a lens edge illumination of $-5.2\ dB$ and a main beam crossover of $-4.5\ dB$. The report of Major and Devan [10] describes a 44 GHz waveguide lens design using short, non-corrugated horns, in which measured horn radiation patterns show an edge illumination of $-3\ dB$ (horn H-plane) and $-5\ dB$ (horn E-plane) for an average edge illumination of about $-4\ dB$; main beam crossovers are in the range of $-4.8\ dB$ to $-5.0\ dB$. In summary, it can be said that, for the two designs described, the edge illumination and the main beam crossover differ by no more than one dB, a result which supports the postulate that these quantities are constrained to be approximately equal, independent of focal length, frequency, horn diameter and lens diameter. This means that, for a multi-beam antenna, closer beam spacing must be accompanied by 1) higher sidelobe level due to a more nearly uniform aperture illumination, and 2) higher spillover due to higher edge illumination. If the spillover resulted in excessive radiation toward the earth, it could be controlled by wrapping the lens and the feed array with an absorbing conical shroud.

2.

Design of Zoned Lenses.

Zoning or stepping one side of a lens surface greatly reduces the weight of the lens and reduces its thickness to the point where thin-lens concepts are applicable. However, the properties of a stepped lens are frequency-dependent because each step changes the optical path by one wavelength at the design frequency. Relative to the path through the centre of the lens, the path through the lens edges will exhibit a phase error at any frequency other than the design frequency. It is well known [1] (and can be shown easily) that an allowable phase error of no more than $\pm\ \pi/4$ radians produces a side-to-side percentage bandwidth of $25/N$ where N is the number of steps. Thus a five percent bandwidth requirement implies no more than five steps; a six-step design; while giving 4.2 percent bandwidth by this measure, still provides a reasonable approximation to a five percent bandwidth as shown by Rotman [1], so in this report the design target will be six steps.

A basic design equation as given by Shinn [2] is

$$\cos \gamma_n = \cos \gamma_o + n\frac{\lambda}{R}\left[1-\frac{t_o \cos \gamma_o}{\mu^2 R \cos \beta_o}\right] \tag{8}$$

in which

$R = F$

α_n is the angle of the nth step as seen from the focus and measured with respect to the axis.

γ_o is the angle of the lens edge.

t_o is the minimum lens thickness.

μ is the refractive index of the lens material.

β_o is given by $\mu \sin \beta_o = \sin \gamma_o$.

Equation (8) establishes the locations and number of the steps. All the designs presented in this report have the minimum number of steps for the given parameters. In other words, for each design, R is adjusted so that a slight decrease in R would cause the formation of a new step in the form of a hole at the centre of the lens. Therefore, the thickness of the lens at its centre is given by

$$t_c = t_o + \frac{\lambda_o}{\mu-1} \tag{9}$$

In addition, the overall thickness of the lens is given by

$$T = R(1-\cos \gamma_o) \tag{10}$$

The minimum lens thickness t_o is assigned the value 7 mm, only a trifle greater than the 1/4" value used by Rotman [1]. The refractive index μ is assigned the value 1.594 for Rexolite 1422.

Table 1 summarizes the designs worked out for a 44.5 GHz satellite antenna. The six-step, fully-zoned design is 2.7 m long, probably too long for satellite use. Reduction by only two steps more than doubles the thickness at centre, increasing the weight and perhaps reducing the scanning capability by making the overall shape of the lens less like a thin spherical shell; however, the length is still a large 2.1 m. Reduction by six steps produces a design with 1.5 m overall length but the central-zone thickness is almost five times the fully-zoned value. These results suggest that probably it would be difficult to make a good one metre diameter multiple-beam lens for operation at 44.5 GHz.

Table 2 gives satellite antenna designs for 20.7 GHz and it can be seen that for the same focal length, the number of steps has been reduced approximately in proportion to the reduction in frequency. The fully-zoned, six-step design has a focal length of 1.3 m and so is reasonably compact. The weight can be estimated very roughly by starting with Rotman's 8.6 lb for a 23.5" 44.5 GHz design and converting to a one metre diameter 20.7 GHz design by multiplying by the area ratio and by the ratio of centre-zone thickness. This leads to a lens weight estimate of 41 lb or 19 kg.

Laboratory lens designs are constrained by the need to keep the region of transition from near to far fields ($2D^2/\lambda$) within the confines of the available test space. A 204 mm diameter cylinder of cross-linked polystyrene equivalent to Rexolite 1422 has been acquired to meet the aperture-size requirement. At 20.7 GHz such a small diameter would produce typically a one-step design which would not have the required thin, spherical shape and would have a bandwidth too wide for easy experimental verification. At 44.5 GHz the situation is much better and three trial designs are shown in Table 3. All three designs appears useful and all could be made and tested to provide a suitable range of experimental data.

3.

Environmental Effects.

3.1.

Thermal expansion.

The thermal expansion coefficient per $^\circ F$ for Rexolite 1422 is in the range of $6.0-7.6\times10^{-5}$. Rexolite 1422 is a form of cross-linked polystyrene, and polystyrene has coefficients in the range $6-8\times10^{-5}$. For comparison, other expansion coefficients per $^\circ F$ are: Teflon 5.5×10^{-5}; Aluminum 1.3×10^{-5}; ceramics $\approx 8\times10^{-6}$; Pyrex 5×10^{-6}; quartz 5.7×10^{-7}. Rexolite 1422 clearly has a high thermal expansion coefficient. Taking the value 7×10^{-5} as typical, a one metre diameter lens would expand 7 mm for a 100 °F increase in temperature which would be possible as a satellite component moves from the satellite shadow into the sunlight. This means that one could expect expansions of the order of one wavelength at 44.5 GHz or a half wavelength at 20.7 GHz, and therefore thermal expansion of the lens could be important from the point of view of beam control.

Even more important might be the thermal stress and possible cracking of the zoned lens as a shadow-sunlight boundary moves across it. Thin aluminized layers on the lens surfaces

would reduce temperature differentials in the material but would also attenuate the signal. A better solution would be a thermal lens cover spaced a short distance away from the lens and consisting of, say, 50 μm of Kapton which could be very lightly metallized on its back surface to increase is reflectivity.

3.2.

Spacecraft charging and arc discharging.

Little is known about this phenomenon when it occurs on thick dielectrics such as lenses. If experience in laboratory tests on thinner materials is any guide then one could expect the occasional occurrence of surface flashover arcs with accompanying microscopic rupture of the surface to a depth of several micrometres. This would probably not affect the lens radiation pattern significantly but it could cause significant electromagnetic interference. Furthermore, it might trigger cracking of the lens in the presence of thermal stress. The solution to this problem would appear to be the thin Kapton cover already proposed as a thermal shield. Metallization of its front and/or back surface might reduce charge accumulation effects on the cover. Kapton 50 μm thick would stop electrons up to about 100 keV and so should reduce very greatly the probability of discharges occurring on the lens.

4.

Loss of Beam Due to Electronic Component Failure.

It has been pointed out by Major and Devan [10] that the 37-beam 44 GHz receiving antenna system studied by them would have only a two percent probability of surviving at full capability for one year with no redundancy in the electronic circuits. For their antenna with its -5 dB crossover, loss of one beam could result in a signal loss of 33 dB if the signals from the two adjacent beams were added. Such a high signal loss would probably mean loss of communication, so that the problem would have to be solved by either redundancy or soft failure in the electronic circuits associated with beam formation.

The loss-of-beam problem could also be addressed by closer beam spacing. In particular, if the beam crossover level were raised to -3 dB, then removal of one beam would leave the crossover between the remaining adjacent beams at a point closer to boresight than the first null. This crossover would be approximately at -20 dB. Adding 6 dB for field addition at crossover and subtracting 3 dB for equal power division between two beams gives a signal loss of at least 17 dB. This calculation was done for an edge illumination of -6 dB and so it is somewhat optimistic. Nevertheless, it can be estimated that, with -3 dB beam crossover and signal

reliability margins of the order of 20 dB, communications with the loss of one beam could probably be maintained by in-phase combining of the remaining adjacent beams. However, lens edge illumination of the order of -3 dB would be required, with the corresponding high spillover level.

5.

Plan for the Next Interval

Zoned lenses will be constructed and tested in the laboratory at frequencies in the vicinity of 44 GHz. A ray-tracing program will be developed and validated by the laboratory measurements, with particular attention to assessing the limits on frequency bandwidth and scanning angle. The validated program will then be used to predict performance of zoned lenses for use on satellites.

6.

Conclusions.

The satellite use of a dielectric zoned lens of one metre diameter at 21 GHz appears to be worthy of further consideration. The lens would have to be completely shrouded for thermal control and control of electrostatic charging. The part of the shroud between the feed and the lens might have to be electromagnetically absorbing to control spillover from the feed horns. The lens weight would be of the order of 41 lb or 19 kg.

The adjacent main beams in a multi-beam antenna will cross over at a relative level approximately equal to the relative lens-edge illumination level. Compensation for loss of a beam by in-phase combining of remaining adjacent beams would require a design crossover level of about -3 dB.

Feed horn design must be such as to control spillover and main-beam crossover. Suitable candidates are long (non-optimum) corrugated horns, and also long to moderately long smooth horns, possibly with some curvature in the flared section.

7.

References.

1. **Rotman, W.,** "EHF Dielectric Lens Antenna for Satellite Communication Systems." *MIT Lincoln Laboratory Technical Report* No. 620, 3 January 1983.

2. **Shinn, D.H.,** "The design of a zoned dielectric lens for wide angle scanning." *The Marconi Review*, Vol. 18, No. 117, pp. 37-47, 1955.

3. **Cheston, T.C. and D.H. Shinn,** "Scanning Aberrations of Radio Lenses." *The Marconi Review*, Vol. 15, pp. 174-184, 1952.

4. **Hansen, R.C.,** "Circular-aperture axial power density." *Microwave Journal*, Vol. 19, No. 2, pp. 50-52, February 1976.

5. **Jones, E.M.T.,** "Paraboloid reflector and hyperboloid lens antennas." *IEEE Trans. on Antennas Propagat.*, Vol. AP-2, pp. 119-127, July 1954.

6. **Hollis, J.S., T.J. Lyon, and L. Clayton,** "*Microwave Antenna Measurements.*" Published by Scientific Atlantic Inc., 1970.

7. **Chan, K.B.,** "Design Handbook for Conical Corrugated Horns." Report KBC/70/6, Queen Mary College, London, England, 1972.

8. **Balanis, C.A.,** "*Antenna Theory, Analysis and Design.*" Harper and Row, 1982.

9. **Dion, A.R. and L.J. Ricardi,** "A variable-coverage satellite antenna system." *IEEE Trans. on Antennas Propagat.*, Vol. AP-59, No. 2, pp. 252-262, 1971.

10. **Major, R.W. and J.M. Devan,** "EHF Multiple Beam Antennas." *Naval Ocean Systems Center Technical Report* No. 730, 21 September 1981.

Table 1: Summary of Satellite Zoned Lens Designs at 44.5 GHz.

Focal length F and front face radius R (mm).	997	1475	2100	2680	3120
F/D	0.997	1.475	2.100	2.680	3.120
Number of steps N for full zoning.	19	12	8	6	5
Bandwidth (%).	1.3	2.1	3.1	4.2	5.0
Half-angle to edge of lens γ_o (degrees).	30.10°	19.81°	13.77°	10.75°	9.22°
Overall lens thickness T (mm).	134.4	87.3	60.4	47.0	40.3
Thickness at centre for full zoning t_c (mm).	18.4	18.4	18.4	18.4	18.4
Number of steps to be deleted for reduction to six steps ΔN	13	6	2	0	
Thickness at centre for a six step design (mm).	165.9	86.5	41.1	18.4	

Parameters: $\lambda_o = 6.74$ mm, $D = 1000$ mm, $\mu = 1.594$, $t_o = 7$ mm.

Table 2: Summary of Satellite Zoned Lens Designs at 20.7 GHz.			
Focal length F and front face radius R (mm).	937.5	1286	1484
F/D	0.9375	1.286	1.484
Number of steps N for full zoning.	9	6	5
Bandwidth (%).	2.8	4.2	5.0
Half-angle to edge of lens γ_o (degrees).	32.23°	22.88°	19.67°
Overall lens thickness T (mm).	154.1	101.2	86.8
Thickness at centre for full zoning t_c (mm).	31.4	31.4	31.4
Number of steps to be deleted for reduction to six steps ΔN	3		
Thickness at centre for a six step design (mm).	104.6		
Parameters: $\lambda_o = 14.49$ mm, $D = 1000$ mm, $\mu = 1.594$, $t_o = 7$ mm.			

Table 3: Summary of Laboratory Zoned Len Designs at 44.5 GHz.			
Focal length F and front face radius R (mm).	150.5	173.2	208.7
F/D	0.738	0.849	1.023
Number of steps N for full zoning.	5	4	3
Bandwidth (%).	5.0	6.3	8.3
Half-angle to edge of lens γ_o (degrees).	42.67°	36.08°	29.26°
Overall lens thickness T (mm).	39.8	33.2	26.6
Thickness at centre for full zoning t_c (mm).	18.4	18.4	18.4
Parameters: $\lambda_o = 6.74$ mm, $D = 204$ mm, $\mu = 1.594$, $t_o = 7$ mm.			

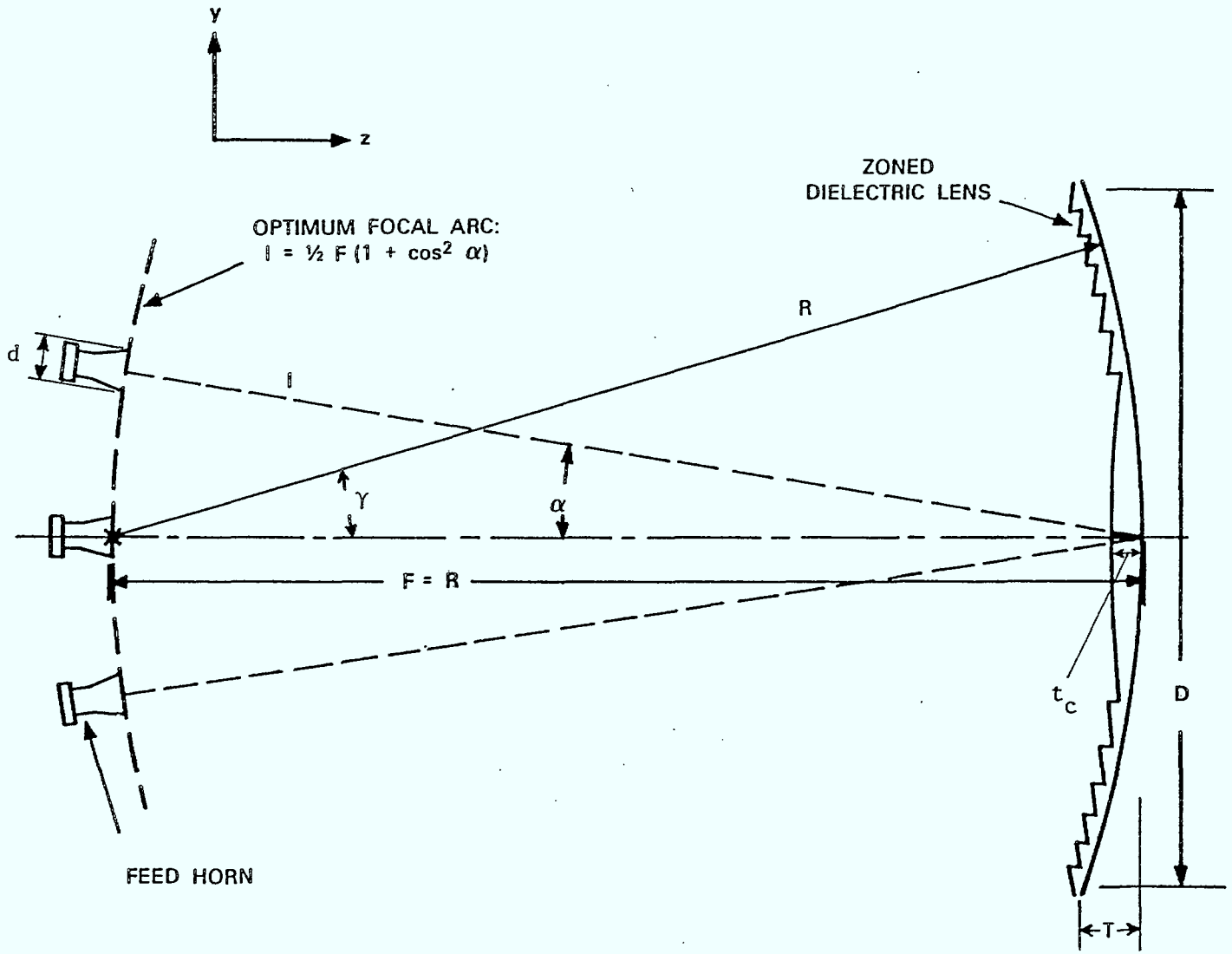

Fig.1 A multi-beam, zoned-lens antenna (adapted from Rotman [1]).

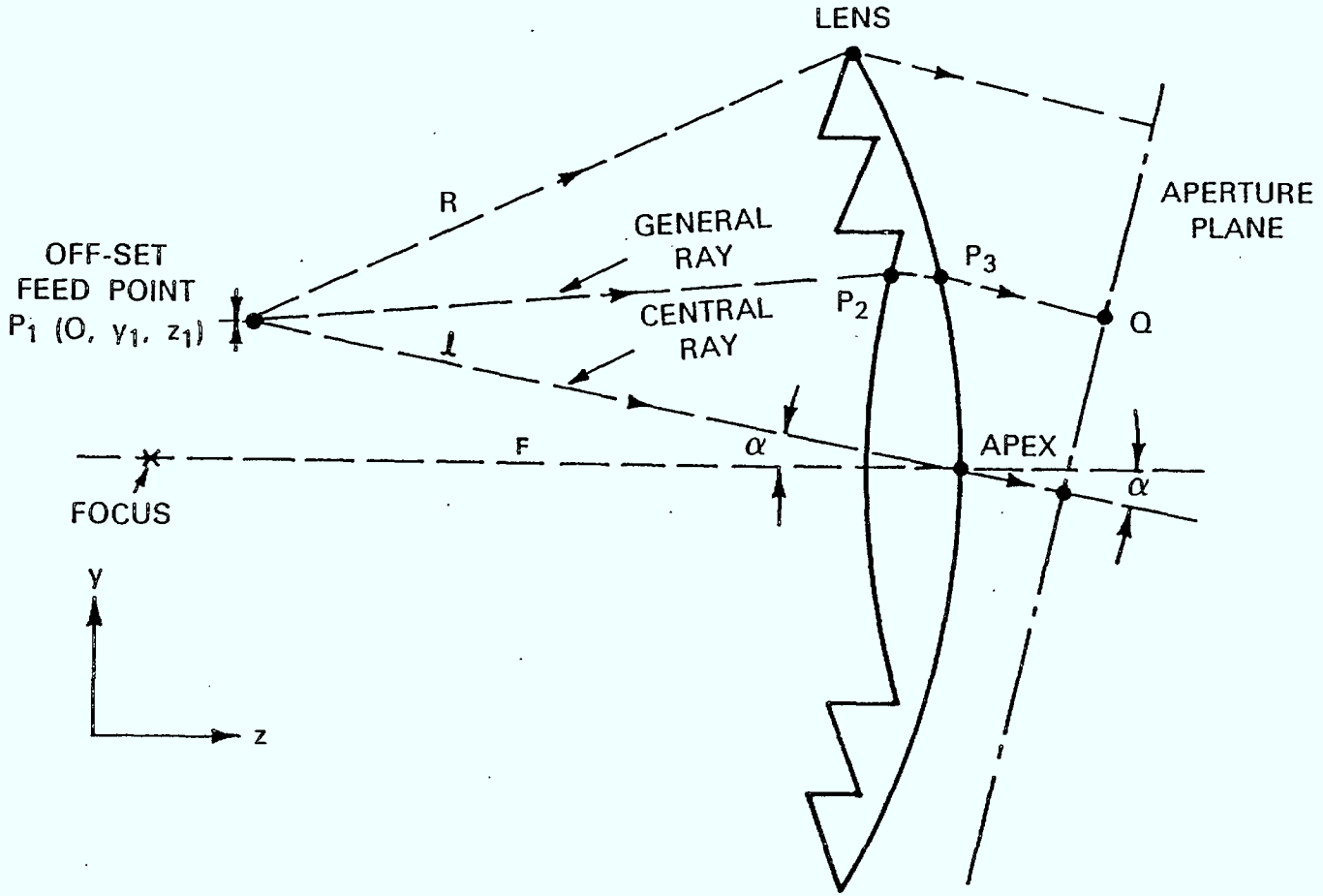

Fig.2 Ray tracing through a zoned-lens antenna (adapted from Rotman [1]).

Chapter 4

UPLINK BEAM CONTROL

J.L. Yen

1.

Introduction

The first task of beam control is to steer or switch the antenna beams toward desired directions according to network command. The second task is in the presence of an adversary's interference, to adaptively steer a null towards each jammer's direction. The effectiveness of the protection depends on the resources and strategies of both the jammer and the anti-jam system. In designing an anti-jam system, one must consider both the system vulnerabilities and jammer alternatives so as to force an adversary to employ much greater resources to successfully disrupt the system service. Although adaptive antennas are very well known [1,2] the unique situation of SATCOM requires the consideration of many question in addition to the usual decisions on nulling criterion, resolution, and algorithm. For instance, how do one interface frequency hopping with nulling? How can location memory be exploited because from the great distance of a spacecraft even mobile users and jammers appear almost stationary? How do one protect a large number of users distributed inside a beam turning on and off in a random manner? How to steer a very narrow antenna beam to a desired direction in the presence of spacecraft motion and thermal distortion of antenna structure? Is it possible to dispense with the concept of a beam and arrange the antenna element configuration to achieve maximum gain to users distributed over an area while minimizing the jammer signals? Finally, in the presence of varying jammer attack how can one devise an intelligent adaptive antenna to counter the jammer? In this Chapter we first review the possible jammer alternatives, then analyze the above questions in detail, finally preferred approaches and their rationale are given.

2.

Jammer Alternatives.

The goal of an adversary's jamming is to deploy available resources in a manner to successfully interrupt communications. At his disposal are power of transmission, nature of jamming signal and to a certain extend locations of transmission. The strategy of the jammer would be first to determine the signal parameters used for communication (the spreading code of course is not likely to be decoded) and then devise signal structures in time and frequency for efficient jamming attack. For instance, knowing that communications is on a frequency hopped signal, multi-tone or partial band jamming with about the same bandwidth and hopping interval can be used. Although not likely, if the jammer can get close enough to an emitter so that the time delay is a fraction of the chip time, he can listen in on the communication transmission and follow the signal.

The power available to a jammer depends on its platform. In the worst case the jammer can use an antenna of a few meters diameter with say kilowatts of power resulting in a 100 dBw eirp. Compared with the smallest communicator terminal there is a 50 to 60 dB advantage in jammer power. The power can of course be reduced to mimic a transmission if it is necessary. Alternatively, higher peak power pulses can be used. From a spectral point of view the alternatives are partial band noise jamming or partial band multi-tone jamming with or without hopping, to attack the inverse linear dependence of bit error rate on signal to jammer power ratio [3] in frequency hopping systems. The same satellite can also be attacked simultaneously from different locations. By using independent atomic frequency standards of 10^{-12} frequency stability it is possible to generate spatially distributed coherent sources with coherent time of hundreds of seconds to jam a satellite in some manner to make it difficult for adaptive nulling processing to converge.

3.

Nulling in a Frequency Hopping System.

In a frequency hopping receiver the RF signal is likely to be first downconverted into a broadband IF and then dehopped into a narrow band IF for FDM to TDM conversion (see Chapter 1). While all the user power are in the dehopped IF, at most only a fraction of the jammer power may occasionally appear in the narrow band IF. Obviously beam control should be implemented at IF to avoid implementation difficulties of millimeter wave control devices. Anti-jam nulling can be performed either in the broadband IF or the dehopped IF [4]. A broadband canceller can be used to remove the entire jamming signal at the broadband IF. As

a reference a version of the user signal can be obtained by rehopping the dehopped IF as shown in Figure 1. If occasional bursts of jamming power appear in the dehopped band, some means can be devised to detect its presence and only the portion of reference signal that does not contain jamming power is used. The response time of the nulling system need not be fast even when the jammer power varies rapidly, as will be discussed in the next section. Alternatively nulling can be performed at the dehopped IF using a narrow band canceller as shown in Figure 2. In this case no reference signal is available and one has to resort to power inversion under beam direction constraint. It is easy to achieve high null depth in narrow band nulling, however, fast adaption is required to handle the bursty nature of jammer power appearing at the dehopped IF. A combination of both type of nulling can be used as in Figure 3. The scheme is more complex but the improved null depth may be required.

4.

Jammer Location and Nulling Response Time.

A distinct nature of communication satellites in geostationary orbit is their great distance from earth. For a 1/2 degree beam at 40,000 km the beam footprint has a diameter of 350 km. A jammer travelling at a velocity of say 1600 km/hr will move across the area in 770 seconds. For such speeds the jammer can be considered as quasi-stationary and very relzed tracking can follow their trajectory.

To exploit the quasi-stationary nature of jammers the anti-jam system should track the jammers with great precision so that a high depth null can be placed on each jammer. The jammers may emit signals of complex time-frequency structure, but their positions cannot change rapidly. The nulling algorithm therefore should concentrate on position determination in the presence of complex signal structure. This means long memory or long time constant algorithm can be toleranted if it is capable to track the quasi-stationary jammer position and slight variations of angle of arrival at the spacecraft caused by propagation effects. To accomplish this the task of scenario analysis and the task of signal separation, as described in Chapter 6 of Phase A Report [5], can be considered separately and a judicious combination of open and closed loop implementation be devised to maximize the null depths. Such considerations are quite different from the usual applications of adaptive arrays where algorithms of fast convergence are often required.

5.

Main Beam Nulling and Multi-User Protection.

To serve the heavy traffic in a theater of operation a beam must first be steered there by a steering vector. If jammers happen to located within the beam then main beam nulling must be activated. For instance, a jammer near the edge of the beam would cause the beam center to shift away and place a null on the jammer. Users adjacent to the jammer are likely to suffer severe gain degradation. The amount of gain degradation as a function of jammer location can be determined from the quiescent beam without interference [6]. The resulting null resolution is principally dependent on the antenna configuration, a problem to be discussed later.

The use of beam direction constraint alone does not ensure the integrity of all user signals. In the presence of steering vector errors user signals can be inadvertently nulled [7]. In addition, adaptive interaction between user and jammer signals often causes signal cancellation [8]. To accomodate multi-user transmissions turning on and off at random, some additional means must be introduced to avoid these pitfalls. For example, one can minimize the broadband IF signal in the presence of the beam constraint to remove the large jammer signal as discussed before. In addition, the dehopped signal can also be maximized because it contains all the user signals. Thus, a constrained mini-max criterion would be the ideal strategy to use.

6.

Accuracy of Beam Steering and Use of Beacons.

With a beam width of 1/2 degree it is essential that steering error be less than 2-4 arc minutes. In addition, as described above, error in steering vector may lead to nulling of user signals. In the presence of spacecraft motion measurements of spacecraft altitude must therefore be made. If the spacecraft is not equipped with high accuracy altitude sensors, means must be provided to establish a position reference.

One possible way is to introduce one or two beacons located far away from possible jammers. The signals should be sufficiently strong so that no antenna nulling is required to protect their transmissions. The directions of the beacons as measured by the spacecraft antenna are then serve as references from which steering vectors for desired beam directions are derived. For a phased array the beacon directions can be determined from the coherence matrix of the beacon signal as received by the different antenna elements. Either ground based or on board processing can be used to derive the steering vector. The former requires two-way telemetering and hence is slow. On board processing on the other hand requires satellite computational capabilities. The operation is repeated to track satellite motion and to correct control signal

errors.

The use of beacons also provide a mean for taking into account thermal deformation of antenna geometry. In addition, they can serve as network command. They are of lesser value in correcting for propagation effects because most of which occur directly over the user station.

7.

Null Depth, Bandwith and Weight Resolution.

The signal separation ability of an adaptive phased array as reflected in its nulls is no different from that of a conventional array except for its ability to steer main beams and nulls according to the signal scenario. The signals received by each element must first be corrected in geometric delay and then summed to form a main beam. In going off the main beam the signal amplitude is reduced due to delay error. This reduction is accompanied by a distortion because the antenna response as a function of frequency and incident wave direction exhibits a series of nulls and maxima as shown in Figure 4. For a fixed frequency the usual antenna pattern shows a series of nulls and maxima in certain directions. As the frequency is changed the nulls and maxima change their directions. At a fixed direction the response will vary between nulls and maxima as the frequency is changed and the rate of variation increases with the distance from the main beam. In order to have a broadband null transversal filters are required at each element to control the group delay so as to minimize the broadband response in that direction. Alternatively a null plateau can be forced in that direction as shown in Figure 5 so that over the frequency band of interest the jammer location does not move out of the plateau [10]. The weights of the array elements are determined from pattern shape constraints in addition to directional constraints in a feedforward manner without using error signals. Deep broadband nulls are generally more difficult to achieve. In a frequency hopping system narrow band nulling at dehopped IF can be used to supplement broadband nulling at undehopped IF to achieve greater overall interference discrimination.

It is important to note that the depth of null depends on how accurately the element weights can be set. For instance, a null depth of 40 *dB* would require complex weight errors to be less than 1 Z_{μ} and phase errors of less than Y_2 degree. Sufficient weight resolution must be provided in digital implementation of phased arrays.

8.

Main Beam Nulling and Antenna Configuration.

Nulling in main beam necessarily causes gain degradation in portions of the main beam. To reduce vulnerability to nearby jammers the only way is to use a smaller beam. With a smaller beam, only a portion of required theater-of-operation is covered, thus one must employ multi-beam coverage. A smaller beam without increaseing the total antenna aperture area can be achieved by means of thinned arrays. However, thinned arrays have grating lobes which, even when smoothed into grating plateaus by non-uniform specing, increases the area of jamming vulnerability. A trade-off must therefore be reached between these conflicting requirements.

One possibility is to use geometrically separated individual antennas in a phased array each with element beam covering the required field of view. With 60—100 elements required they can be distributed quite sparsely over say a 3 m diameter area. This would reduce the main beam foot prints from 350 km to 120 km diameter, greatly reducing main beam vulnerability. The grating plateaus would then have levels of about -20 *dB* below main beam. Nulling in such plateaus can be relatively effective. With such a large number of antennas it may be possible to form multiple outputs covering the theater-of-operation having appropriate nulls without well defined beams, for instance, an output may have a split beam shape. An alternative approach is to use a larger central antenna and with a ring of smaller elements say 5-9, distributed around it for nulling. With a judicious choice of configuration as discussed in Chapter 6 of Phase A Report [5] proper trade-off between vulnerability, performance and complexity may be obtained.

9.

An Intelligent Adaptive Antenna.

Based on the above considerations an intellegent adaptive antenna must first determine the jammer directions and track their slow movements. The jammers may turn on and off and change their signal structures but their locations will not change rapidly. Reference from secure beacon transmissions may be necessary to account for satellite attitude uncertainty. A slow acting broadband nulling before dehopping is first used to remove the majority of jamming power. This is followed by a fast acting narrow band nulling at the dehopped IF to remove remaining jamming power. Knowledge of jammer location can be used to compute weights for each frequency hop in a feed forward mode. A suitable combination of feed forward and feedback weight setting using directions of jammers and users and maximizing user power while

minimizing jammer power, perhaps in a time varying manner, should be employed so as to provide maximum protection in all jamming situations.

The simplest implementation scheme is the use of the LMS algorithm under directional constraint. The complexity of the system is proportion to the number of elements N. A very small step size is used to have very long memory of jammer location. The performance of such an approach is probably inferior to the more flexible method of first analyse the signal scenario and then discriminate jammers. This latter approach however would have complexity of the system proportional to N^2, hence is only applicable to moderate values of N.

To protect against nearby jammers small main beams must be used. This would imply a non-uniform thinned array with moderate number of elements so that the grating lobes are smeared out in both direction and frequency. Multiple broadband beams are formed by controllable delay lines to each elements. Several beams would be required to service an area of ½ °× ½ °. Such an antenna achieves high performance by means of greater complexity, size and weight.

10.

References.

1. **Munzingo, R.A. and T.W. Miller,** "*Introduction to Adaptive Arrays.*" Wiley Inter-Science Publications, 1981.

2. **Hudson, J.E.,** "*Adaptive Array Principles.*" Peter Peregrinus, 1981.

3. **Levitt, B.K.,** "Use of Diversity to Improve FH/MFSK Performance in Worst Case Partial Band Noise and Multitime Jamming." *IEEE Eastcom*, Paper No. 28-2, June 1982.

4. **Castro, A.A.,** "Uplink antenna nulling for high data ratio EHF satellite communications." *IEEE Eastcom*, Paper No. 25.4, June 1982.

5. **Yen, J.L., et al.,** "Study of EHF Controlled-Beam Antennas for SATCOM." Final Report, Phase A Study, DSS Contract Serial No. OSO-81-00336, May 1982.

6. **Gupta, I.J. and A.A. Ksienski,** "Prediction of adaptive array performance." *IEEE Eastcom*, Paper No. 30-1, June 1982.

7. **Compton, Jr., R.T.,** "The effect of random steering vector errors in the Applebaum adaptive array." *IEEE Transactions on Aerospace and Electronic Systems*, Vol., AES-18, pp. 392, September 1982.

8. **Widrow, B., K.M. Duvall, R.P. Gooch and W.C. Newman,** "Signal Cancellation Phenomena in Adaptive Antennas: Causes and Cures." *IEEE Transactions on Antennas and Propagat.*, Vol., AP-30, pp. 469, May 1982.

9. **Bar-Neis, Y.,** "Steered Beam and LMS Interference Canceller Comparison." *IEEE Transactions on Aerospace and Electronic Systems,* Vol., AES-19, pp. 30, January 1983.

10 **Steyskal, H.,** "Synthesis of antenna patterns with prescribed nulls." *IEEE Transactions on Antennas and Propagat.*, Vol., AP-30, p. 273, March 1982.

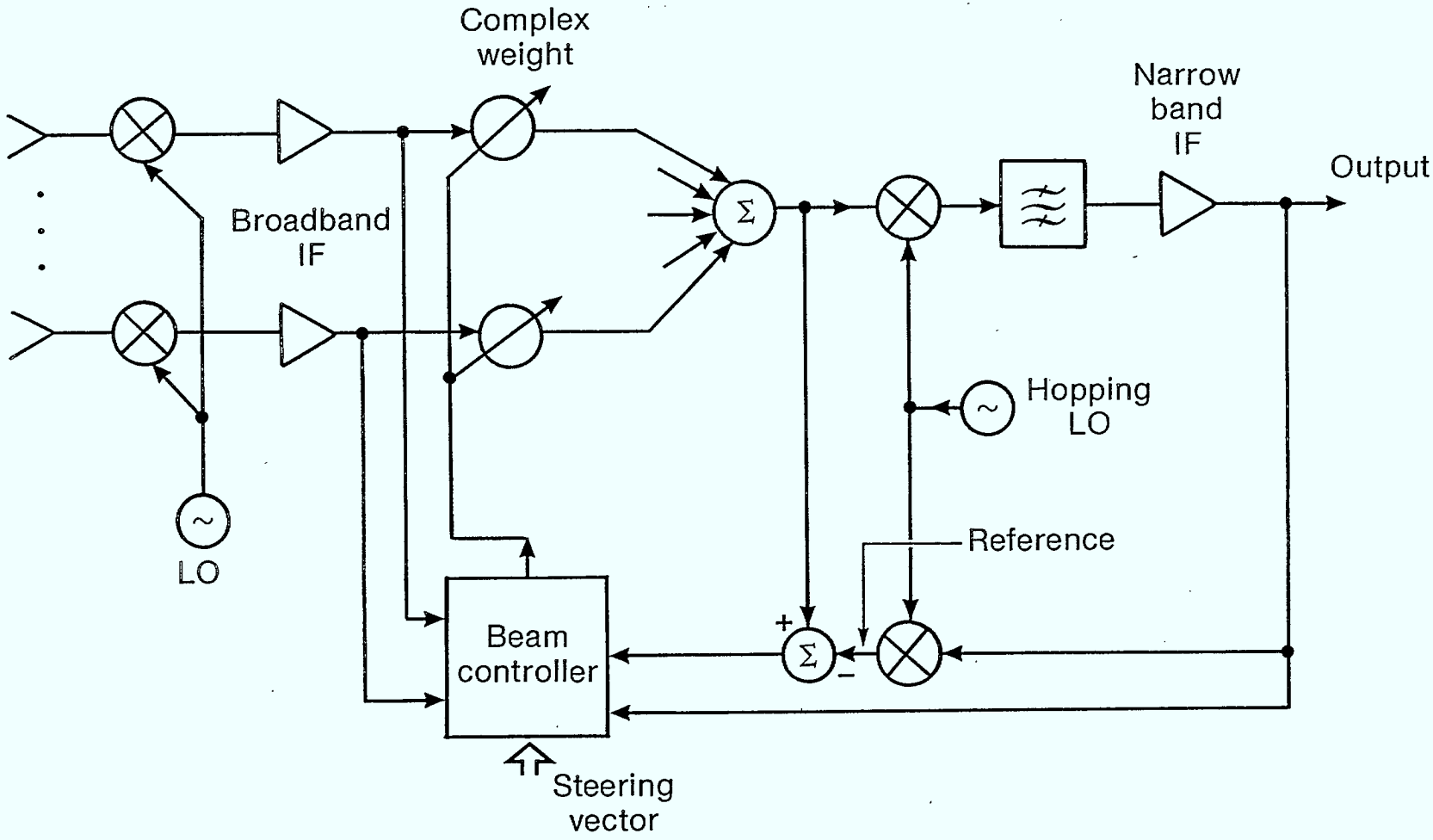

Fig. 1. Broadband beam control

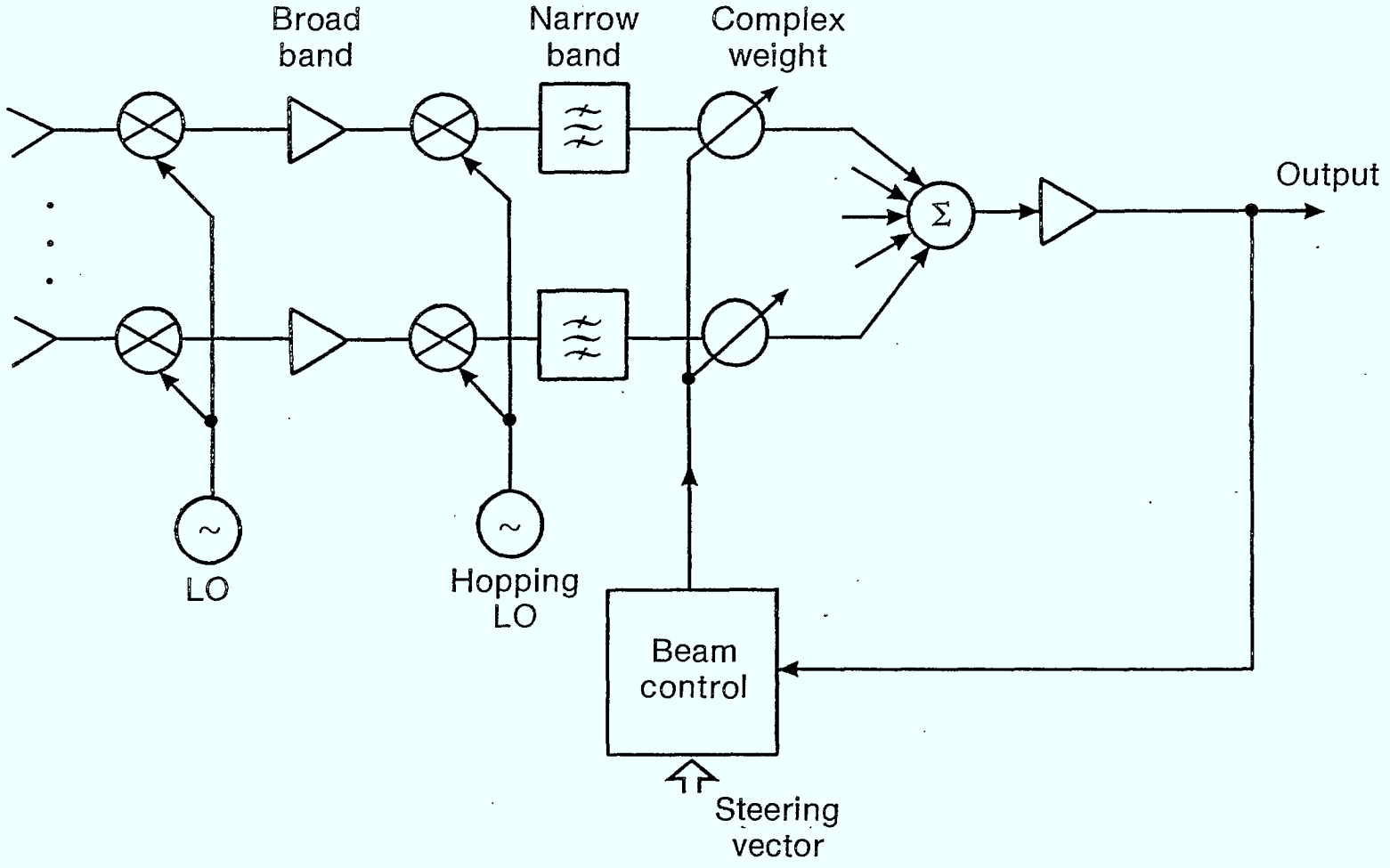

Fig. 2. Narrow band beam control

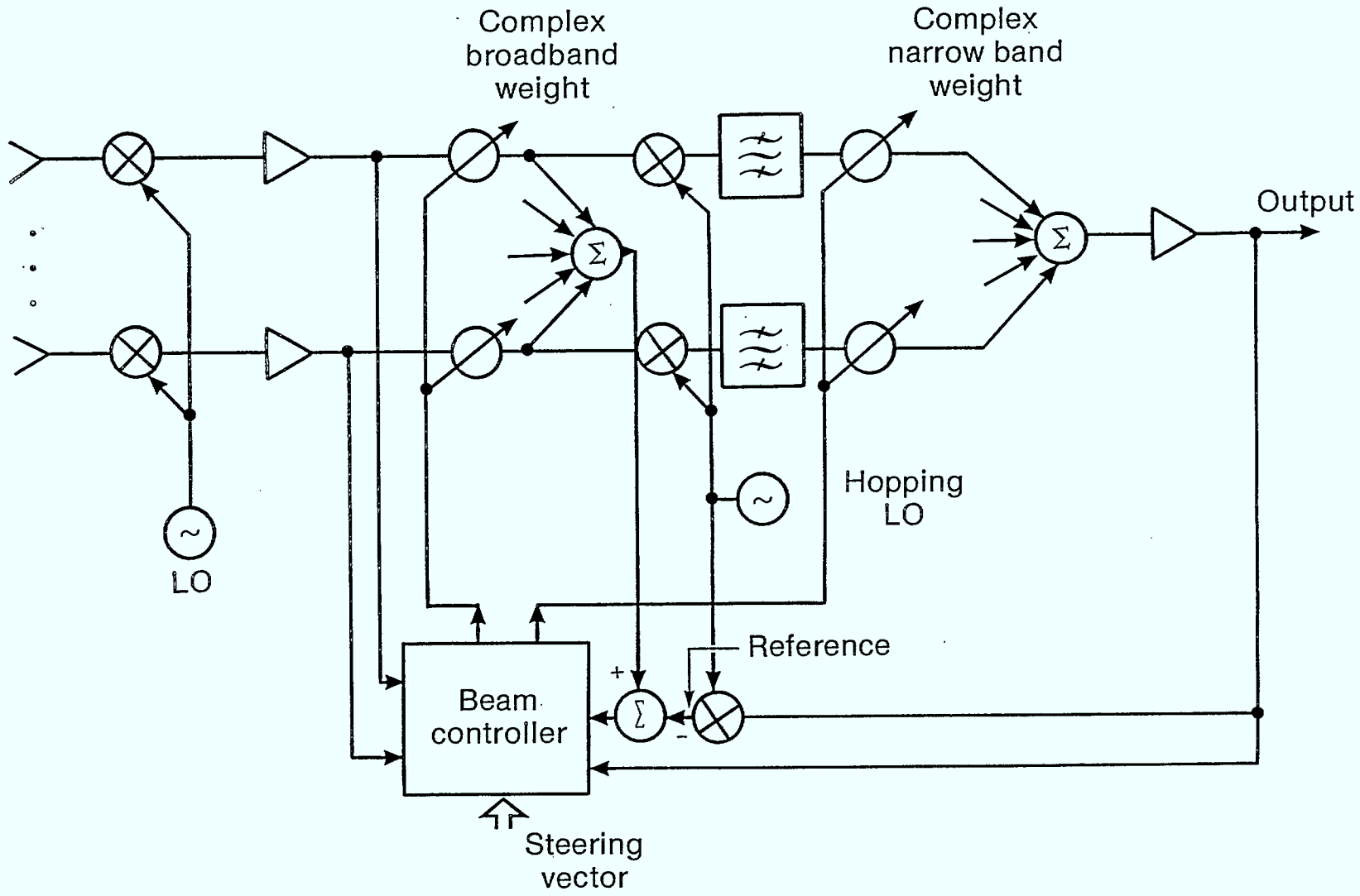

Fig. 3. Two band beam control

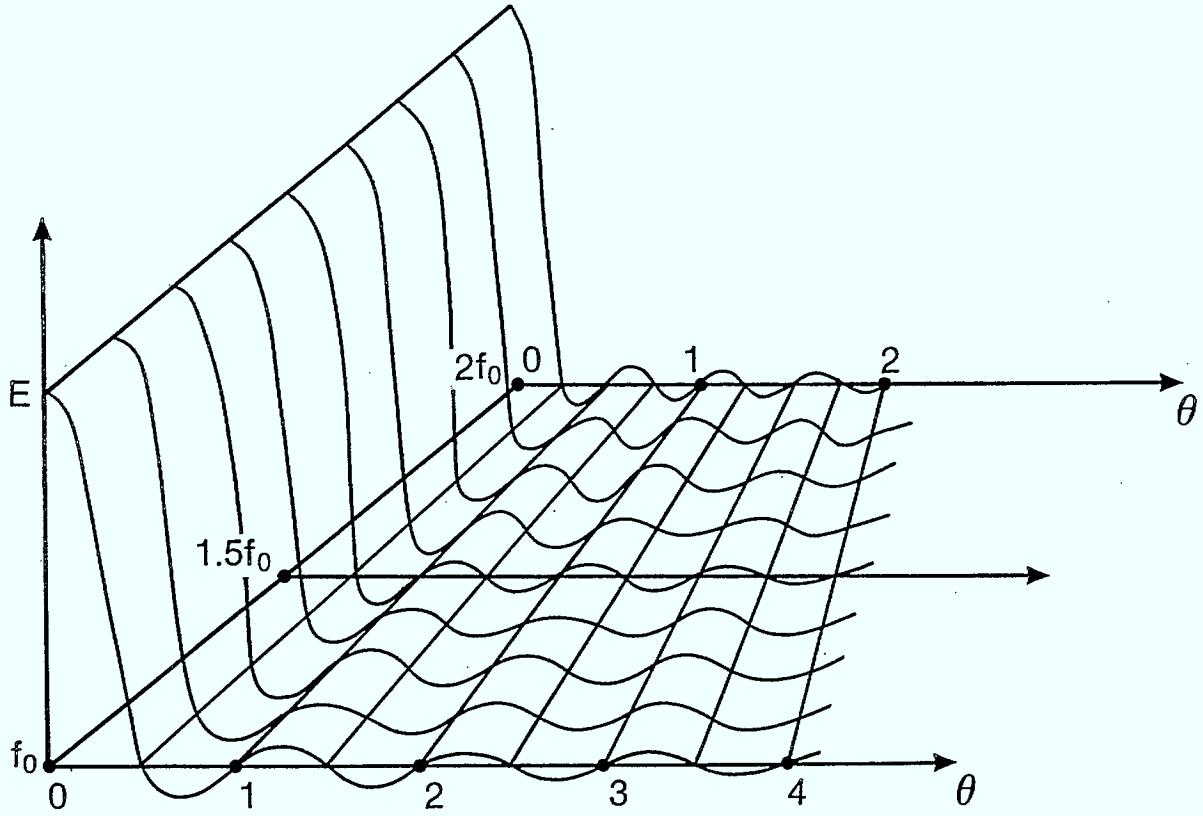

Fig. 4. Frequency-angular beam structure

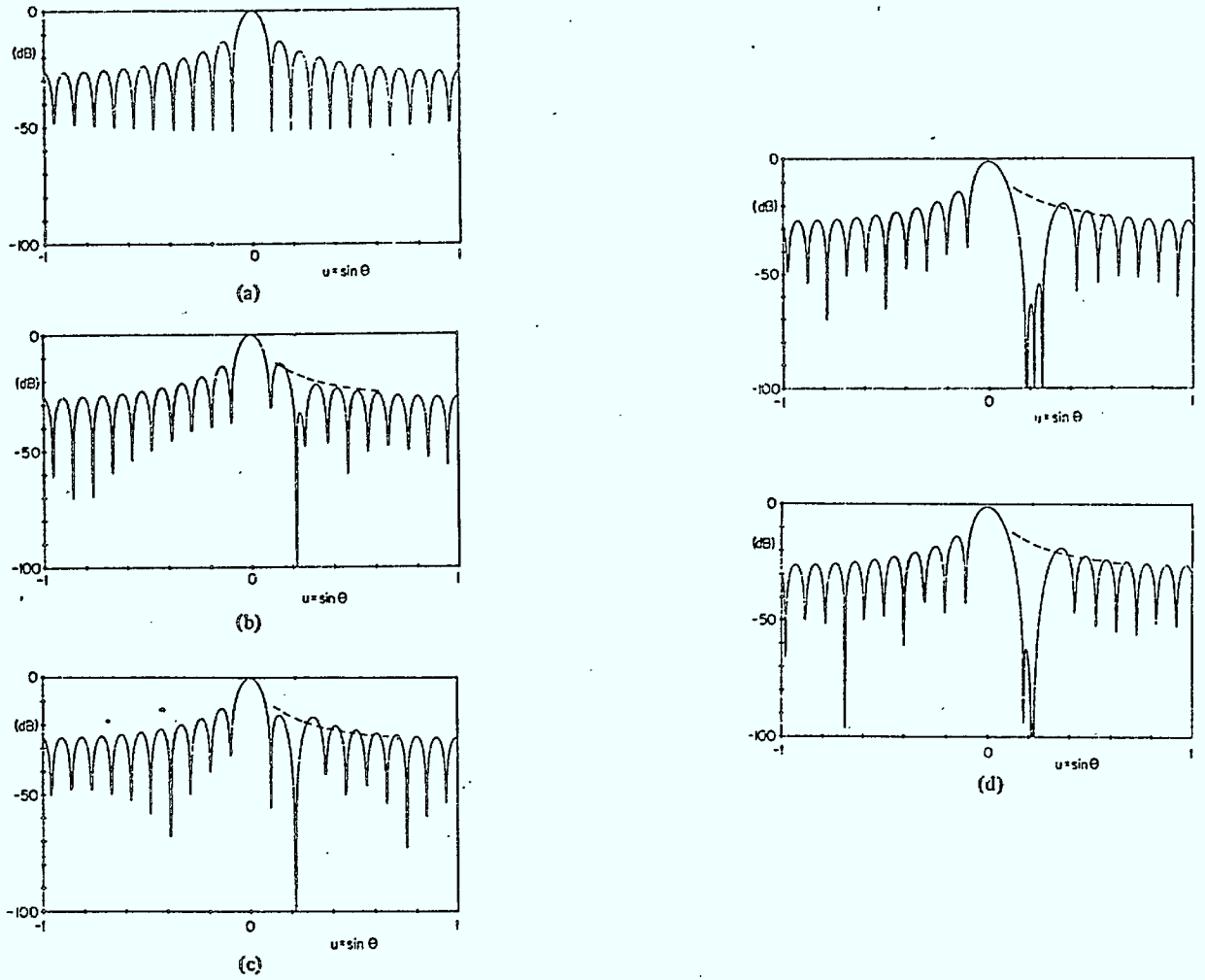

Figure 5 Shaped nulls after [10].

Chapter 5

Recent Results of Experiments with a Microwave Adaptive Array.

K. Iizuka and M. Klemes

1.

Introduction

In order to obtain insight into the actual operation of a hardware adaptive array antenna system, a two-element microwave adaptive array was built and tested in our laboratory. Of primary interest was the behaviour of its receiving gain pattern when the system was confronted with various interference situations and system parameters. The following is a brief description of the system (in its current stage of development) and its principles of operation. Results of recent experiments are presented and interpreted, to illustrate its performance.

2.

Functional Description of the Hardware System.

Figure 1 shows schematically the experimental set-up. For reasons of availability of components the array was built to operate at X-band, with 12.4 GHz RF. A track was built to move the scanning antenna in a semi-circular arc of radius R = 85 cm around the phase centre of the array. This satisfied the far-field approximation. To enhance the far-field effect, the receiving horns were tilted to make their axes converge at $\approx$ 85 cm, resulting in greater depths of nulls in the array patterns and also in coinciding the individual element patterns.

Figure 2 shows the detailed functional diagram of the whole system, excluding the measuring apparatus. The 12.4 GHz RF was down-converted to a 60 MHz IF and the adaptive functions were implemented at that frequency. The system was fairly narrow-band (BW = 5 MHz), thus permitting the use of relatively simple components in the adaptive processor, as well as simplifying mathematical treatment somewhat.

The continuous-time version of the least mean square (LMS) algorithm was used. This algorithm is robust in control, simple in implementation and higher in speed than its digital counterpart.

The signals were separated into in-phase and quadrature phase components each of which was controlled by an adaptive loop. The outputs of all four weighters are summed directly to generate the output signal of the system, $y(t)$. This is then subtracted from a reference signal, $r(t)$, and the resulting error signal, $\epsilon\ (t)$, is amplified and fed back to the weighter control loops. The IF signals are monitored through directional couplers with - 30 *dB* coupling constant, the weighter control signals by high-impedance oscilloscope probes. The reference signal is practically an exact replica of the desired signal which is CW, converted to 60 MHz IF. (The reference modulator was not used except to tune the system at the start of an experiment). The gains of the low-noise mixer preamps preceding the adaptive processor are set, but those of the IF amplifiers in each loop are variable. These amplifiers serve to boost the signal level (while maintaining phase coherence) high enough for the high-level double-balanced mixers used as correlator multipliers. Being narrow-band (5 MHz) they help to block undesired mixer products as well as the mixer noise and also act as buffers for the loops. The same kind of IF amplifiers are used to control the feedback gain applied to the error signal, thus affecting the system's convergence rate towards optimal adjustment. Attenuators were used to adjust signal levels to minimize amplifier saturation, and to balance the amplitudes of signals from the mixer-preamps of each element.

It is important to note that the RF frequency of the jammer was incoherent with the desired RF and slightly offset from it (but still within the passband of the system at IF). It was also pulsed at 1 KHz while the desired signal was CW. Only one RF filter was available; the other horn was fitted with an attenuator to balance the RF inputs of both mixer preamps.

Finally, Figure 3 depicts the details of the integrator (low-pass filter) used in the correlator of each loop. They are 'leaky' and have inverted outputs. A passive single-pole RC filter precedes the integrator and removes the high-frequency outputs of the correlation mixer, which the op-amps cannot handle. (This filter makes the actual adaptive loops into second-order systems, causing small oscillations in control signals, to be discussed later). The integrator outputs are buffered and augumented by an extra output stage (which is included in the buffer feedback loop to linearize it) which drives the 50 Ω current-controlled attenuators that weight the element signals.

It is important to note that the integrators are disconnected from the weighters and the weighters are instead connected to regulated D.C. power supplies set to pre-measured control-voltage values when pattern measurements are being made. Otherwise, the loops would keep adapting to follow the desired signal (which is used as the test-source in this mode) and the

pattern would tend to look uniformly level. The jamming signal is also extinguished during pattern measurements.

In many experiments, a beamforming network (as shown in Figure 4) was inserted after the mixer-preamps, giving a sum-beam ($\sum$) output to one channel and a difference beam (Δ) output to the other channel of the adaptive processor.

3.

Outline of Principles of Operation*.

The LMS algorithm strives to minimize the cost function, in this case the mean square error signal, $\overline{|\epsilon(t)|^2}$. It does so by causing the vector of weighting coefficients (W-coefficients) to descend the gradient of the constant error-power surface (in weighting-coefficient coordinates). With reference to Figure 5, the mean square error (power) is, in assuming independence of the input, $X(t)$, and weighting signals $W(t)$,

$$\overline{|\epsilon(t)|^2} = \overline{W^T(t)}\, R\, \overline{W(t)} - 2\, \overline{W^T(t)}\, D - \overline{d(t)^2} \tag{1}$$

where

$$R = \overline{X(t)\, X^T(t)}\,, \quad D = \overline{r(t)\, X(t)}$$

The gradient of mean error power in W-coordinates is therefore,

$$\nabla_W\ \overline{|\epsilon(t)|^2} = 2R\overline{W(t)} - 2D \tag{2}$$

The algorithm causes the W-coefficients to change in the opposite direction in W-space as time increases, according to

$$\frac{dW(t)}{dt} = -\mu \nabla_W\ \overline{|\epsilon(t)|^2} \tag{3}$$

where μ is a constant of proportionality.

It is clear from equation (2) and (3) that in the steady state when $\frac{dW(t)}{dt} = 0$ the W-coefficients have reached an optimum state and satisfy

$$\overline{W(t)}_{\text{steady state}} = R^{-1} D = W_{opt} \tag{4}$$

*real-number representation is used except when noted otherwise.

which is recognized as the Wiener filter solution for a spatial filter.

However, the gradient is not an instantaneous quantity since R and D are really steady-state average quantities, and it is necessary to use an estimate of the gradient for every instant before the algorithm reaches steady-state. An unbiased estimate is taken to be the instantaneous version of equation (2), namely

$$\hat{\nabla}_W = 2\,X(t)\,\epsilon(t)$$

This is then used at every instant of continuous time in the algorithm, according to

$$\frac{dW(t)}{dt} = -2\mu\,X(t)\,\epsilon(t) \tag{5}$$

and ensures that equation (4) is still satisfied at steady-state, on the average. The ideal solution for the weight vectors is obtained from equations (2) and (3) by solving

$$\frac{d}{dt}\,W_{opt}(t) = -2\mu(R\,W_{opt}(t) - D) \tag{6}$$

to yield

$$W_{opt}(t) = 2\mu\int_0^t \exp\left[-2\mu\,(t-\tau)\,R\right]\,D\,d\tau + W(0)\exp\left[-2\mu t\,R\right] \tag{7}$$

From the Laplace transform of (6), which is

$$W_{opt}(s) = 2\mu\,[\,sI + 2\mu R\,]^{-1}\,D/s$$

it is evident that $\mu > 0$, to give poles in the left half-plane and ensure stability of all modes of the system, since the eigenvalues of R are all >0.

Next, the equivalent of equation (7) is computed by the hardware adaptive loops but with shorter averaging times. Analysis of Figure 5 reveals that the weighting vector is the solution of the governing differential equation

$$\frac{d}{dt}\,W(t) + \left[\frac{1}{R_2C}\,I + \frac{2\alpha}{R_1C}\,X(t)\,X^T(t)\right]W(t) = \frac{2\alpha}{R_1C}\,X(t)\,r(t) \tag{8}$$

which is found by variation of parameters to be

$$W(t) = \frac{2\alpha}{R_1C}\int_0^t \exp\left[-\int_\tau^t \left[\frac{1}{R_2C}\,I + \frac{2\alpha}{R_1C}\,X(\xi)\,X^T(\xi)\right]d\xi\right]X(\tau)\,r(\tau)\,d\tau +$$

$$+ W(0)\exp\left[-\int_0^t \left[\frac{1}{R_2C} I + \frac{2\alpha}{R_1C} X(l)\, X^T(l)\right] dl\right]$$

Mixer conversion losses (about 6 dB) and power divider/combiner loses have been ignored for the moment. In Figure 3 we find a passive RC filter preceding the integrator. If we represent its effect simply as low-pass averaging, denoted by $\overline{(....)}^{LPF}$, we can write the solution for $W(t)$ as

$$W(t) = \frac{2\alpha}{R_1C}\int_0^t \exp\left[-\int_\tau^t \left[\frac{1}{R_2C} I + \frac{2\alpha}{R_1C}\,\overline{X(\xi)\, X^T(\xi)}^{LPF}\right] d\xi\right] \overline{X(\tau)\, r(\tau)}^{LPF}\, d\tau + \qquad (9)$$

$$+ W(0)\exp\left[-\int_0^t \left[\frac{1}{R_2C} I + \frac{2\alpha}{R_1C}\,\overline{X(l)\, X^T(l)}^{LPF}\right] dl\right]$$

even though in reality it is a second-order system. Rearrangement of (9) makes it easily comparable to (7).

$$W(t) = \frac{2\alpha}{R_1C}\int_0^t \exp\left[\frac{-2\alpha}{R_1C}\int_\tau^t \left[\frac{1}{2\alpha G} I + \overline{X(\xi)\, X^T(\xi)}^{LPF}\right] d\xi\right] \overline{X(\tau)\, r(\tau)}^{LPF}\, d\tau + \qquad (10)$$

$$+ W(0)\exp\left[\frac{-2\alpha}{R_1C}\int_0^t \left[\frac{1}{2\alpha G} I + \overline{X(l)\, X^T(l)}^{LPF}\right] dl\right]$$

If the $\overline{(....)}^{LPF}$ quantities can be treated as nearly constant, the following correspondence exists between the ideal weight vector solution (7) and the hardware-computed solution (10), in the LMS algorithm:

$$W(t) \rightarrow W(t)$$

$$2\mu > 0 \rightarrow \frac{2\alpha}{R_1C} > 0$$

$$R(t-\tau) \rightarrow \int_\tau^t \left[\frac{1}{2\alpha G} I + \overline{X(l)\, X^T(l)}^{LPF}\right] dl, \quad G = R_2/R_1$$

$$D \rightarrow \overline{X(\tau)\, r(\tau)}^{LPF}$$

Due to the finite value of R_2, the integrators leak, which has the effect of augmenting the eigenvalues of R by $\frac{1}{2\alpha G}$, and changing the optimum weight solution to

$$W_{opt_L} = R_L^{-1} D = \left[R + \frac{1}{2\alpha G} I \right]^{-1} D \tag{11}$$

This is comparable to injection of (synthetic) uncorrelated noise with power $\frac{1}{2\alpha G}$ into each antenna. Usually the leakage is small and $2\alpha G >> Tr\, R$ so its effect on W_{opt} is negligible. When α and G are large, the error in W_{opt} can be shown to be approximately

$$\Delta W = \overline{W(t)} - W_{opt} \approx \frac{1}{2\alpha G} \; R^{-1} W_{opt}$$

near steady state. Slight leakage in the integrator prevents the accumulation of D.C. offset voltages at its output. It also improves the conditioning of R in case it has a zero eigenvalue. Since convergence of each mode is exponential with time-constant proportional to its eigenvalue (recall that

$$\begin{aligned} \exp[R] &= \exp[Q \Lambda Q^T] = [I + Q \Lambda Q^T + \tfrac{1}{2} (Q \Lambda Q^T) \;\; (Q \Lambda Q^T) + \cdots] \\ &= Q[I + \Lambda + \tfrac{1}{2}(\Lambda)^2 + \cdots] Q^T \\ &= Q \exp[\Lambda]\, Q^T \quad , \quad Q^T = Q^{-1} \end{aligned}$$

where the columns of Q are the eigenvectors of R) the leakage will reduce the eigenvalue disparity when some of them become very small, thus improving slightly the overall convergence rate.

Integrator offsets can be modelled by a D.C. source V_{off} at the non-inverting input of the op.amp. By superposition $V_{out}(t)$ then becomes $W(t) + (1 + R_2/R_1)\, V_{off}$ and the system differential equation (8) becomes

$$\frac{dW(t)}{dt} + \left[\frac{1}{R_2 C} I + \frac{2\alpha}{R_1 C} \; X(t)\, X^T(t) \right] \; W(t) = \frac{2\alpha}{R_1 C} \; X(\tau)\, r(\tau) + \left[\frac{1 + R_2/R_1}{R_2 C} \right] V_{off}$$

In the steady state the average weighting vector is then

$$\overline{W(t)} = \left[\frac{1}{2\alpha G} I + R \right]^{-1} \left[D + \frac{1}{2\alpha} \; V_{off} \right]$$

so once again, when $\alpha >> 1$ the error in the weighting vector is negligibly small. V_{off} has a magnitude of $< 10\,mV$ while the magnitude of the $W(t)$ signals was measured to be generally < 350 mV.

The mixer conversion loss and losses in power splitters/combiners generally reduce the effective magnitude of $\frac{2\alpha}{R_1 C}$ (multiplicatively), so it is advisable to keep $\frac{2\alpha}{R_1 C}$ large, since there is no danger of instability. However, if the adaptive loop is solved as a second-order system instead of using $\frac{LPF}{}$, it is found that when

$$\alpha \geqslant \frac{R_o + R_1}{2R_1\,\lambda_{max}} \left[\frac{(\tau_{01} + \tau_2)^2}{4(\tau_{01}\,\tau_2)} - \frac{1}{G} \right]$$

the weights begin to oscillate. The oscillations are always damped exponentially by $\exp\left[-\tfrac{1}{2} \left[\frac{\tau_{01} + \tau_2}{\tau_{01}\,\tau_2} \right] t \right]$ so stability prevails. The quantities above are defined with reference to Figure 4 as

$$\tau_{01} = \left[\frac{R_0 R_1}{R_0 + R_1} \right] C_o$$

$$\tau_2 = R_2\,C_2$$

$$G = R_2/R_1$$

Reference [1] claims that when this occurs the convergence rate doubles over that of a first-order loop with the same W-coefficient variance. It is, however, advisable to limit the magnitude of the feedback gain $\frac{2\alpha}{R_1 C}$ to prevent the system from acting instantaneously on the signals before allowing time for averaging, so that information in the desired signal would not be destroyed by making the output $y(t)$ identical with the internal reference $r(t)$ at every instant.

There is thus an apparent trade-off between convergence rate and loop noise, both being increased by increase of α, and/or of the eigenvalues. See also Gabriel's paper [2] for limits on μ.

4.

Experimental Results

In Figures 6 (a), (b) and (c) are recorded gain patterns (at IF) of the receiver before the adaptive processor. Figure 6(a) shows the element patterns of each horn in the presence of the other, after the IF channel outputs were balanced with an attenuator and the horns converged (focused) at $\approx$ 85 cm. The gain scale has an arbitrary reference (0 *dB*). The 3 *dB* element beamwidth is $\approx$ 20 ° and good pattern coincidence is maintained to a beamwidth of $\approx$ 90 °. All receiving and transmitting antennas were the same.

Figure 6(b) shows the patterns of the $\sum$ and Δ beams superposed. There is a slight phase error in the hardware beamformer (compared to Figure 3) as evidenced by the slight deviation of the peak of the $\sum$ beam from 90 °. The beams are orthogonal in the sense that the nulls of one beam coincide with the peaks of the other, and also because their beamforming matrix is composed of the orthogonal vectors $[1\ ,\ -1]^T$, $[1\ ,\ 1]^T$.

Figure 6(c) shows the conformity of the 'envelope' of the $\sum$ beam with the element pattern. Orthogonal beams were used in many of the experiments; they tend to let the weighting channels operate more independently (due to their orthogonality) resulting in somewhat clearer control-signal traces.

The above results illustrate proper operation of the receiver-downconverter section; there is no amplifier saturation, negligible pattern distortion due to mutual coupling and external reflections, and the lobe and null spacing agrees with simple far-field geometry ($N\lambda = d\sin\theta$, where d is the element spacing = 3.8 λ, θ is angle from broadside, N is an integer denoting the grating lobes.). Since $\Delta N = 1$ and $\Delta N\lambda/d \approx \Delta\theta\cos\theta$, the null sepration is $\Delta\theta \approx \lambda/(D\cos\theta)$ which works out to be $\approx$ 15 ° near the centre and $\approx$21 ° around θ = 45 ° from centre of the pattern. This can be verified for the $\sum$ and Δ beams in the figures.

Interference rejection is demonstrated in Figures 7 (a) and (b). The interference signal is a 1 KHz pulsed RF signal, slightly off-set in frequency from the CW desired RF signal, as noted earlier. The jammer RF power was $\approx$20 *dB* greater than the desired RF power, but the jamming source was at a larger radius ($\approx$100 cm). Element separation was 4.2 λ. In all experiments, 'quiescent' pattern refers to the gain pattern arrived at by the adaptive processor in the steady state when no interference source is active, and 'adapted' pattern refers to the steady state pattern obtained by the processor in response to an activated jamming source. (In both cases the patterns have been actually adapted.). The oscilloscope traces show the jammer RF pulse (10 μs risetime), the error burst (analogous to the 'learning curve' [3] of the processor) and weighter control signal transients, all on synchronized timebases.

Evolution of the optimum pattern is shown in the superposed pattern recordings of Figure 7(b). Minimization of error power is in effect a maximization of signal to noise-plus-interference ratio. This is clearly evident as the array adapts to give the highest gain to the desired signal and develops a null in the direction of the interference signal, resulting in about 33 *dB* rejection of the jammer. The DFT beamformer was used here, but the receiving horns were focused at ∞. The total time for adaptation was 65 μs. This depends on the feedback gain and eigenvalues of R_L, which have not yet been experimentally determined, but the existence of their corresponding modes is evident in the different risetimes of the W-signals, each being a different linear combination of the two possible exponential modes.

Figures 8 (a) and (b) show the effect of the DFT transformation on the patterns. The two-element array has two degrees of freedom when trained to receive one desired signal. In the absence of an interference signal one degree of freedom is unused, and R is ill-conditioned having one very small eigenvalue corresponding to total thermal noise power, the other being total signal power. Since the noise conditions can be time-varying and unpredictable in the time it takes to insert the beamformer, the quiescent patterns in the two cases were quite different.

However, when the jammer turns on and is in a position not too close to the equivalent position of the desired signal and has comparable power, the eigenvalues of R become less disparate and less random. Now, it is a simple matter to show that when the (complex) input signal vector is transformed by a matrix B, the optimum W-coefficient vector becomes $B^{T^{-1}} W_{opt}$, where W_{opt} is the optimum W-coefficient vector without input transformation, and also that the gain pattern remains unchanged from that without the B-transformation [4]. It can be verified from Figure 8 that this was very nearly achieved experimentally, as the adapted patterns are nearly the same except for the exact null depths, which are very sensitive to small errors in adjustment of the W-coefficients (especially on a log-scale). Transformation of the W-vector can be verified numerically when the lengths of the lines connecting the power-combiners in the DFT beamformer in Figure 4 are accounted for by phase-shifts.

The actual transformation performed by the beamformer on the complex input signal vector $X(t)$ was obtained by measurement to be

$$B = \begin{bmatrix} -e^{-j81^\circ} & e^{-j84^\circ} \\ -e^{-j79^\circ} & -e^{-j79^\circ} \end{bmatrix}$$

therefore

$$B^{T^{-1}} = \tfrac{1}{2} \begin{bmatrix} -e^{j82.5^\circ} & e^{j82.5^\circ} \\ -e^{j77.5^\circ} & -e^{j80.5^\circ} \end{bmatrix}$$

When the control voltages were converted to their corresponding weighting coefficients (which were measured), the weighting-coefficient vectors became the following:

without DFT

$$W_X = \begin{bmatrix} 1.53 & +j250 \\ -j2.70 & -j2.25 \end{bmatrix} \times 10^{-2} \qquad \text{(measured)}$$

with DFT

$$W_Y = \begin{bmatrix} 2.60 & -j2.40 \\ 0.100 & +j0.380 \end{bmatrix} \times 10^{-2} \qquad \text{(measured)}$$

The predicted weight vector W_Y was then calculated from W_X according to

$$W_Y = B^{T^{-1}} W_X$$

with the result that

$$W_Y = \begin{bmatrix} 2.08 & -j2.41 \\ 0.168+j0.498 & \end{bmatrix} \times 10^{-2} \qquad \text{(predicted)}$$

Comparison of the measured W_Y coefficients with those predicted from measured W_X coefficients reveals reasonable agreement. One major source of error arises from the measurements of attenuation effected by the weighters, which was found to vary among the four individual devices, especially at the extreme low and high attenuations. For example at an attenuation 0.100×10^{-2} the control voltages ranged from 0.0030 to 0.0170, and around 2.7×10^{-2} they ranged from 0.22 to 0.26. Since the patterns were not exactly identical, an additional source of error was present, probably due to frequency drift in the system while the beamformer was being installed. Nevertheless, this result indicates fairly consistent operation of the system. When the $B^{T^{-1}}$ transformation was performed on the control voltages themselves, similar agreement was found, indicating that the operation of the hardware was nearly linear over about 17 *dB* range of coefficients.

The array can also be operated without a reference signal if the direction of the desired signal is known and a constraint is implemented to keep gain undisturbed in that single direction. This is precisely what is achieved by an orthogonal beamformer such as the one used here. Reference [4] explains the theory behind this approach. Briefly, one beam output is constrained and that beam is directed onto the desired signal. The other beams are adaptive and all are orthogonal to the constrained one (have nulls in direction of desired signal) and to each other. The reference signal is disconnected and total output power, $\overline{|y(t)|^2}$, is minimized instead, with the above constraint. The result is that the adaptive beams settle to such gains as

they require to subtract out the interference signals intruding on the constrained beam via its sidelobes, or on a side-direction of its main lobe or grating lobes.

Such experiments were conducted and samples of the results appear in Figures 9 (a) and (b). The evolution of the resultant pattern as well as that of the unconstrained beam are shown separately, and superimposed on the sample patterns in Figure 9(b). The desired signal is on the null of the adaptive Δ-beam and on the main lobe of the constrained $\sum$-beam, while the jammer intrudes on a side-direction of the first grating lobe. Cancellation of the jammer is accomplished by the Δ-beam, which is clearly seen to reduce its gain of the lobe on which the jammer is initially incident. Slight saturation of the IF buffer amplifiers is still evident in the separate beam patterns.

5. Conclusions.

A two-element microwave hardware adaptive array was built and tested in the laboratory. The testing was not complete and is continuing, but the results obtained to date, as exemplified by those contained herein, indicate that the system has good adaptive nulling capabilities and its operational characteristics are consistent with theoretical predictions. The system can suppress one directional incoherent interference source by about 30 dB, while maintaining constant gain on the desired signal. Its response time to a step transient interference pulse is 60 to 120 μs, though it was observed to be as low as 20 μs and as long as 200 μs, depending on system parameters and signal environment. The system was operated also in the constrained power-minimization mode (without a reference signal) and found to perform well, although there are indications that its dynamic range was reduced (not shown in these results).

Certain degeneracies arise from the fact that the array has only two elements: all lobes are grating lobes, only one degree of freedom is available (not really a degeneracy) and non-uniform element spacing is impossible. Since grating lobes are particularly vulnerable to jamming, the performance of this array was limited by this degeneracy (to be analyzed in subsequent experiments). When a jammer has considerable bandwidth, more than one degree of freedom may be required of the array to null it effectively. The hardware available was in some cases non-ideal (especially the multipliers) but the inherent robustness of the algorithm was relied upon initially to minimize problems of this nature.

A greater IF bandwidth is desirable in the case of dehopping at the IF stage. The only difference between such a system and this system is the correlators and weighters. The correlator is implemented by a balanced mixer and is available at almost all microwave frequencies, whereas the weighter can be implemented by an RF amplifier with electronic gain controls.

GaAs FET devices are available up to 18 GHz. No problem is foreseen in extending the present system to a system capable of dehopping over a range of 1 GHz.

These and other effects are currently being investigated in the laboratory.

6.

References

[1] **Brennan L.E., E.L. Pugh and I.S. Reed** "Control-loop Noise in Adaptive Array Antennas." *IEEE Transactions on Aerospace and Electronic Systems*, Vol., AES-7, No. 2, pp. 254-262, March 1971.

[2] **Gabriel, W.F.,** "Adaptive Arrays - An Introduction." *Proceedings of the IEEE*, Vol. 64, No. 2, pp. 239-272, February 1976.

[3] **Widrow, B, P.E. Mantey, L.J. Griffiths and B.B. Goode,** "Adaptive Antenna Systems" *Proceedings of the IEEE*, Vol., 55, No. 12, pp. 2143-2159, December 1967.

[4] **Hudson, J.E.,** "Adaptive Array Principles". (IEE Electromagnetic Wave Series 11), Peter Peregrinus Ltd., on behalf of IEE, 1981.

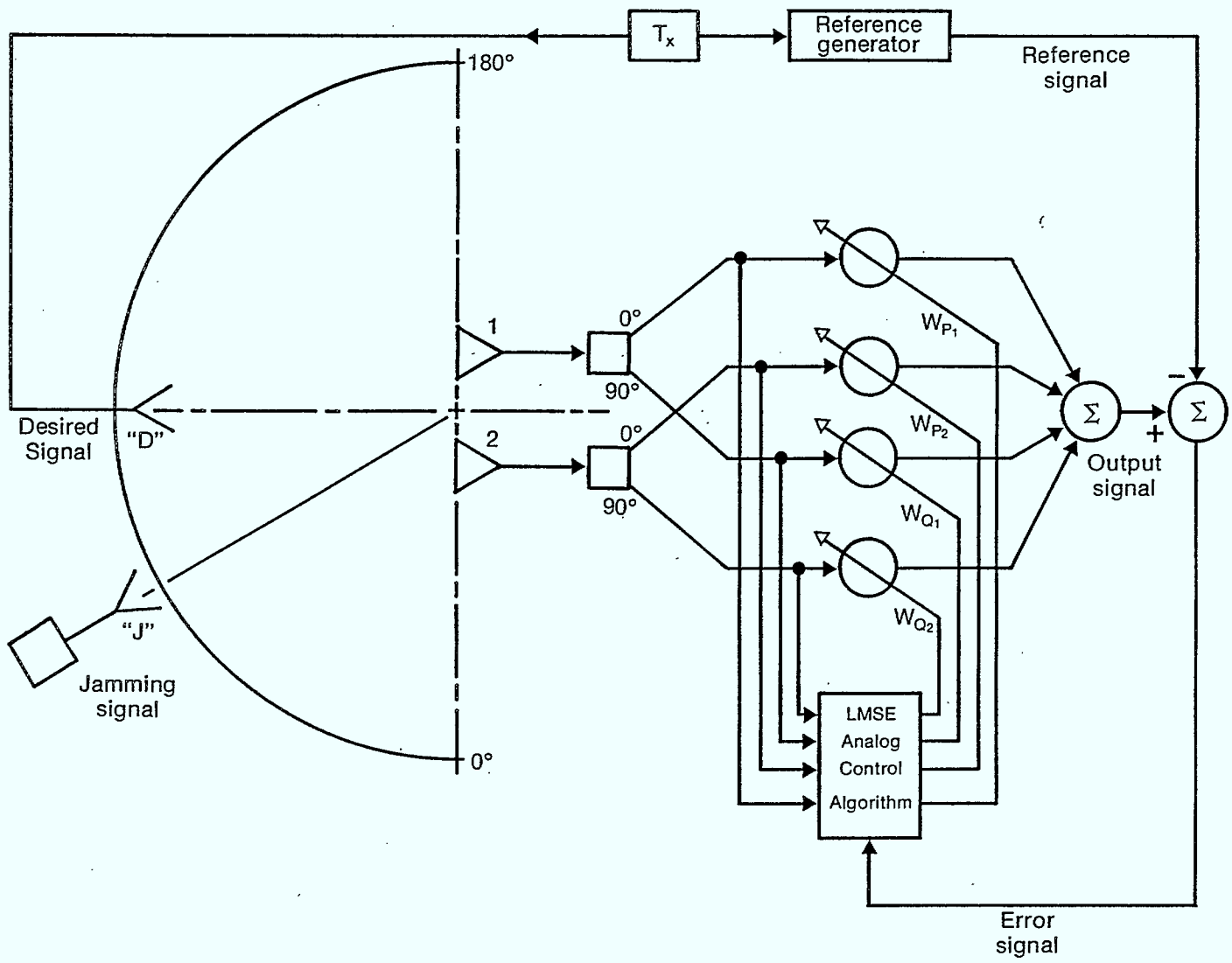

FIGURE 1. SCHEMATIC OF EXPERIMENTAL SETUP

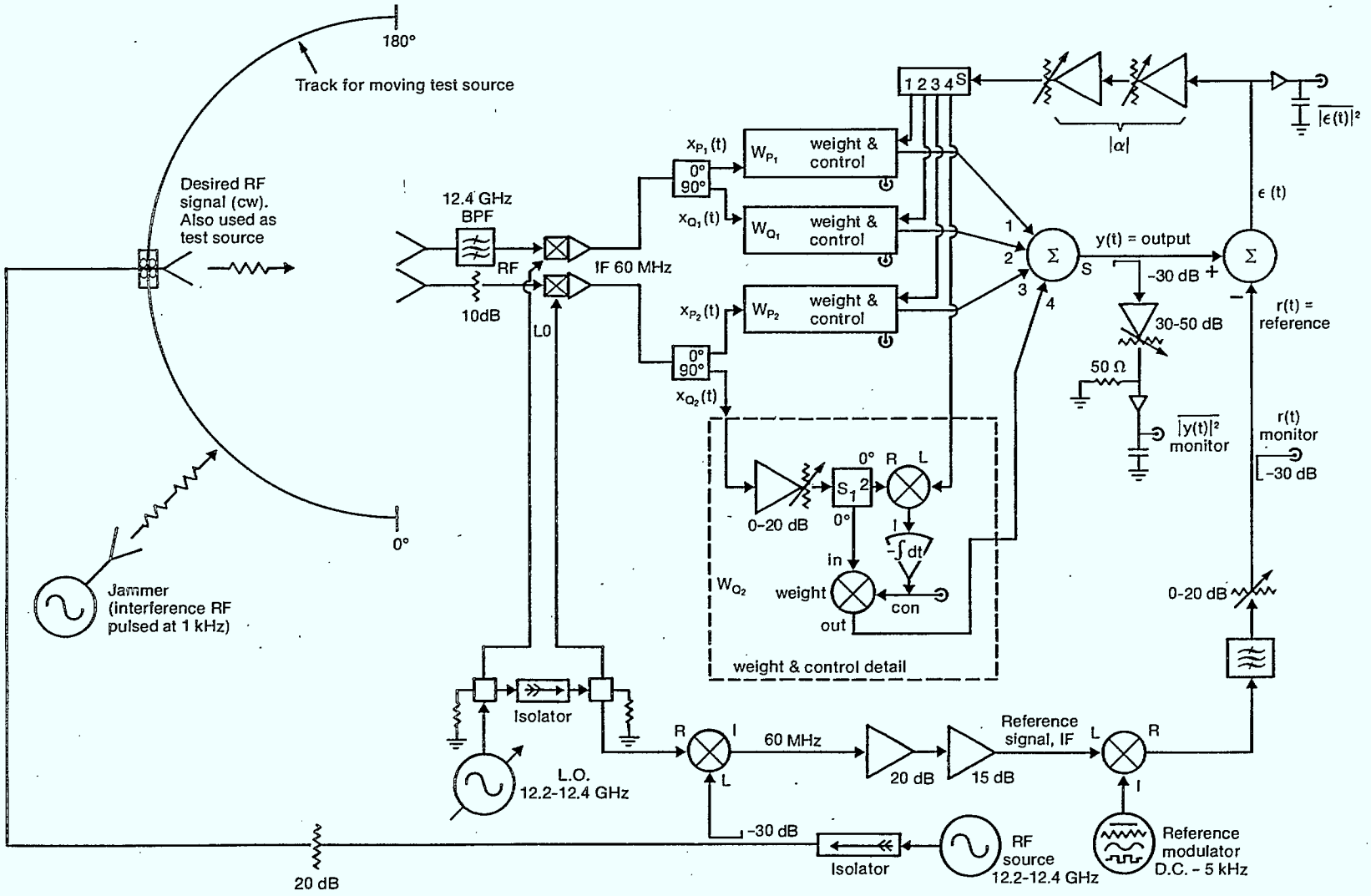

FIGURE 2. EXPERIMENTAL SYSTEM

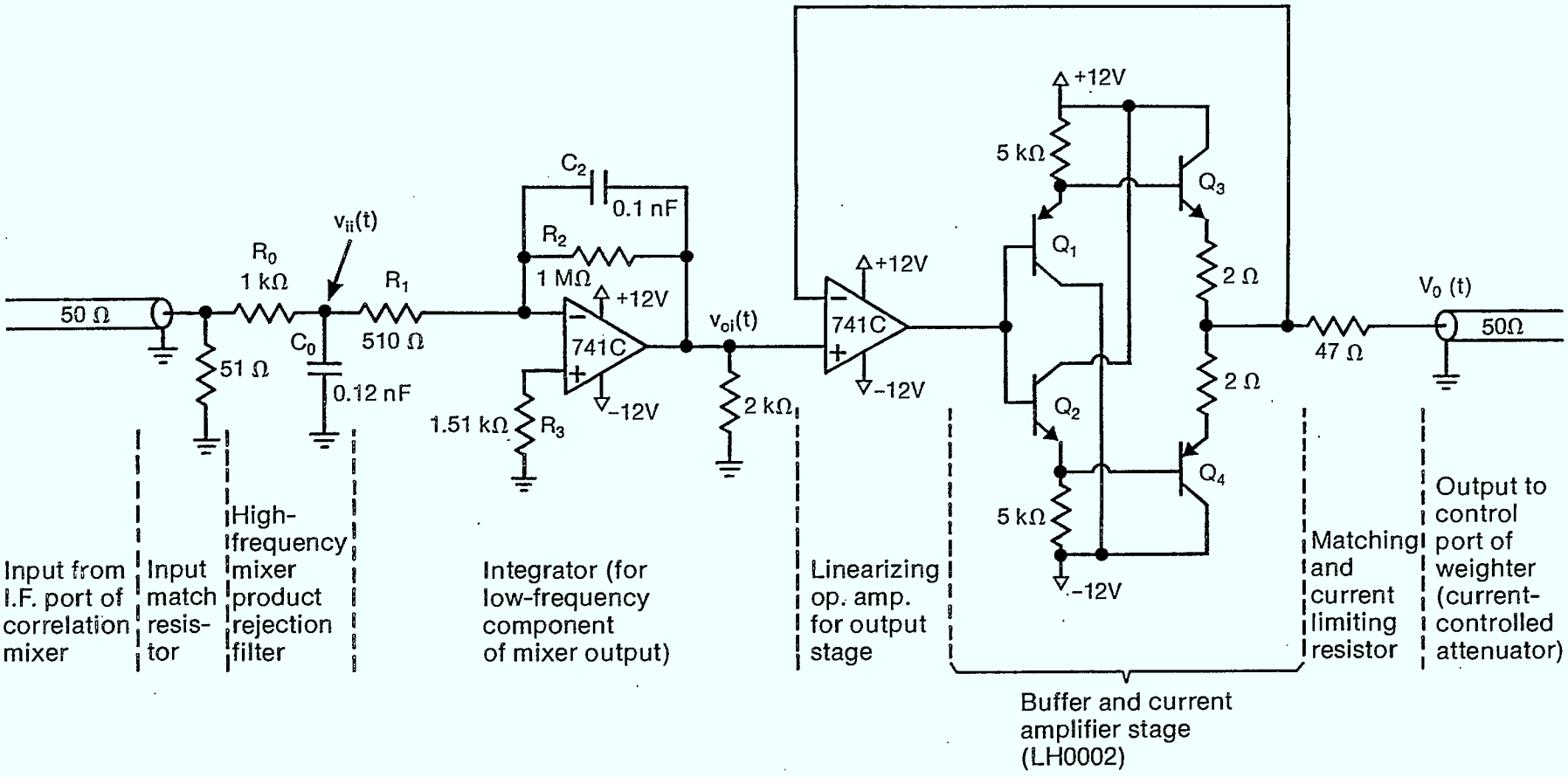

FIGURE 3. CIRCUIT DETAILS OF INTEGRATORS

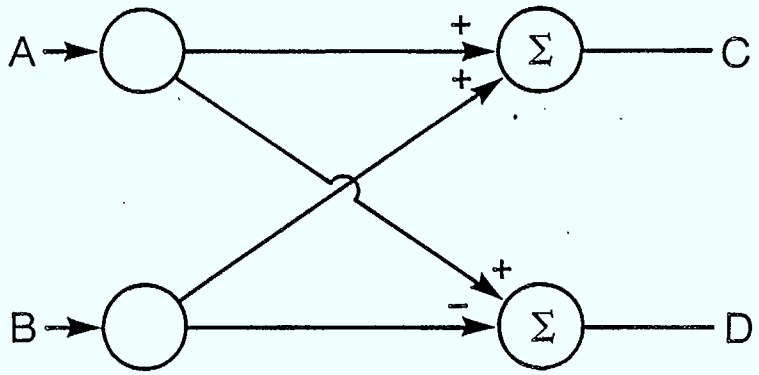

$$\begin{bmatrix} C \\ D \end{bmatrix} = \begin{bmatrix} 1 & 1 \\ 1 & -1 \end{bmatrix} \begin{bmatrix} A \\ B \end{bmatrix} = \begin{bmatrix} \Sigma \\ \Delta \end{bmatrix}$$

FIGURE 4. ORTHOGONAL BEAMFORMING NETWORK (2 POINT DFT), PRECEDING THE ADAPTIVE PROCESSOR. (FUNCTIONAL SCHEMATIC ONLY)

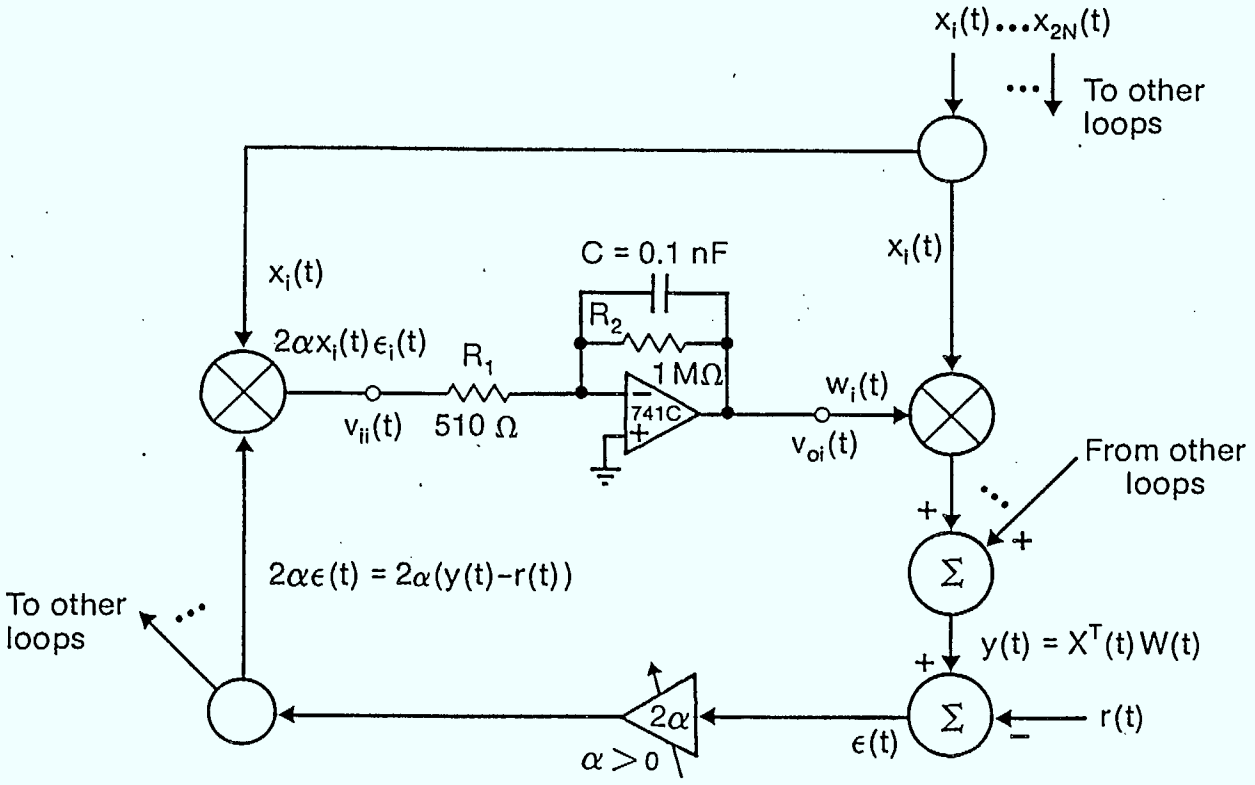

$$c\frac{d}{dt}v_{oi}(t) + \frac{1}{R_2}v_{oi}(t) = -\frac{1}{R_1}v_{ii}(t)$$

$$v_{ii}(t) = 2\alpha x_i(t)\epsilon(t), \quad V_i(t) = 2\alpha X(t)\epsilon(t)$$
$$v_{oi}(t) = w_i(t), \quad V_o(t) = W(t)$$
} for all loops

FIGURE 5. SIMPLIFIED CIRCUIT OF ADAPTIVE LOOP FOR PURPOSE OF ANALYSIS

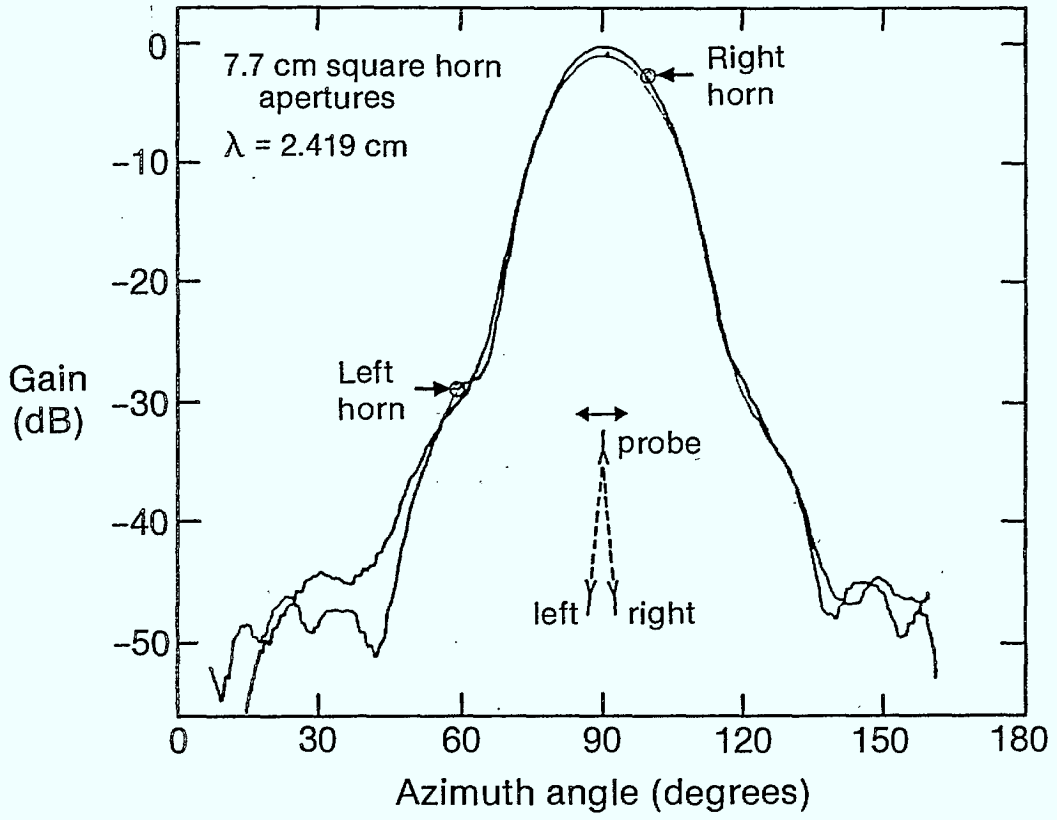

FIGURE 6(a). SUPERIMPOSED ELEMENT PATTERNS AT I.F. WITH HORNS CONVERGING

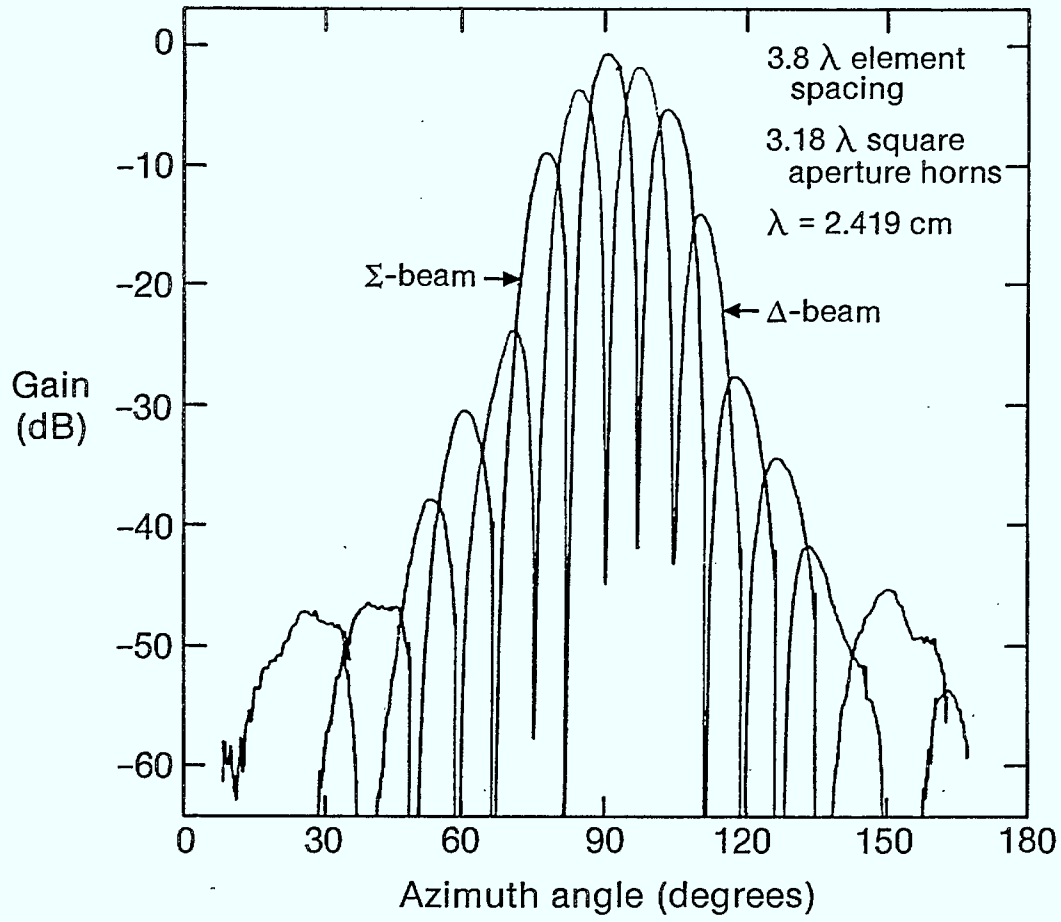

FIGURE 6(b). SUPERIMPOSED SUM (Σ) AND DIFFERENCE (Δ) BEAM PATTERNS AT I.F. TO SHOW RELATIVE POSITIONS OF LOBES AND NULLS

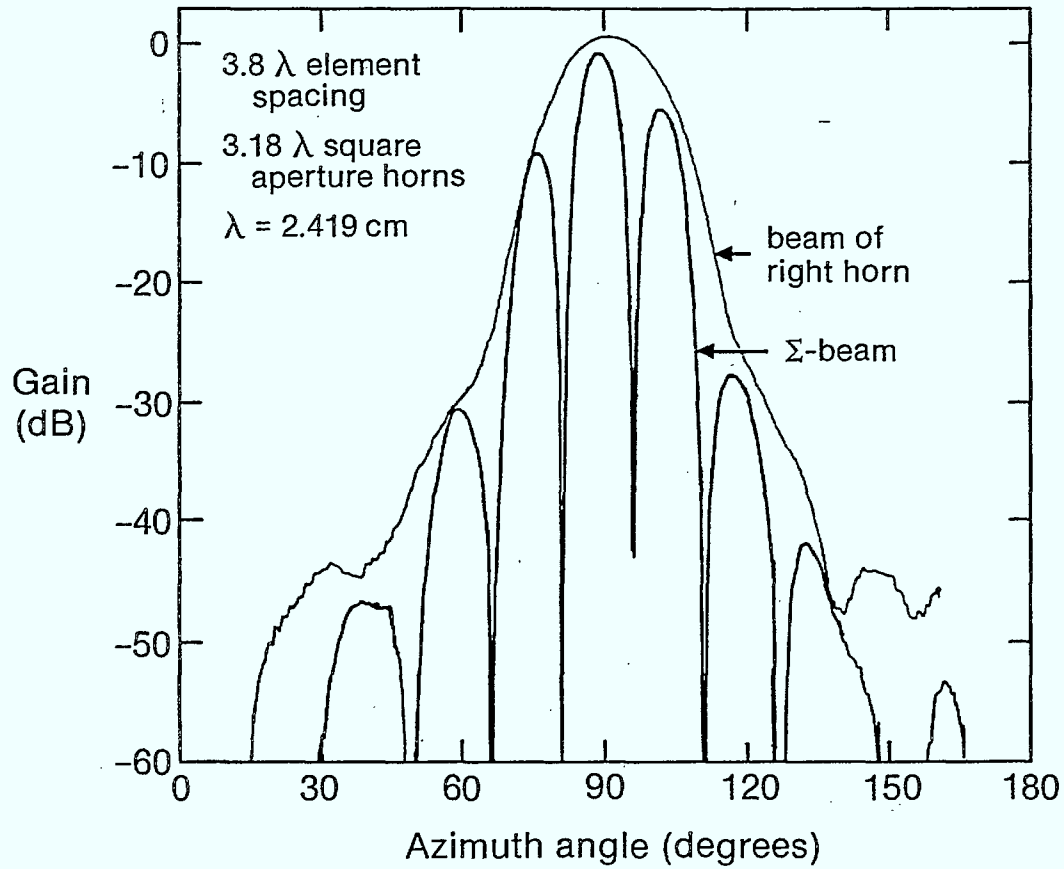

FIGURE 6(c). Σ-BEAM PATTERN WITH (RIGHT) HORN ELEMENT PATTERN, AT I.F.

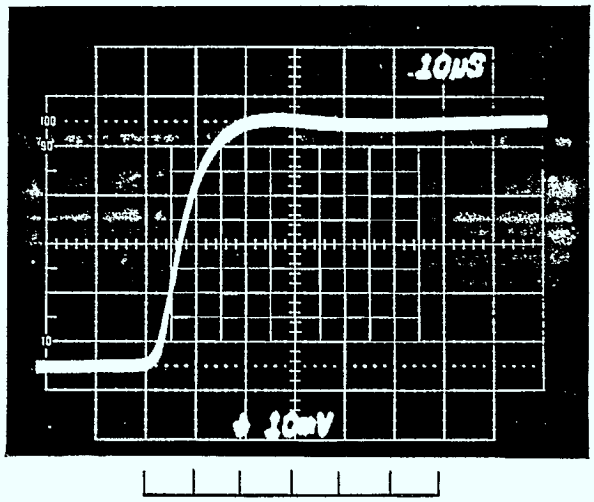

Leading edge of envelope of RF interference pulse.

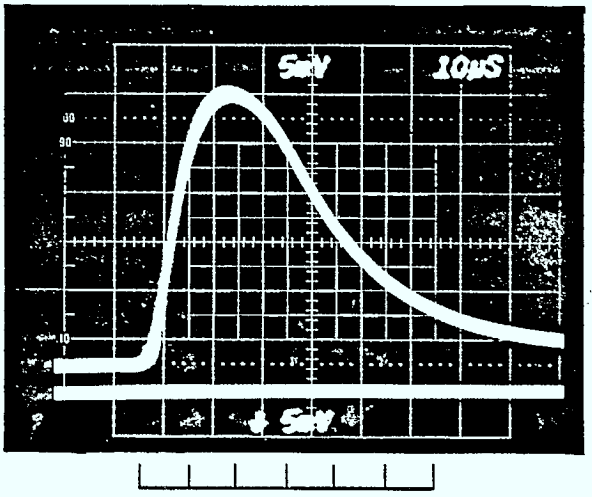

Envelope proportional to magnitude of mean square error.

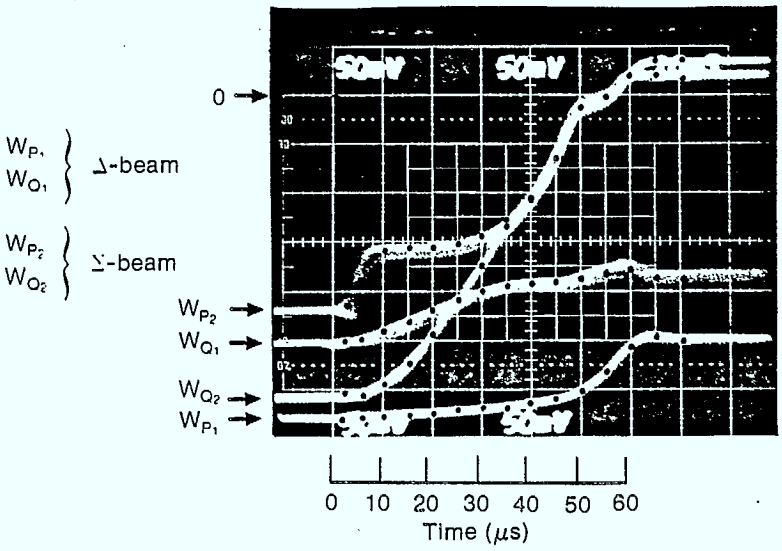

Transients of weight controlling signals in response to the interference pulse.

FIGURE 7(a). EVOLUTION OF JAMMER, ERROR, AND CONTROL SIGNALS

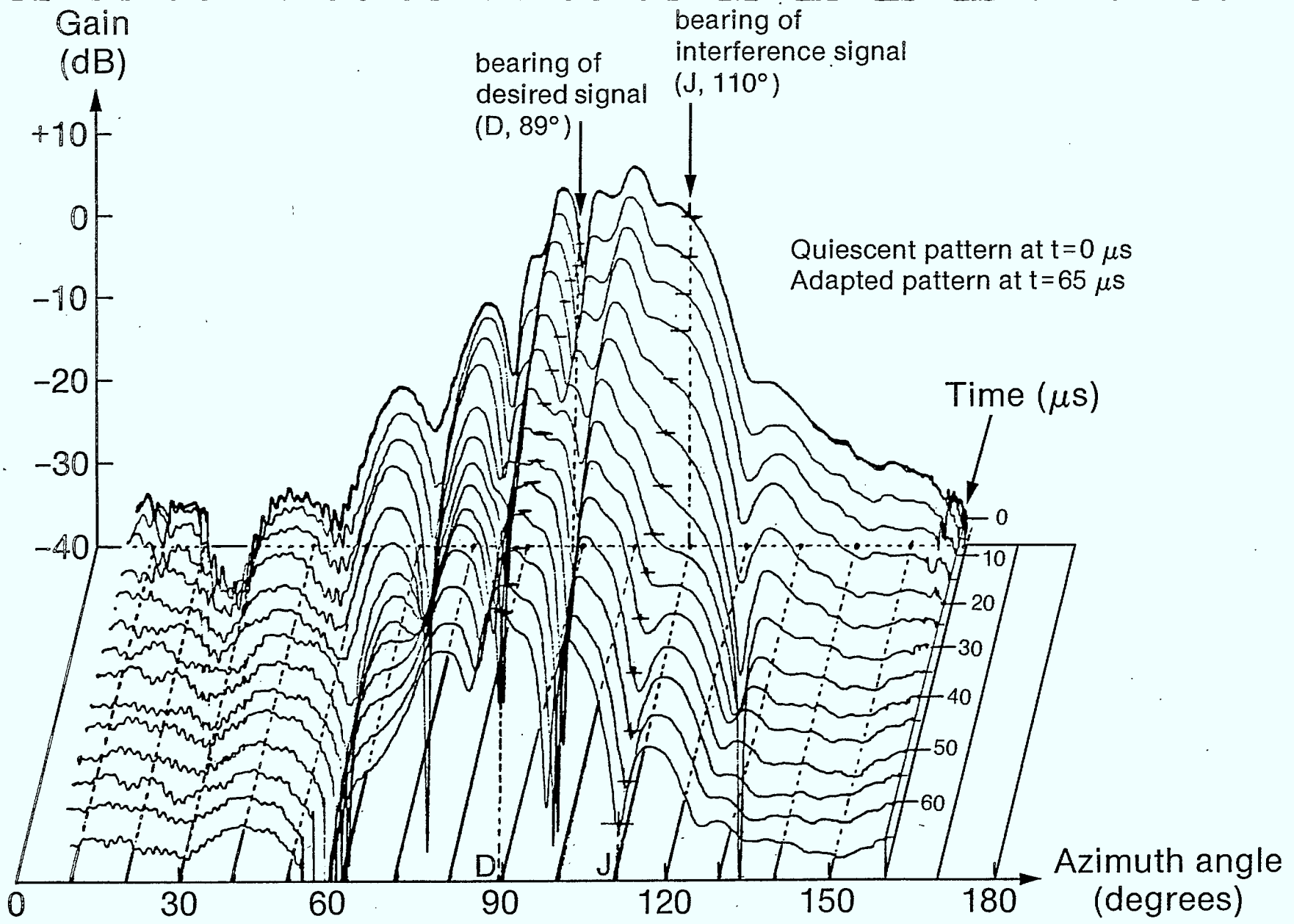

FIGURE 7(b). EVOLUTION OF ANTENNA GAIN PATTERN IN RESPONSE TO A JAMMER ACTIVATED IN A STEP-FUNCTION MANNER AT T=0 μs

Weighter voltages	Quiescent	Adapted
W_{P_1}	−0.0036	+0.1500
W_{Q_1}	+0.0490	+0.2260
W_{P_2}	−0.2705	−0.2274
W_{Q_2}	−0.3286	−0.1926

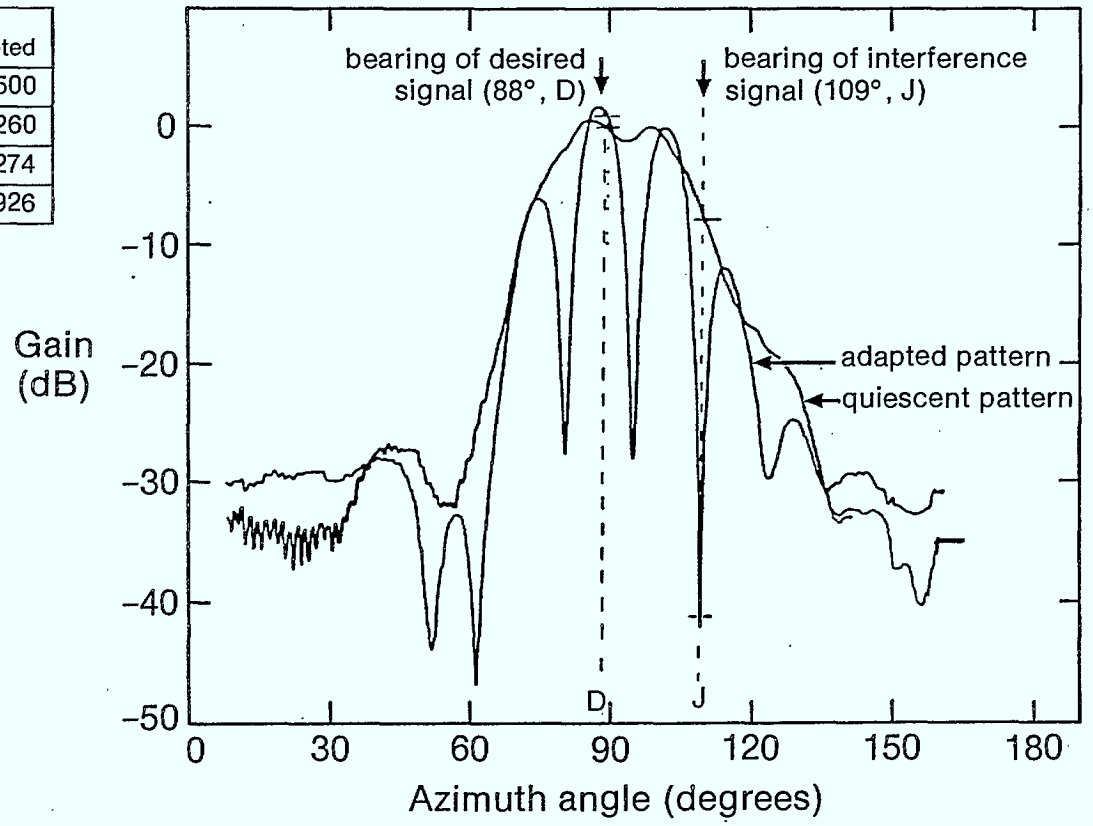

FIGURE 8(a). STEADY-STATE BEAM PATTERNS WITHOUT DFT (Σ·Δ) BEAMFORMER

Weighter voltages	Quiescent	Adapted
Δ port W_{P_1}	+0.3120	+0.2617
W_{Q_1}	-0.1800	-0.2182
Σ port W_{P_2}	-0.2306	+0.0022
W_{Q_2}	-0.3159	+0.0348

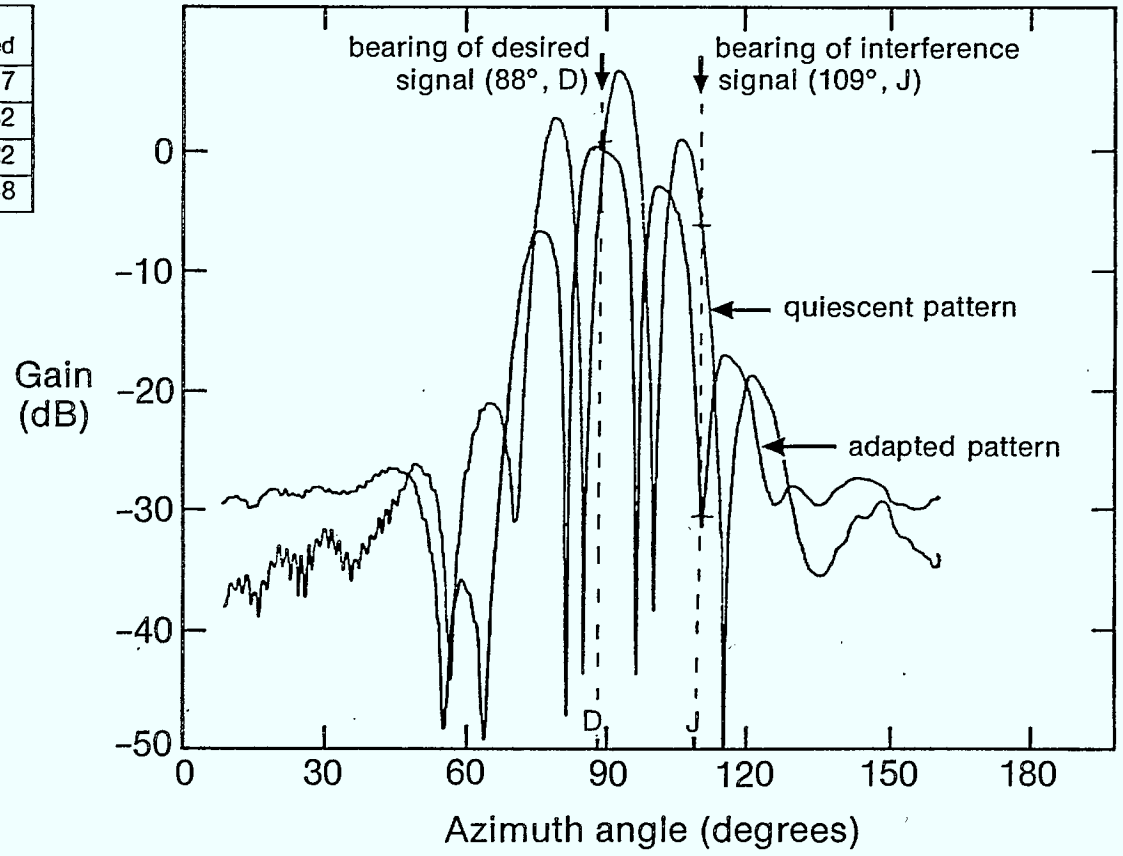

FIGURE 8(b). STEADY-STATE BEAM PATTERNS WITH DFT ($\Sigma \cdot \Delta$) BEAMFORMER.

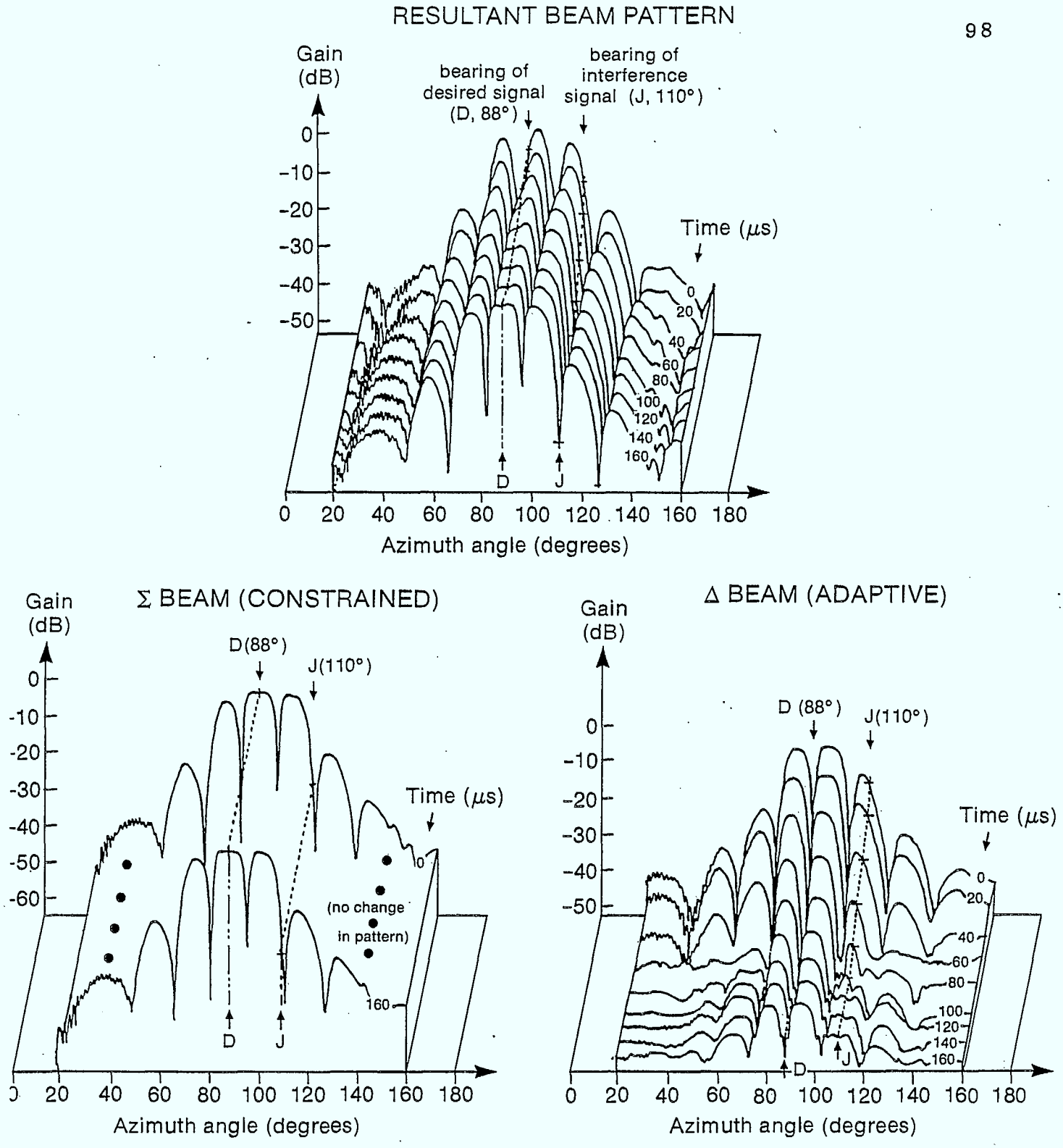

FIGURE 9(a). DECOMPOSITION OF THE EVOLVING PATTERN INTO Σ AND Δ PATTERNS

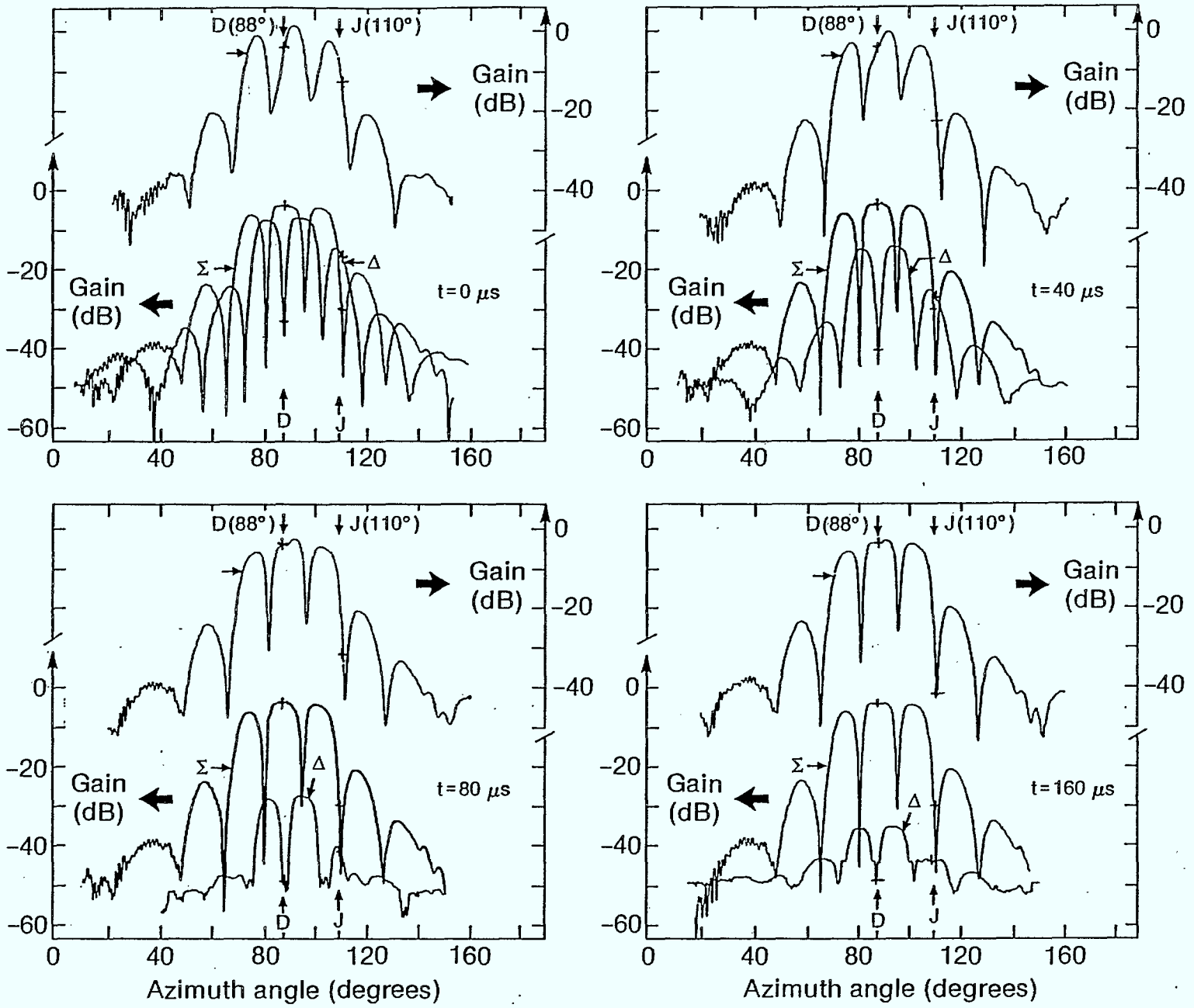

FIGURE 9(b). SAMPLE OF EVOLVING PATTERNS AND THEIR DECOMPOSITION INTO Σ AND Δ PATTERNS AT t=0, 40, 80, AND 160 μs.

Chapter 6

RECOMMENDATIONS AND CONCLUSIONS

For the Phase C Study we propose the following:

1. Design, fabricate, test and evaluate a small element number phased array fed reflector antenna with appropriate feed horns suitable for uplink service.
2. Fabricate, test and evaluate a small multi-beam lens antenna with appropriate feed horns suitable for downlink.
3. Implement and evaluate a small element number intellegent adaptive array for frequency hopping signals incorporating broadband slow acting nulling and fast acting narrow band nulling using a combination of feed forward and feed back modes. The phased array reflector of section 1 will be used for this at 44 GHz uplink frequency.
4. Experimental determination of the features, capabilities and drawbacks of the above will be verified against detailed analysis.

APPENDIX

DESIGN OF CORRUGATED FEEDS FOR EHF REFLECTOR AND LENS ANTENNAS.

TIL-TEK LIMITED

The most commonly used feed for reflector and horn antennas is the hybrid mode corrugated conical horn [1]. The usual way of deriving the fields is to expand the aperture distribution in an infinite series of spherical wave functions. The method being looked at here is due to Narasimkan [2] and simplifies the above procedure by replacing the spherical Bessel functions by Lommel functions. This still leaves a rather complex infinite series of Bessel and Lommel functions and their derivatives. The work done here simplifies this formulation making it much more amenable to computation by microcomputers. The simplification consists of two parts. First the series involved are made to converge more quickly, and secondly the need for taking derivatives of the infinite series is obviated by the derivation of relationships between the derivations and the functions themselves.

The fields of a corrugated horn may be expressed in terms of Lommel functions [2]. The relevant formulae are:

$$\bar{E} = C_{11}(1+\cos\theta)\ M\ I^{j\phi}\ \ (\bar{a}_\theta + j\bar{a}_\phi)$$

where

$$M = b_3 \cdot W_a^3(2v,\beta) + b_2 \cdot W_a^2(2v,\beta) + b_1\ W_a^1(2v,\beta) + b_a\ W_a^a(2v,\beta)$$

$$W_a^n(x,\beta) = \left[\frac{2}{j}\right]^n \left\{ \frac{\partial^n}{\partial x^n}\left[\frac{U_1(x,\beta)}{x}\right] + j\frac{\partial^n}{\partial x^n}\left[\frac{U_2(x,\beta)}{x}\right]\right\}$$

$$U_1(x,\beta) = -\sum_{n=1}^{\infty} (-1)^n\ J_{2n-1}(\beta)\cdot\left(\frac{x}{\beta}\right)^{2n-1}$$

$$U_2(x,\beta) = -\sum_{n=1}^{\infty} (-1)^n\ J_{2n}(\beta)\cdot\left(\frac{x}{\beta}\right)^{2n}$$

- o $v = \frac{\pi a^2}{\lambda L}$,
- o $\beta = ka \sin \theta$,
- o $k = 2\pi/\lambda$,
- o $L =$ axial length of horn from vertex to aperture,
- o $a =$ aperture radius,
- o U_1 and U_2 are Lommel functions.

The above series for the Lommel functions may be evaluated either in terms of powers of $(\frac{x}{\beta})$ or $(\frac{\beta}{x})$ by making use of relations derived here:

First we note that

$$\cos(\beta \cos \phi) = J_o(\beta) + \sum_{n=1}^{\infty} (-1)^n \cdot J_{2n}(\beta) \left[e^{j2n\phi o} + e^{-j2n\phi o} \right]$$

From this we can deduce with a little maniputation that

$$\cos\left[\frac{\beta}{2} \left(u + \frac{1}{u} \right) \right] = J_o(\beta) + \sum_{n=1}^{\infty} (-1)^n J_{2n}(\beta) \left[u^{2n} + u^{-2n} \right]$$

Thus if it is easier to sum the series in u^{-2n} than u^{2n} we may do so and vice versa.

In a similar fashion it may be shown that

$$\sin\left[\frac{\beta}{2} \left[u + \frac{1}{u} \right] \right] = -\sum_{n=1}^{\infty} (-1)^n J_{2n-1}(\beta) \left[u^{2n-1} + u^{-(2n-1)} \right]$$

The derivates of U_1 and U_2 are derived as follows:

Let

$$U_1 = -\sum_{n=1}^{\infty} (-1)^n J_{2n-1}(\beta) u^{2n-1}$$

$$\frac{\partial U_1}{\partial u} = -\sum_{n=1}^{\infty} (-1)^n (2n-1) J_{2n-1}(\beta) u^{2n-2}$$

$$= -\sum_{n=1}^{\infty} (-1)^n \frac{\beta}{2} \left[J_{2n-2}(\beta) + J_{2n}(\beta) \right] u^{2n-2}$$

$$= \frac{\beta}{2} J_o(\beta) + \frac{\beta}{2} \sum_{n=1}^{\infty} (-1)^n J_{2n}(\beta) u^{2n} \left(1 - \frac{1}{u^2}\right)$$

Thus

$$\frac{\partial U_1}{\partial u} = \frac{\beta}{2} J_o(\beta) - \frac{\beta}{2}\left(1-\frac{1}{u^2}\right) U_2$$

Similarly for U_2

$$U_2 = -\sum_{n=1}^{\infty} (-1)\, J_{2n}(\beta)\, U^{2n}$$

$$\frac{\partial U_2}{\partial u} = -\sum_{n=1}^{\infty} (-1)^n\, 2n\, J_{2n}(\beta)\, u^{2n-1}$$

$$= -\sum_{n=1}^{\infty} (-1)^n \frac{\beta}{2}\left[J_{2n-1}(\beta) + J_{2n+1}(\beta) \right] u^{2n-1}$$

$$= \frac{\beta}{2u} J_1(\beta) - \frac{\beta}{2}\left(1-\frac{1}{u^2}\right) \sum_{n=1}^{\infty} (-1)^n\, J_{2n-1}(\beta)\, u^{2n-1}$$

so that

$$\frac{\partial U_2}{\partial u} = \frac{\beta}{2u} J_1(\beta) + \frac{\beta}{z}\left(1-\frac{1}{u^2}\right) U_1$$

with these formulae only U_1, U_2 and some other simple functions need be calculated.

References

1. **Clarricoats, P.J.B.,** "Feeds for Reflector Antennas - A Review." Second International Conference on Antennas and Propagation, IEEE Conference Publication, No. 195, 1981.

2. **Narasimhan, N.S.,** "Corrugated Conical Horns with Arbitrary Corrugation Depth." Radio Electron. Eng., Vol. 43, March 1973.

E-PLANE PATTERN OF CORRUGATED HORNS.

THETA	E	PHASE	E (dB)
0	1	30.26	0
10	0.8584	30.17	1.325
20	0.5356	29.85	5.421
30	0.2264	28.97	12.89
40	0.481	24.30	27.3
50	0.0244	143	32.23
60	0.082	147.2	29.89

Aperture radium 1.25 cm.
Axial length 80 cm.
Frequency = 30 GHz.
Axis gain is 16.3 dB.

THETA	E	PHASE	E (dB)
0	1	9.715	0
10	0.8517	11.60	1.394
20	0.5181	17.16	5.71
30	0.2184	33.72	18.21
40	0.0771	82.64	22.25
50	0.0553	138.3	25.14
60	0.0396	162.7	26.03

Aperture radius 1.3 cm.
Axial length 5.02 cm.
Frequency = 30 GHz.
Axis gain 16.39 dB.

THETA	E	PHASE	E (dB)
0	1	28.05	0
10	0.7492	27.71	2.507
20	0.283	26.04	10.96
30	0.0113	17.08	38.87
40	0.0366	147.9	28.72
50	7.658	157.1	42.31
60	9.311	35.52	40.61

Aperture radium 1.7269 cm.
Axial length 80 cm.
Frequency = 30 GHz
Axis gain 19.10 dB.

THETA	E	PHASE	E (dB)
0	1	26.55	0
10	0.6817	25.94	3.327
20	0.1681	21.92	15.48
30	0.0352	141.3	29.04
40	0.0155	154.5	36.17
50	0.0114	35.17	38.85
60	8.495	30.03	41.47

Aperture radius 1.965 cm
Axial length 80 cm
Frequency = 30 GHz.
Axis gain 20.31 dB.